

Summer 2024

# Optimizing the Reliability Improvement of Power Electronic Converters Using Different Computational Optimization Techniques

Valentin A. Dun

Follow this and additional works at: <https://digitalcommons.georgiasouthern.edu/etd>



Part of the [Computational Engineering Commons](#), and the [Power and Energy Commons](#)

---

## Recommended Citation

Dun, Valentin A., "Optimizing the Reliability Improvement of Power Electronic Converters Using Different Computational Optimization Techniques" (2024). *Electronic Theses and Dissertations*. 2834.

<https://digitalcommons.georgiasouthern.edu/etd/2834>

This thesis (open access) is brought to you for free and open access by the Jack N. Averitt College of Graduate Studies at Georgia Southern Commons. It has been accepted for inclusion in Electronic Theses and Dissertations by an authorized administrator of Georgia Southern Commons. For more information, please contact [digitalcommons@georgiasouthern.edu](mailto:digitalcommons@georgiasouthern.edu).

# OPTIMIZING THE RELIABILITY IMPROVEMENT OF POWER ELECTRONIC CONVERTERS USING DIFFERENT COMPUTATIONAL OPTIMIZATION TECHNIQUES

by

VALENTIN DUN

(Under the Direction of Masoud Davari)

## ABSTRACT

The implementation of renewable energy and decentralization of power generation over the last years created the need for superior technology to be implemented into the grid, which had to transform and integrate these variable renewable energy sources into the existing grid. This technology aims to completely replace the traditional technology in the grid by providing more efficient electricity generation, transmission, and distribution, as well as ensuring benefits such as high reliability, lower cost, higher efficiency, and more compactness, among others. However, the inclusion of power electronic converters into the grid brings many challenges, such as harmonic distortions introduced by power electronic converters and non-linear operation. In addition, power electronic converters can bring challenges related to the quality of the power generated, as well as the stability of the system. In other words, converter design will be critical depending on its application. The most optimum design can be done after a thorough study of the behavior of the converts as well as how to optimize its characteristics. Therefore, this work develops the modeling process of the reliability of power electronic converters at the component, sub-system, and power system level and the optimization of the proposed reliability improvement model. This optimization will be done by using different computational optimization techniques, also called metaheuristic algorithms, such as the Harris Hawk Optimization (HHO) algorithm, the Artificial Bee Colony (ABC) algorithm, and the Particle Swarm Optimization (PSO) algorithm. The objective is to compare each algorithm's performance in terms of convergence rate and the fitness of the parameters in terms of constraints provided by the designer.

**INDEX WORDS:** Power converter reliability, Reliability Modeling, Reliability Optimization, Metaheuristic Optimization Algorithms.

OPTIMIZING THE RELIABILITY IMPROVEMENT OF POWER ELECTRONIC  
CONVERTERS USING DIFFERENT COMPUTATIONAL OPTIMIZATION TECHNIQUES

by

VALENTIN DUN

B.Sc., Georgia Southern University, United States, 2024

A Thesis Submitted to the Graduate Faculty of Georgia Southern University

in Partial Fulfillment of the Requirements for the Degree

MASTER OF SCIENCE

© 2024

VALENTIN DUN

All Rights Reserved

OPTIMIZING THE RELIABILITY IMPROVEMENT OF POWER ELECTRONIC  
CONVERTERS USING DIFFERENT COMPUTATIONAL OPTIMIZATION TECHNIQUES

by

VALENTIN DUN

Major Professor:  
Committee:

Masoud Davari  
Rocio Alba-Flores  
Fernando Rios-Gutierrez

Electronic Version Approved:

July 2024

## DEDICATION

This work is dedicated to my family, who have supported me since I started my bachelor's degree four and a half years ago; I could not have done it without them.

## ACKNOWLEDGMENTS

I want to express my warmest gratitude to my supervisor, Dr. Masoud Davari, who supported me throughout this research. Thank you very much, Dr. Davari, for all your ideas, contributions, and pieces of advice that you have given me since we started to do research together. I genuinely appreciate the trust that you put in me. I also want to thank Felix Adabla for introducing me to the topic of reliability of power converters when I joined the research team and for the many ideas and contributions he made to my research along the way. Thank you very much, Felix; being on the same research team as you was a pleasure.

## TABLE OF CONTENTS

	Page
ACKNOWLEDGMENTS .....	3
LIST OF TABLES .....	7
LIST OF FIGURES.....	8
LIST OF SYMBOLS .....	10
CHAPTER	
1 INTRODUCTION .....	14
Purpose of Study .....	15
Contribution.....	16
2 LITERATURE REVIEWS .....	17
Reliability in power systems.....	17
Power electronics in power systems .....	19
AC to DC converters .....	20
DC to DC converters .....	21
AC to AC converters.....	21
DC to AC converters.....	22
Power converter's role in modernized power systems .....	22
Power converter's reliability analysis.....	23
Metaheuristic optimization methods.....	24
3 RELIABILITY MODELING .....	27
Power system level reliability modeling .....	27

	5
Loss of load probability (LOLP) .....	28
Loss of load expectation (LOLE) .....	28
Expected energy that is not supplied (EENS) .....	28
Sub-system level reliability modeling .....	29
Component level reliability modeling .....	35
Reliability enhancement .....	37
<b>4 METAHEURISTIC OPTIMIZATION ALGORITHMS.....</b>	<b>39</b>
Harris Hawk Optimization (HHO) Algorithm.....	39
Initialization phase .....	41
Exploration phase .....	41
Transition from exploration to exploitation phase.....	41
Exploitation phase .....	42
Soft besiege stage.....	42
Hard besiege stage .....	43
Soft besiege with progressive rapid dives stage .....	43
Hard besiege with progressive rapid dives stage .....	44
HHO Pseudocode.....	45
Particle Swarm Optimization (PSO) Algorithm .....	46
PSO principles of execution .....	46
Development of the algorithm .....	47
Initialization phase .....	48
Exploration and exploitation phase.....	49
Constriction coefficients .....	49
PSO Pseudocode .....	51

	6
Artificial Bee Colony (ABC) Algorithm .....	52
ABC principles of execution.....	52
Employed bees' phase .....	53
Onlooker bees' phase.....	54
Scout bees' phase.....	54
ABC pseudocode .....	55
5 RELIABILITY STUDIES AND RESULTS .....	57
Harris Hawk Optimization Algorithm Results .....	58
Particle Swarm Optimization Algorithm Results .....	65
Artificial Bee Colony Algorithm Results .....	72
Number of components vs Performance.....	80
Global Optimization (useful time phase) .....	82
Global Optimization (wear out phase).....	86
6 CONCLUSION AND FUTURE WORK .....	90
REFERENCES.....	91

## LIST OF TABLES

Table	Page
3.1 Input variables boundaries .....	38
3.2 Parameters constrictions.....	38
5.1 Capacitor failure rate optimized parameters (HHO).....	58
5.2 Single Capacitor lifetime optimized parameters (HHO).....	60
5.3 Switching device failure rate optimized parameters (HHO).....	62
5.4 Single switching device lifetime optimized parameters (HHO) .....	63
5.5 Capacitor failure rate optimized parameters (PSO) .....	65
5.6 Single capacitor lifetime optimized parameters (PSO).....	67
5.7 Switching device failure rate optimized parameters (PSO) .....	69
5.8 Single switching device lifetime optimized parameters (PSO) .....	71
5.9 Capacitor failure rate optimized parameters (ABC) .....	73
5.10 Single capacitor lifetime optimized parameters (ABC).....	75
5.11 Switching device failure rate optimized parameters (ABC) .....	77
5.12 Single switching device lifetime optimized parameters (ABC).....	79
5.13 Useful time phase optimized results (Part 1) .....	83
5.14 Useful time phase optimized results (Part 2) .....	84
5.15 Failure rate optimization parameters.....	86
5.16 Wear out phase optimized results (Part 1) .....	86
5.17 Wear out phase optimized results (Part 2) .....	87
5.18 Lifetime optimization parameters .....	89

## LIST OF FIGURES

Figure	Page
1.1 Annual $CO_2$ emissions from fossil fuel by world region estimate in ( $GtCO_2$ ).....	14
2.1 Typical bathtub curve describing failure rate of an item .....	19
2.2 A dual-output half-bridge converter with three switches.....	20
2.3 General overview and interconnection of overall reliability-related topics.....	24
2.4 Classification of meta-heuristic techniques (meta-heuristic diamond).....	25
2.5 General framework of the swarm intelligence algorithms.....	26
3.1 Correlation between PE and power system reliability concepts .....	27
4.1 Exploration and exploitation phases of Harris Hawks optimization (HHO) .....	40
4.2 The exploration phase and the four types of exploitation phases in HHO.....	40
4.3 The taxonomy of PSO applications.....	46
4.4 The flowchart of PSO .....	48
4.5 Schematic diagram of the artificial bee colony algorithm .....	53
5.1 Single capacitor failure rate ( $\lambda_{cap}$ ) convergence (HHO).....	59
5.2 Capacitor with redundancy failure rate ( $\lambda_{cap}$ ) convergence (HHO).....	59
5.3 Single capacitor lifetime ( $L_{cap}$ ) convergence (HHO).....	61
5.4 Single switching device failure rate ( $\lambda_{SD}$ ) convergence (HHO).....	62
5.5 Switching device with redundancy failure rate ( $\lambda_{SD}$ ) convergence (HHO).....	63
5.6 Single switching device cycles to failure ( $N_f$ ) convergence (HHO) .....	64
5.7 Single capacitor failure rate ( $\lambda_{cap}$ ) convergence (PSO) .....	66
5.8 Capacitor with redundancy failure rate ( $\lambda_{cap}$ ) convergence (PSO).....	66
5.9 Single capacitor lifetime ( $L_{cap}$ ) convergence (PSO) .....	68

5.10 Single switching device failure rate ( $\lambda_{SD}$ ) convergence (PSO) .....	70
5.11 Switching device with redundancy failure rate ( $\lambda_{SD}$ ) convergence (PSO) .....	70
5.12 Single switching device cycles to failure ( $N_f$ ) convergence (PSO).....	72
5.13 Single capacitor failure rate ( $\lambda_{cap}$ ) convergence (ABC) .....	74
5.14 Capacitor with redundancy failure rate ( $\lambda_{cap}$ ) convergence (ABC).....	74
5.15 Single capacitor lifetime $L_{cap}$ convergence (ABC).....	76
5.16 Single switching device failure rate ( $\lambda_{SD}$ ) convergence (ABC).....	78
5.17 Switching device with redundancy failure rate ( $\lambda_{SD}$ ) convergence (ABC) .....	78
5.18 Single switching device cycles to failure ( $N_f$ ) convergence (ABC).....	80
5.19 Number of capacitors vs performance .....	81
5.20 Number of switching devices vs performance .....	82
5.21 Failure rate optimization convergence .....	85
5.22 Lifetime optimization convergence.....	88

## LIST OF SYMBOLS

Symbol	Description	Symbol	Description
$\lambda_{Physical-cap}$	Contribution of physical stresses on the capacitor	$D_{Cap}$	Diameter of Cap
$\lambda_{Physical-SD}$	Contribution of physical stresses on the SD	$L_{Cap}$	Length of Cap
$\Pi_{PM}$	Quality and technical control that goes into the capacitor's and SD's manufacturing.	$h_{tot}$	Total heat transfer coefficient of Cap
$\Pi_{Process}$	Quality and technical control of the development, manufacturing, and operating processes of the converter as a system	$h_{rad}$	Radiation heat transfer coefficient of Cap
$\delta_1 \& \alpha_1$	Correlating factors that determine the size of the impact of $\Pi_{PM}$ on reliability. [ $\delta_1 = 1.39, \alpha_1 = 0.69$ ]	$h_{free}$	Convection heat transfer coefficient of Cap
<i>Part_Grade</i>	Estimation from the audit indicating the influence of the manufacturer's QA, the component's QA & RA, and where applicable, the buyer's past experience ( $\epsilon$ ) [assume best = 1 (supplier superior/under control)]	$\epsilon$	Radiation coefficient (emissivity) [ $\epsilon = 0.85$ ]
$\delta_2$	Correlating factor that determines the range of variation of $\Pi_{Process}$ . [ $\delta_2 = 2.079$ ]	$\sigma$	Stefan Boltzmann constant for radiation [ $\sigma = 5.67 \times 10^{-8} W/m^2K^4$ ]
<i>Process_Grade</i>	Estimation from an audit indicating how the factors influencing the design rules for the components are managed [assume = 1 (best process)]	$G_{RMS,Cap}$	Stress associated with the Cap's random vibration phase. Assuming worst case scenario ( $G_{RMS,Cap} = 40 G_{rms}$ )
$\Pi_{PW}$	Acceleration factor related to the impact of the component's development.	$G_{RMS,SD}$	Stress associated with the SD's random vibration phase. Assuming worst case scenario ( $G_{RMS,SD} = 40 G_{rms}$ )
$\delta \& \alpha$	Correlating factors that determine the size of the impact of $\Pi_{PW}$ on reliability. [ $\delta = 3.401, \alpha = 0$ ]	$\lambda_{0TH}$	Basic failure rate of a SD due to thermal contribution [assume usage of SMD, high power, large heatsink, lead, plastic type of package ( $\lambda_{0TH} = 0.56$ )]
$\Pi_{Induced}$	Contribution of the induced/overstress factors inherent to a particular field of application.	$\lambda_{0TCyCase}$	Basic failure rate of a SD due to thermal cycling contribution [= 0.013371]
$\Pi_{Placement}$	Influence of the Cap's and SD's functions in the system [assume power analog interface function = 2.5]	$\lambda_{0TCySolderjoints}$	Basic failure rate of a SD due to contribution of thermal cycling of the soldered joints [= 0.066853]

$\Pi_{Application}$	Influence of the environment of use during application on the converter's reliability [assume best case (controlled environment) = 1]	$\lambda_{0RH}$	Basic failure rate of a SD due to relative humidity contribution [0.487813]
$W_{scores,k}$	Weightings for the scores assigned to each criterion of condition [assume favorable condition, i.e. $\Pi_{Application} = 1$ ]	$\lambda_{Mech}$	Basic failure rate of a SD due to mechanical contribution [0.001337]
$W_{OS,k}$	Weight of each criterion	$\Pi_{TH}$	The acceleration factor indicating thermal stress sensitivity on the SD during operation.
$\Pi_{Ruggedizing}$	Influence of the policy of building overstress tolerance into the Cap or SD	$\Pi_{TCyCase}$	Acceleration factor indicating thermal cycling stress sensitivity on the SD during operation.
$Recom\_Grade$	Weighted recommendation score assigned to the Cap or SD [assume all recommendations have been applied = 1]	$\Pi_{TCySolderjoints}$	Acceleration factor indicating thermal cycling stress sensitivity on the SD's soldered joints during operation.
$C_{Sens}$	Overstress sensitivity coefficient inherent to the technology of the Cap or SD $C_{sens} = \alpha EOS + \beta MOS + \gamma MOS = 6.3$	$\Pi_{RH}$	Acceleration factor indicating relative humidity stress sensitivity on the SD during operation [during operation = 0]
$\lambda_{0Cap}$	Basic failure rate of the Cap (assume the value of ceramic capacitor [ $\lambda_{0Cap} = 0.4$ ])	$\Pi_{Mech,SD}$	Acceleration factor indicating mechanical stress sensitivity on the SD during operation.
$t_{phase}$	Duration of the operation and maintenance phase [We assume only this phase to reduce mathematical complexity. Also, assume a 24-hr operation ( $t_{phase} = 24hrs$ )]	$T_{j-IGBT}$	SD's junction temperature during an operating phase
$T_{total}$	Reference duration in a year ( $T_{total} = 8760hrs$ )	$\Delta T_{cycling,SD}$	Amplitude of temperature variation associated with the SD's cycling phase ( $^{\circ}C$ ) [equation determined from curve-fitting technique in MATLAB]
$T_{Ref} = T_{amb}$	Reference/ambient temperature [ $T_{Ref} = 25^{\circ}C$ ]	$T_{max-cycling}$	Maximum temperature on the board during the SD's cycling phase ( $^{\circ}C$ )
$\Pi_{Thermo-electrical}$	Thermo-electrical acceleration factor indicating thermal and electrical stress sensitivity on the capacitor during operation.	$RH_{amb}$	Ambient relative humidity
$\Pi_{TCy}$	Thermal cycling acceleration factor indicating thermal cycling stress sensitivity on the capacitor during operation.	$P_A, P_{IGBT}^{Cond}, P_{IGBT}^{SW}$	Total power losses, conduction losses, and switching losses in the SD
$\Pi_{Mech,Cap}$	Mechanical acceleration factor indicating mechanical stress sensitivity on the capacitor during operation.	$R_{th,hs}, R_{th}^{IGBT}$	Thermal resistance of heat sink, thermal resistance of SD (assume = 1.72 W/K)

$\gamma_{TH-EL}$	Thermo-electrical stress sensitivity factor of the Cap [ $\gamma_{TH-EL} = 0.69$ ]	$v_{ce0}$	Collector-emitter voltage [(@150°C, $T_j$ ) and (@20A, $i_c$ ) = 0.82V]
$\gamma_{TCY}$	Thermal cycling stress sensitivity factor of the Cap [ $\gamma_{TCY} = 0.26$ ]	$R_{on,S}$	On-state resistance of IGBT [(@150°C, $T_j$ ) and (@20A, $i_c$ ) = 0.051Ω]
$\gamma_{Mech}$	Mechanical stress sensitivity factor of the Cap [ $\gamma_{Mech} = 0.05$ ]	$i_{c,SD}, I_{ref}, V_{ref}$	IGBT collector current, reference/nominal current, reference/nominal voltage
$S_{ref}$	Reference level of electrical stress on the Cap [= 0.3]	$E_{sw}$	Total switching energy losses of IGBT
$E_a$	Activation energy of capacitor material [assume value for ceramic material (= 0.122 eV)]	$E_{sw,ref}$	Reference switching energy losses of IGBT (assume = $0.625 \times 10^{-3} J$ )
$K_b$	Boltzmann constant (= $8.617 \times 10^{-5} eV$ )	$K_i, K_v, TC_{sw}$	Exponent modelling current dependency (= 0.729), exponent modelling voltage dependency (= 1.3), temperature coefficient of switching losses (= 0.003)
$V_{applied}$	Operation voltage	$T_{j,SD,max}$	Maximum temperature constrained within the model (= 125°C)
$V_{rated}$	Rated blocking voltage of Cap, nominal blocking voltage of SD (= 650V)	$k_{hs}, t_{b,hs}$	Thermal conductivity of the heat sink (assuming aluminum = 160), heat sink base thickness
$N_{cy}$	Number of cycles associated with each cycling phase of Cap (cycles) [= 730]	$A_{hs}, A_{hs,SD,max}$	Surface area of heatsink, maximum heat sink size (can assume different constraint values) (= $100 \times 10^{-3} \times 100 \times 10^{-3}$ )
$\theta_{cy}$	Cycle duration of Cap (hours) [ $\theta_{cy} = t_{phase}/N_{cy}$ ]	$k_{bw,SD}$	Thermal conductivity of bond wire (assuming Cu) (= 390)
$\Delta T_{cycling,Cap}$	Amplitude of temperature variation associated with the Cap's cycling phase (°C)	$\rho_{bw,SD}$	Resistivity of bond wire (assuming Cu) (= $1.68 \times 10^{-8}$ )
$T_{max-cycling,Cap}$	Influence of the Cap's maximum temperature on the board during a cycling phase (°C)	$D_{bw,SD}$	Diameter of bond wire of SD
$I_{rip}, I_{rip,max}$	Percent ripple current in the application, maximum allowed ripple current percent (=50%)	$l_{bw,SD}$	Length of bond wire of SD (= $1.7 * 10^{-3}$ )
$ESR$	Equivalent series resistance of Cap	$\Delta T_{bw,SD}$	Temperature variation between two ends of bond wire of SD (assume constant) = 1.1°C
$R_{th}^{Cap}$	Thermal resistance of Cap	$Der, Der_{max}$	Voltage and current deration, maximum deration (assume 0.8)

$R_0$	Approximate constant ohmic resistance of Cap ( $R_0 = 0.01 \Omega$ )	$Space_{pcb}$	Space available on PCB for mounting components [assume $Space_{max} = 20 \cdot (64.3 \times 105.7) mm^2$ ]
$R_d$	Frequency dependent resistance of Cap	$Cost_{comp}$	Cost of components [assume $Cost_{max} = \$500/\$750$ ]
$R_e$	Temperature dependent resistance of Cap	$N_{cap}$	Number of capacitors in total including redundant Caps
$D_{ox}$	Dissipation factor of the Cap's dielectric (assume 0.015)	$N_{SD}$	Number of SD in total including redundant Caps
$f_{sw}$	Switching frequency in application	$AR$	Aspect ratio constraint [ $AR = L_{cap}/D_{cap}$ ]
$C$	Capacitance of Cap [ $C = 7.312 mF$ ]	$\lambda_{tot}$	Total failure rate considering only SDs or Caps and assuming parallel redundancy configuration
$R_{e0}$	Temperature dependent resistance of Cap at room temperature (assume $= 0.5\Omega$ )	$R(T), R, N$	Total reliability in a given period, T(assume $T = t_{phase}$ ), reliability of a single component, number of components
$T_{c,cap}, T_{s,cap}$	Core temperature of Cap, surface temperature of Cap (assume maximum model value $= 125^\circ C$ )	$R_{cap}, R_{SD}$	Reliability of a single Cap, reliability of a single SD
$A_{cap}$	Surface area of Cap	$L_0$	Useful lifetime of the capacitor at nominal conditions (hrs) (assume 1)
$K_T$	Temperature factor (ambient temperature) / model of lifetime on temperature	$K_R$	Ripple current factor (self-heating) / model of lifetime on ripple current
$K_V$	Voltage factor (operating voltage) / model of lifetime on voltage	$K_i$	Empirical safety factor (assuming maximum core temperature) [ $K_i = 4$ ]
$DuCy$	Duty cycle of application [= 0.585]	$n$	Exponent for non-linearity of deration $0.8 \leq \frac{V_{applied}}{V_{rated}} \leq 1 \rightarrow n = 5$
$N_f$	Number of cycles to failure of the IGBT (calculated)	$A, \beta_1 - \beta_6$	Base number of cycles to failure of the IGBT (assume $= 2.8 \times 10^4$ ), lifetime model constants [ $\beta = (-3.483, 1917, -0.438, -0.717, -0.751, -0.564)$ ]
$T_{j-IGBT}, \Delta T_j, T_a$	SD's mean junction temperature, junction temperature swing (assume constant $= 1.1$ ), and ambient temperature ( $= 25^\circ C$ )	$t_{on}$	On-time of IGBT ( $= t_{phase}$ ) duration of the operation and maintenance phase [assume a 72-hr operation ( $t_{phase} = 72hrs$ )]
$I_{C,SD}$	IGBT collector current		

## CHAPTER 1

### INTRODUCTION

The consumption of electricity in the whole world does nothing but increase with the years, and the fact that we need to find a balance between energy generation and energy consumption while trying to keep greenhouse gas emissions as low as possible is a challenge that we are going to face for the next decades.

The harsh truth is that about 60% of electricity production depends mainly on burning fossil fuels like coal and natural gas, with significant greenhouse gas emissions and irreversible fossil fuel depletion. Fig. 1.1 from [3] depicts the annual global  $CO_2$  emission from fossil fuels. These are some reasons why renewable energy is becoming an obvious solution to traditional non-renewable energy, offering more reliable, eco-friendly, and economically viable energy sources. However, connecting renewable energy power systems to the grid is a highly challenging task, which might impose challenges related to power quality and stability control [2].

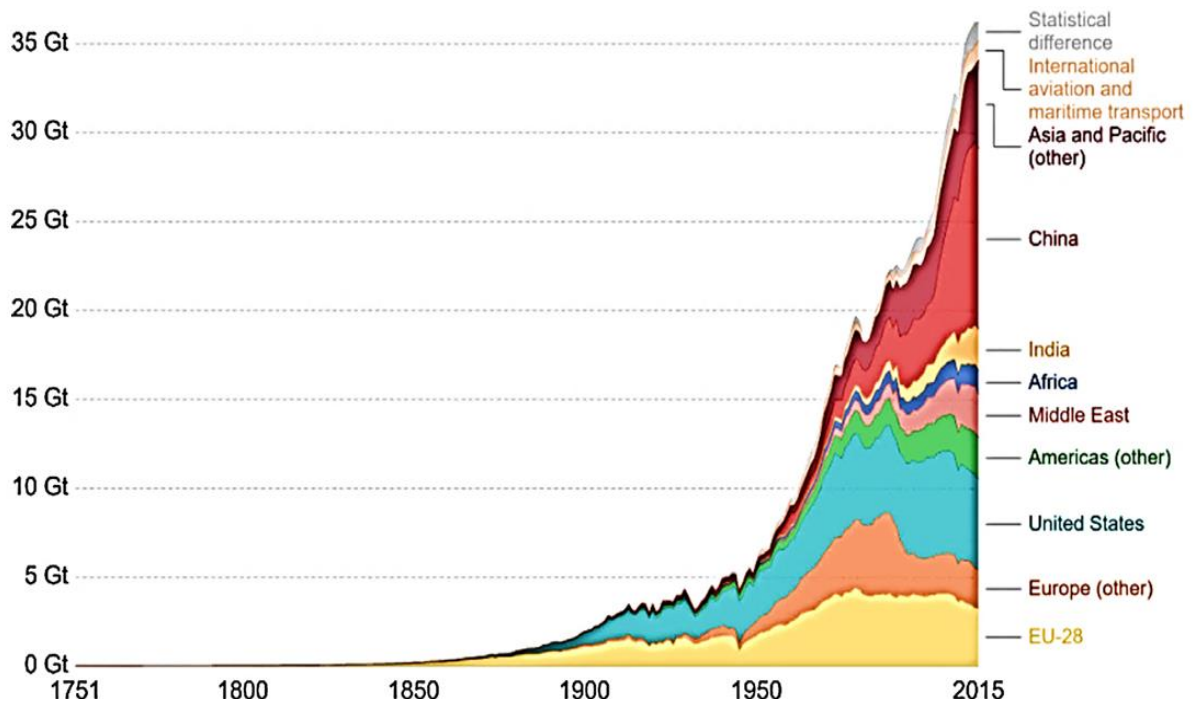


Fig. 1.1: Annual  $CO_2$  emissions from fossil fuel by world region estimate in gigatons  $CO_2$  per year ( $GtCO_2$ ) [3].

Studies were made on the control aspect of renewable energy integration into the grid. [4], [5], [6], [7], [8], [9], and [10] elaborate on the control robustness aspect, while focusing on the importance of this characteristic when integrating renewables into the energy grid. The integration of renewables into the grid was also considered from an adaptive controlling perspective, with studies such as [11] and [12]. In addition to the previously mentioned controllers, other controllers were analyzed, such as unmatching impedances grids controllers such as [13], unbalanced grids controllers such as [14], modernized grid controllers such [15] and [16], three-phase Z-source inverters such as [17], and islanded modern microgrids such as [18].

One crucial technology that makes it easier to include renewables into the grid is the implementation of power electronic converters. Power electronic technologies offer high reliability and renewable energy conversion efficiency, thus contributing to energy conservation, improving energy efficiency, and helping mitigate harmful global emissions. This is why they are considered one of the main solution to tackle carbon emission and global warming problems [3]. Multiple studies have analyzed renewable energy applications, especially for solar and wind energy, as shown in [19], [20], [21], and [22]. Furthermore, different topologies such as [23], [24], and [25] were analyzed with different purposes such as stabilization, robustness, adaptability, and grid integration.

However, a converter's topology will change depending on its applications, and its performance will be strongly related to its reliability. Reliability means that maintenance costs are reduced, and the power distribution is safer. Therefore, finding the most reliable converter is important nowadays, as choosing the correct parameters for designing a converter can significantly improve its lifetime and performance.

## 1.1 PURPOSE OF STUDY

In recent years, multiple attempts have been made to accurately model converters' reliability to improve this reliability afterward. Power converters are key in power systems, and their failure affects the whole system, translating into shortages in power, supply and the extra cost of maintenance. Therefore, this research aims to provide a clear and concise model of the behavior of power converters based on their two main components which are the most prone to failure: the switching device and the capacitor. Once this model is created, different optimization algorithms

such as Harris Hawk Optimization, Particle Swarm Optimization, and Artificial Bee Colony Optimization will be used to find the optimal parameters for the design of a converter. This optimization in the design will increase the converter's reliability, increasing the power system's overall reliability.

## 1.2 CONTRIBUTION

The main contribution of this study is the reliability modeling of a power converter in a power system, sub-system, and component level in terms of the two components that are more prone to failure: the capacitor and the switching device. In addition, the reliability of the converter will be analyzed and improved based on the parameters that are considered variable, related to the voltage, current, frequency, and sizes of the different parts of the power electronic converter.

## CHAPTER 2

### LITERATURE REVIEWS

Reliability is a crucial characteristic in every type of system. It is defined as the quality of being consistent in performing a certain function over a specific period of time. When talking more specifically about power systems, reliability refers to the ability of the system to continuously provide consumers with electricity, especially during harsh conditions where its components are prone to failure.

A reliable system is a predictable system, and predictability is the key to its correct functioning. This is even more true in power systems, where a failure in any system level could cause a failure in the whole system. Because of this, it is important to estimate the reliability of the system at each of its levels.

The concept of reliability analysis consists of estimating a system's reliability by studying the behavior of each component that forms it. In other words, the main objective when analyzing the reliability of a system as a whole is to use the knowledge of the reliabilities of individual components and how these components interact to investigate the reliability of the system that the components constitute [1].

A well-known alternative method to analyze a system's reliability is the Monte Carlo simulation, which can estimate the damage the converters experience over the years. Different studies have been conducted on the application of the Monte Carlo simulation method in power converters, such as [26], [27], and [28].

Monte Carlo simulation consists of imitating the stochastic behavior of a physical system. In general, Monte Carlo simulation methods can be used to imitate any system that exhibits any form of random behavior. In the context of reliability evaluation, Monte Carlo simulation is used to determine how random failures of the system's components affect its reliability [1].

#### 2.1 RELIABILITY IN POWER SYSTEMS

Estimating a power system's reliability is crucial to our society, as many aspects of it, such as the economy, health, quality of life, and several other sectors, depend on it. Power converters are

one of the elements on which a power system depends the most when it comes to reliability. Over the years, multiple attempts have been made to determine how reliable these components are and to try to estimate their lifetime and performance over time.

On the converter level, the reliability model of a power electronic converter is developed based on the power electronic devices that the converter is composed of, for which various hourly-based input profiles and converter topologies are considered. The analysis on a component level aims to determine the failure rate that a converter exhibits in the useful time phase.

On the system level, a non-sequential Monte-Carlo simulation estimates reliability metrics such as expected energy not served (EENS) and loss of load expectation (LOLE). Machine regression models, such as support vector regression (SVR) and random forests (RF), are implemented to bridge the nonlinear reliability relationship between two levels [29]. The analysis can also be done at a subsystem level, where the capacitor's lifetime and cycles to failure of the switching device could be determined, focusing on the wear-out phase of the converter.

Many mathematical models have been developed through the years to model the reliability of power converters, and these varieties of models mainly differ in the topologies and variables considered to model the converters. The main variables that need to be considered when modeling a power electronic converter are related to the capacitor's characteristics and the switching device of power converters because these components are highly prone to failure.

The different characteristics of these main components of the converters will make the converter's lifetime longer or shorter, depending on how carefully their values are picked. Once the most effective values are chosen, the manufacturers can design these converters that theoretically have a longer lifetime and better performance.

Fig. 2.1 depicts the aforementioned useful lifetime phase of the converter, where the failure rates of the capacitor and switching device are analyzed, as well as the wear-out phase, where the lifetime of the capacitor and the cycles to failure of the switching device are analyzed.

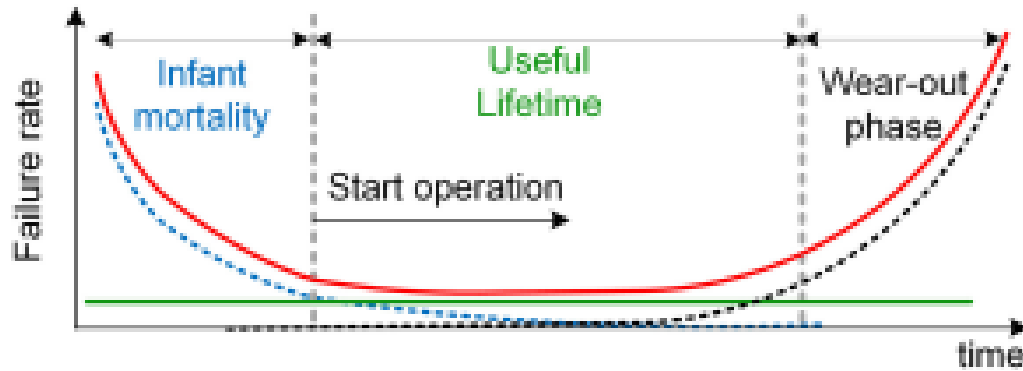


Fig. 2.1: Typical bathtub curve describing failure rate of an item [30].

## 2.2 POWER ELECTRONICS IN POWER SYSTEMS

According to the International Renewable Energy Agency (IRENA), renewable technology is the main pathway to reach zero carbon dioxide ( $CO_2$ ) emissions by 2060. Power electronics have played and will continue to play a significant role in this transition by providing efficient electrical energy conversion, distribution, transmission, and utilization [31]. However, implementing converters will add challenges in terms of the control and stability of the system, which need to be overcome to ensure that the energy supplied is enough to satisfy the demand.

Power electronic converters have four main categories: AC to DC converters, DC to DC converters, DC to AC converters, and AC to AC converters. In addition, some categories, such as AC to DC converters and AC to AC converters, have further classifications. The half-bridge converter will be the type of converter analyzed for this work, and one of the most novel converters is presented in [32], which uses two half-bridge DC-AC converters in parallel to reduce the number of switches used. This converter topology is illustrated in Fig. 2.2, and it will be like the one used for this work, with the difference that the number of switches and capacitors is a variable to be optimized by the optimizing algorithms to increase the converter's reliability.

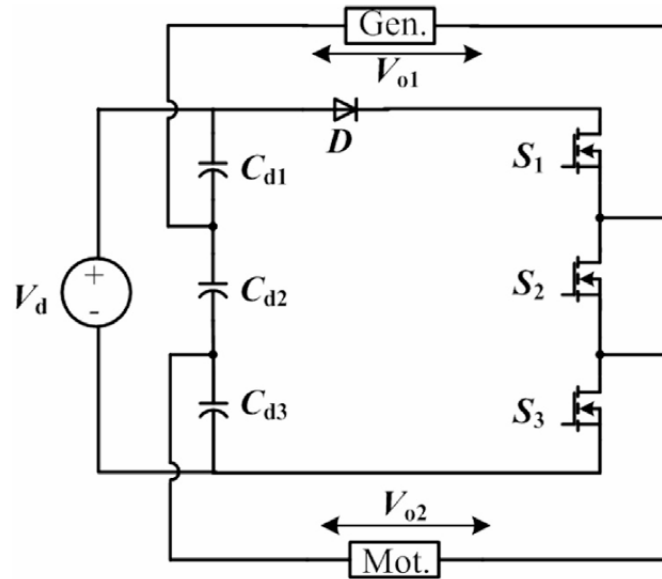


Fig. 2.2: A dual-output half-bridge converter with three switches [32].

### 2.2.1 AC TO DC CONVERTERS

AC-to-DC converters convert an AC input signal into a DC output signal. These types of converters are also known as rectifiers, and there are two main types in the industry: diode rectifiers and phase controller rectifiers.

Diode rectifiers represent a compact, lightweight superconducting conversion chain that can significantly reduce the carbon footprint in critical sectors [33]. These rectifiers can rectify a variable AC input signal into a stable, fixed output DC signal. Some examples of diode rectifiers are developed in [34], [35], and [36], with applications in wireless power transfer, RF energy harvesting, and power distribution.

On the other hand, phase-controlled rectifiers convert a fixed AC input signal into a variable output DC signal. In works like [37], this technology uses the existing variable DC bus voltage control strategy based on a two-level AC/DC converter rather than the traditional fixed DC bus control.

### 2.2.2 DC TO DC CONVERTERS

DC-to-DC converters convert a DC input signal into a DC output signal. These converters, also known as choppers, use semiconductors such as power transistors to control the output with a very low-power signal.

DC-to-DC converters are widely used in applications such as electric vehicles, electronic devices such as phones and laptops, and renewable energy. These converters can be either step-up DC to DC converters, also known as boost converters, or step-down DC to DC converters, also known as buck converters. Studies such as [38] are a great example of the utilization of DC-DC converters to enhance the charging speed of an electric car. On the other hand, applications such as [39] show how DC-DC converters are helpful when implementing wind turbines into the DC grid, which seems to have advantages such as reactive power harmonics. Furthermore, DC-DC converters are essential in HVDC (High voltage direct current) networks, where they interconnect two different types (LCC (line commutated converter) / VSC (voltage source converter)) of the network, with examples such as [40] and [41].

### 2.2.3 AC TO AC CONVERTERS

AC-to-AC converters convert an AC input signal with fixed frequency into an AC output signal with variable voltage. They are classified into two main types: cycloconverters and AC voltage controllers.

Cycloconverters are power electronic devices that produce adjustable voltage and frequency AC power from a constant voltage constant frequency AC source without any DC link. Cycloconverters produce significant harmonics and non-standard frequency components in their output voltage that will depend on their structure [42]. Therefore, different structures could be implemented with other purposes, ranging from hybrid cycloconverters [43] to high-frequency cycloconverters [44] and cycloconverters to control the power quality of the grid [45].

On the other hand, AC voltage regulators function by changing the input AC signal with fixed voltage into an output AC signal with variable voltage and the same frequency as the input. The topology of AC voltage regulators could vary, depending on the application of the converter. Studies such as [46] have developed a topology for an AC voltage regulator with a high-frequency link. In contrast, studies such as [47] and [48] explored the efficiency improvement that could be

done to an AC voltage regulator.

#### 2.2.4 DC TO AC CONVERTERS

DC to AC converters are the type of converters that convert a DC input signal to an AC output signal. These converters are also known as inverters and are crucial in sectors such as power transmission and distribution. In addition, due to the global energy challenge, grid-tied inverters for renewable energy sources are becoming widely used nowadays [49]. In this case, DC-AC converters will be essential to be able to produce a larger-scale integration of wind and photovoltaic power. Studies such as [50] and [51] explore the challenges of integrating wind power into the grid. In contrast, study [52] examines the same difficulties regarding integrating photovoltaic power into the grid.

### 2.3 POWER CONVERTER'S ROLE IN MODERNIZED POWER SYSTEMS

The energy system is undergoing significant changes due to the decentralization of power generation. These changes have, as a consequence, the replacement of large synchronous generators by the implementation of more power electronics converters. However, introducing power converters into the grid can create harmonics/stability issues that increase the loading stresses of power electronic components systems, accelerate the wear out, or even induce catastrophic failure. Wear out or failure of power electronic components alternate the electrical parameters or the system architecture, which is undesirable because it may cause new harmonic/stability issues.

In addition, introducing converters in the power systems industry affects power generation, transmission, and distribution. On the generation side, the introduction of converter-interfaced generators has features such as intermittent input resources and small unit sizes with low or synthetic inertia, replacing the traditional approach used with synchronous generators. When talking about transmission, the increasing implementation of FACTS and HVDC converters has enhanced power transmission by providing flexibility in controlling power network parameters, having the only downside of new control and stability challenges. Regarding the distribution level, small-scale converter-interfaced generators, electric vehicles, and inverter-based battery energy

storage systems have significantly complicated the distribution and utilization systems [53].

## 2.4 POWER CONVERTER'S RELIABILITY ANALYSIS

Depending on the level of interest of the study, the reliability analysis could relate to the individual performance of the device, converter, or power systems in terms of lifetime, availability, probability of failure, LOLE, security, and so on. The standard performance measure of a power system in terms of LOLE is that it doesn't exceed 4-8 hours/year.

Articles such as [54] present a device-level and converter-level analysis of converter failure rates according to physics. Therefore, once the weaknesses of the converters are found in terms of the design, planning, operation, and maintenance of these power electronic converters, an optimal decision-making process needs to be done. Moreover, these modeling systems for the reliability analysis of power converters must consider how this random chance of failure and the wear-out failures on power systems can affect their performance.

Moreover, reliability has become a crucial topic in applications such as continuous power delivery, low-frequency maintenance, and applications with high safety requirements. The challenges faced in the design of converters for these applications are related to the reliability of the overall system once these converters are implemented. In many cases, the power electronic converters do not have redundant systems in place, which means that a fault in a device, component, or subsystem level can cause the entire system to fail [55].

A failure in the entire system would increase the cost of repairing, which leads to the conclusion that the system must be designed while considering the reliability of each one of the parts that form that system so that when they are assembled, the overall reliability of the system could be determined by analyzing how these parts interact. This approach will help avoid unexpected system failures that will cause undesired results related to safety and maintenance. Fig. 2.3 depicts a general overview of the different aspects of reliability that need to be considered when optimizing the reliability improvement of a system.



Fig. 2.3: General overview and interconnection of overall reliability-related topics [55].

## 2.5 METAHEURISTIC OPTIMIZATION METHODS

Nowadays, many decisions are machine-learning decisions, processing large amounts of data to make accurate decisions. However, the data size increases with the years, and this is where many machine-learning-based decisions have a weakness. Despite the struggles of increasing the amount of data, many artificial intelligence approaches succeeded in the lifetime estimation of power electronics such as PV systems [63]. Moreover, algorithms such as the interior-point algorithms were proposed to control modernized microgrids [64].

The rapid increase in data volume and feature dimensionality negatively influences machine learning and many other fields, such as decreasing classification accuracy and increasing computational cost [65]. Therefore, applying older but reliable methods, such as the well-known

metaheuristic optimization algorithms, is beneficial in many scenarios. These algorithms work great when the objective is to find approximate solutions to optimization problems, especially when the problem to be optimized is a nonlinear problem, which is the case with power electronic converters.

As seen in Fig. 2.4, metaheuristic optimization methods are divided into multiple categories, such as physics-based optimization algorithms, swarm-based optimization algorithms, human-based optimization algorithms, and evolutionary optimization algorithms.

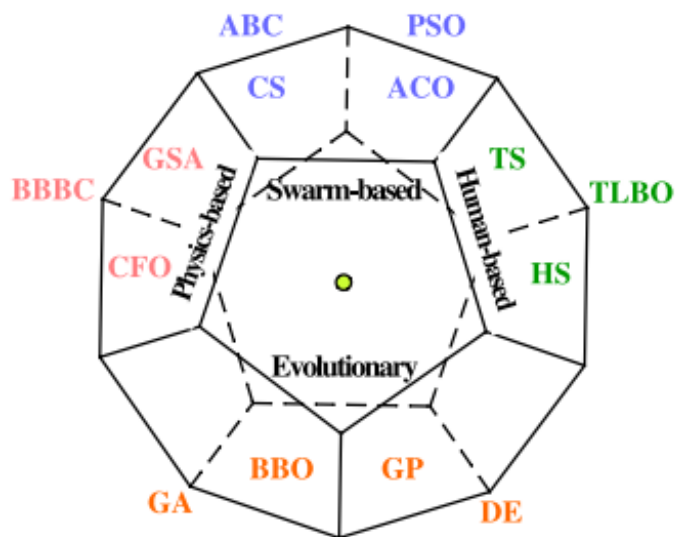


Fig. 2.4: Classification of meta-heuristic techniques (meta-heuristic diamond) [62].

This study will focus on swarm-based optimization algorithms, which are inspired by natural processes such as swarm behavior. The main types of swarm optimization are Particle swarm optimization, ant colony optimization, and artificial bee colony optimization. In addition to the previously mentioned algorithms, a recently developed swarm-based algorithm called the Harris Hawk optimization algorithm, a gradient-free optimization algorithm tested with excellent results in non-linear optimization problems, has been created.

All swarm-based optimization algorithms have the characteristic of having a certain number of particles, also called a population, in charge of searching for an optimum solution in a defined search space. This search space will be determined by the constraints provided by the user, and in

there, the particles will interact with each other, influencing their positions and their neighbors' positions, to collectively find the best solution possible.

Fig. 2.5 depicts the traditional functioning of swarm intelligence algorithms when searching for an optimum solution.

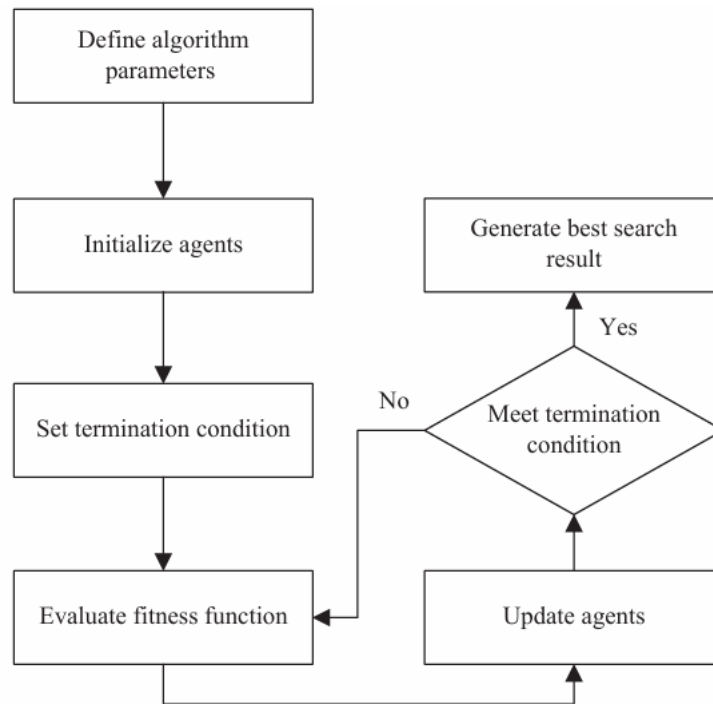


Fig. 2.5: General framework of the swarm intelligence algorithms [94].

## CHAPTER 3

### RELIABILITY MODELING

Reliability modeling can be done at each of the three levels presented in a system. The first level is the power system level, governed by system reliability indices and indicators such as LOLE, EENS, and LOLP. The second level for analyzing a system is the subsystem level, where availability modeling is done to predict the failure probability and failure rate ( $F$ ,  $\lambda$ ,  $\Pi$ ). The third level is the component level, where wear-out modeling is executed to find lifetime indicators ( $N_f$ ,  $L_0$ ).

Fig. 3.1 from [54] depicts the different levels explained and their correlation.

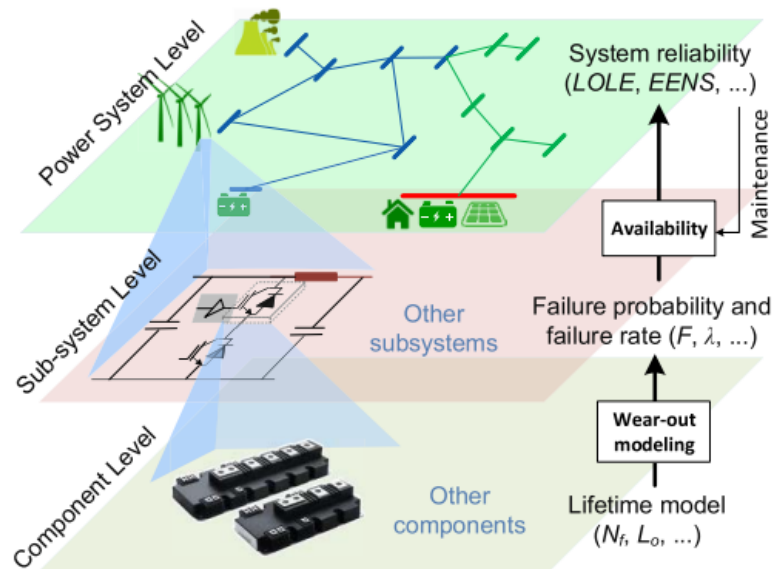


Fig. 3.1: Correlation between PE and power system reliability concepts [54].

### 3.1. POWER SYSTEM LEVEL RELIABILITY MODELING

Power system reliability modeling is a crucial aspect of ensuring the correct operation of the system without interruptions. The power system level reliability has three widely used reliability indicators: LOLP, LOLE, and EENS. In addition, various alternative standard test systems for modern power system analysis are proposed in [56].

### 3.1.1. LOSS OF LOAD PROBABILITY (LOLP)

The LOLP is a fundamental index in power systems, especially regarding reliability. This index refers to the Loss of Load Probability, and it quantifies the likelihood that the current power supply will not be enough to meet the demands at a given time, which, in other words, could be defined as a shortage of power supply for the market. The LOLP is defined by [57] as a sum of all mathematical expectations for all units defined in Eq. (1).

$$LOLP = \sum_{i=1}^n p_i \cdot t_i \quad (1)$$

where  $p_i$  is the probability of loss of capacity and  $t_i$  is the duration of loss of capacity in percent.

### 3.1.2. LOSS OF LOAD EXPECTATION (LOLE)

The LOLE is a probabilistic index used in power system applications for more than 70 years and is one of the most well-known ways to measure a system's shortage risk. This index refers to the likelihood that consumption  $L$  would not surpass the operating power capability  $C$ , where  $p_i$  is the individual likelihood of capability in an outage, as defined in Eq. (2), described by [58].

$$LOLE = \sum_{i=1}^n p_i \cdot (c_i - L_{i-1}) \quad (2)$$

### 3.1.3. EXPECTED ENERGY THAT IS NOT SUPPLIED (EENS)

The EENS indicator is also one of the crucial indicators used at the power system level to indicate the amount of energy demand that is not matched by the sufficient electricity supply. This indicator is very important to ensure the constant and reliable functioning of a power system, as well as to perform economic analysis and system planning. The classical numerical method to calculate the EENS is shown in Eq. (3).

$$EENS = \sum_{i=1}^n P_i \cdot E_i \quad (3)$$

where  $P_i$  shows the load loss and  $E_i$  shows the curtailed energy.

More advanced EENS algorithms are proposed in [59] and [60], where this indicator is calculated while considering the total average active loads of transformer substations disconnected after the fault for the service time. This modified algorithm to approach the calculation of the EENS allows for reducing the ENNS in an MV distribution system by placing sectionalizers strategically in the power lines.

### 3.2. SUB-SYSTEM LEVEL RELIABILITY MODELING

The sub-system and component level reliability modeling were developed using the FIDES Guide 2022 for Reliability Methodology for electronic systems [61]. The sub-system level reliability modeling is assessed by targeting the formulation of rates, such as  $F$  and  $\lambda$  (failure rates) and  $\Pi$  (stress coefficients), that will determine the overall reliability on a sub-system level, modeling the behavior of a converter regarding its useful lifetime phase. The general aim of the modeling at a sub-system level is to develop an equation that describes the total failure rate of the system, defined in Eq. (4).

$$\lambda_{tot} = \frac{-\frac{\delta}{\delta t}R(T)}{R(T)} \quad (4)$$

where  $R(T)$  is the reliability of a single converter, defined in Eq. (5).

$$R(T) = 1 - [1 - R]^N \quad (5)$$

where  $R$  corresponds to the  $R_{SD}$  (individual reliability of the switching device) and  $R_{Cap}$  (individual reliability of the capacitor), defined in Eq. (6) and Eq. (7), respectively. In addition,  $N$  is the number of switching devices ( $N_{SD}$ ) and capacitors ( $N_C$ ) used in the converter.

$$R_{SD} = e^{-\lambda_{SD}(T)} \quad (6)$$

$$R_{Cap} = e^{-\lambda_{cap}(T)} \quad (7)$$

Eq. (8) and Eq. (9) both model the reliability of the switching device and capacitor, respectively, by using  $\lambda_{SD}$  (switching device useful failure rate) and  $\lambda_{Cap}$  (capacitor useful failure rate). These two coefficients model the random phase of the bathtub curve modeled in Fig. 2.1, considering only the operational and maintenance phases.

As  $\lambda_{Cap}$  and  $\lambda_{SD}$  model the failure rate of the capacitor and switching device, they must be minimized to increase the reliability of the power converter. However, the model these two coefficients must be created for the minimization objective.

The failure rate of the capacitor  $\lambda_{Cap}$  depends on the contribution of physical stresses on the capacitor ( $\lambda_{physical-cap}$ ), the quality and technical control that goes into the capacitor manufacturing ( $\Pi_{PM}$ ), and the quality and technical control of the development, manufacturing, and operating processes of the converter as a system ( $\Pi_{Process}$ ), as defined by Eq. (8).

$$\lambda_{Cap} = \lambda_{physical-cap} * \Pi_{PM} * \Pi_{Process} \quad (8)$$

On the other hand, the failure rate of the switching device  $\lambda_{SD}$  depends on the contribution of physical stresses on the switching device ( $\lambda_{physical-SD}$ ), the acceleration factor related to the impact of the component's development ( $\Pi_{PW}$ ), the quality and technical control that goes in the switching device manufacturing ( $\Pi_{PM}$ ), and the quality and technical control of the development, manufacturing, and operating processes of the converter as system ( $\Pi_{Process}$ ), as defined by Eq. (9).

$$\lambda_{SD} = \lambda_{physical-SD} * \Pi_{PW} * \Pi_{PM} * \Pi_{Process} \quad (9)$$

The contribution of physical stresses on the capacitor ( $\lambda_{physical-cap}$ ) and physical stresses on the switching device ( $\lambda_{physical-SD}$ ) are modeled in Eq. (10) and Eq. (11), while the rest of the variables related to quality and control are modeled in Eq. (12), Eq. (13), and Eq. (14).

$$\lambda_{Physical-Cap} = \lambda_{0Cap} \left[ \left( \frac{t_{phase}}{T_{total}} \right) (\Pi_{Thermo-electrical} + \Pi_{TCy} + \Pi_{Mech,Cap}) \Pi_{Induced} \right] \quad (10)$$

$$\lambda_{Physical-SD} = \left( \frac{t_{phase}}{T_{total}} \right) \left( \lambda_{0TH} \Pi_{TH} + \lambda_{0TCyCase} \Pi_{TCyCase} + \lambda_{0RH} \Pi_{RH} + \lambda_{0TCySolderjoints} \Pi_{TCySolderjoints} + \lambda_{Mech} \Pi_{Mech,SD} \right) (\Pi_{Induced}) \quad (11)$$

$$\Pi_{PM} = e^{\delta_1(1-PartGrade)-\alpha_1} \quad (12)$$

$$\Pi_{PW} = e^{\delta(1-Process_Grade)-\alpha} \quad (13)$$

$$\Pi_{Process} = e^{\delta_2(1-Process_Grade)} \quad (14)$$

Eq. (12), Eq. (13), and Eq. (14) are calculated using constant values provided in the Table of Symbols, where  $\delta_1$  and  $\delta_2$  are correlating factors that determine the size of the impact of  $\Pi_{PM}$  on reliability,  $\delta_2$  is the correlating factor that determines the range of variation of  $\Pi_{Process}$ ,  $\alpha$  and  $\delta$  are correlating factors that determine the size of the impact of  $\Pi_{PW}$  on reliability, *PartGrade* is the estimation from the audit indicating the buyer's past experience, and *Process\_Grade* is the estimation from an audit indicating how the factors influencing the design rules for the components are managed.

Meanwhile, Eq. (10) and Eq. (11) need some other equations to be developed. For the contribution of physical stresses on the capacitor ( $\lambda_{physical-cap}$ ) in Eq. (10),  $\lambda_{0Cap}$  corresponds to the basic failure rate of the capacitor,  $t_{phase}$  refers to the duration of the operation and maintenance phase,  $T_{total}$  refers to the reference duration in a year,  $\Pi_{Thermo-electrical}$  refers to the thermo-electrical acceleration factor indicating thermal and electrical stress sensitivity on the capacitor during operation,  $\Pi_{TCy}$  is the thermal cycling acceleration factor indicating thermal cycling stress sensitivity on the capacitor during operation,  $\Pi_{Mech,Cap}$  refers to the mechanical acceleration factor indicating mechanical stress sensitivity on the capacitor during operation, and  $\Pi_{Induced}$  refers to the contribution of the induced/overstress factors inherent to a particular field of application.

Some of the afore mentioned variables' equations are developed below, while some are assumed constant (refer to Table of Symbols).

$$\Pi_{Thermo-electrical} = \gamma_{TH-EL} \left( \frac{1}{S_{ref}} \cdot \frac{V_{applied}}{V_{rated}} \right)^3 \cdot e^{\frac{E_a}{K_b} \left[ \frac{1}{293} - \frac{1}{T_{amb}+273} \right]} \quad (15)$$

$$\Pi_{TCy} = \gamma_{TCy} \left( \frac{12 \times N_{cy}}{t_{phase}} \right) \cdot \left( \frac{\min(\theta_{cy}, 2)}{2} \right)^{\frac{1}{3}} \cdot \left( \frac{\Delta T_{cycling, Cap}}{20} \right)^{1.9} \cdot e^{\frac{E_a}{K_b} \left[ \frac{1}{313} - \frac{1}{T_{max-cycling, Cap} + 273} \right]} \quad (16)$$

$$\Pi_{Mech, Cap} = \gamma_{Mech} \times \left( \frac{G_{RMS, Cap}}{0.5} \right)^{1.5} \quad (17)$$

$$\Pi_{Induced} = \left( \Pi_{Placement} \times \Pi_{Application} \times \Pi_{Ruggedizing} \right)^{0.511 \ln(C_{sens})} \quad (18)$$

$$\Pi_{TH} = e^{11604 \times 0.7 \left( \frac{1}{T_{Ref} + 273} - \frac{1}{T_{j-IGBT} + 273} \right)} \quad (19)$$

$$\Pi_{TCyCase} = \left( \frac{12 \times N_{cy}}{t_{phase}} \right) \times \left( \frac{\Delta T_{cycling, SD}}{20} \right)^4 \times e^{\frac{E_a}{K_b} \left( \frac{1}{313} - \frac{1}{T_{max-cycling} + 273} \right)} \quad (20)$$

$$\Pi_{TCySolderjoints} = \left( \frac{12 \times N_{cy}}{t_{phase}} \right) \times \left( \frac{\min(\theta_{cy}, 2)}{2} \right)^{\frac{1}{3}} \times \left( \frac{\Delta T_{cycling, Cap}}{20} \right)^{1.9} \times e^{\frac{E_a}{K_b} \left( \frac{1}{313} - \frac{1}{T_{max-cycling} + 273} \right)} \quad (21)$$

$$\Pi_{Mech, SD} = \left( \frac{G_{RMS, SD}}{0.5} \right)^{1.5} \quad (22)$$

From Eq. (15),  $\gamma_{TH-EL}$  is the thermo-electrical acceleration factor indicating thermal and electrical stress sensitivity on the capacitor during operation,  $S_{ref}$  is the reference level of electrical stress on the capacitor,  $V_{applied}$  is the operation voltage,  $V_{rated}$  is the blocking voltage of the capacitor and nominal voltage of the switching device,  $E_a$  is the activation energy of the capacitor material,  $K_b$  is the Boltzmann constant, and  $T_{amb}$  is the ambient temperature.

From Eq. (16),  $\gamma_{TCy}$  is the thermal cycling stress sensitivity factor of the capacitor,  $N_{cy}$  is the number of cycles associated with each cycling phase of the capacitor,  $\theta_{cy}$  is cycle duration of the capacitor in hours,  $\Delta T_{cycling, Cap}$  is the amplitude of temperature variation associated with the capacitor's cycling phase, and  $T_{max-cycling, Cap}$  is the influence of the capacitor's maximum temperature on the board during a cycling phase.

From Eq. (17) and Eq. (18),  $\gamma_{Mech}$  is the mechanical stress sensitivity factor of the capacitor,  $G_{RMS, Cap}$  is the stress associated with the capacitor's random vibration phase.  $\Pi_{Placement}$  is the influence of the capacitor's and switching device's functions in the system,  $\Pi_{Application}$  is the influence of the environment of use during application on the converter's reliability,  $\Pi_{Ruggedizing}$  is the influence of the policy of building overstress tolerance into the capacitor or switching device,

and  $C_{sens}$  is the overstress sensitivity coefficient inherent to the technology of the capacitor or switching device.

From Eq. (19), Eq. (20), Eq. (21) and Eq. (22),  $T_{ref}$  is the reference temperature,  $T_{j-IGBT}$  is the switching device's junction temperature during an operating phase,  $\Delta T_{cycling,SD}$  is the amplitude of temperature variation associated with the switching device's cycling phase,  $T_{max-cycling}$  is the maximum temperature on the board during the switching device's cycling phase, and  $G_{RMS,SD}$  is the stress associated with the switching device's random vibration phase.

The afore mentioned variables that don't correspond to constant values are defined by the next equations.

$$\Delta T_{cycling,Cap} = I_{rip}^2 \cdot ESR \cdot R_{th}^{Cap} \quad (23)$$

where,

$$I_{rip} = \frac{DuCy}{2R_0C f_{sw}} \quad (24)$$

$$R_d = \frac{D_{ox}}{2\pi f_{sw}C} \quad (25)$$

$$R_e = R_{e0} \cdot 2^{-\left(\frac{T_{s,Cap}-T_{Ref}}{40}\right)^{0.6}} \quad (26)$$

$$ESR = R_0 + R_d + R_e \quad (27)$$

$$h_{free} = 1.32 \times \left(\frac{T_{s,Cap}-T_{Ref}}{D_{Cap}}\right)^{0.25} \quad (28)$$

$$h_{rad} = \varepsilon \cdot \sigma \cdot (T_{s,Cap} + T_{Ref})(T_{s,Cap}^2 + T_{Ref}^2) \quad (29)$$

$$h_{tot} = h_{free} + h_{rad} \quad (30)$$

$$A_{Cap} = \frac{\pi}{4} \cdot D_{Cap} \cdot (D_{Cap} + 4L_{Cap}) \quad (31)$$

$$R_{th}^{Cap} = \frac{1}{h_{tot} \cdot A_{Cap}} \quad (32)$$

From Eq. (23),  $I_{rip}$  refers to the percent ripple current in the application,  $ESR$  refers to the equivalent series resistance of the capacitor,  $R_{th}^{Cap}$  refers to the thermal resistance of the capacitor,  $R_0$  refers to the approximate constant ohmic resistance of the capacitor,  $R_d$  refers to the frequency dependent resistance of the capacitor,  $R_e$  refers to the temperature dependent resistance of the capacitor,  $DuCy$  refers to the duty cycle of application,  $C$  refers to the capacitance of the capacitor,  $f_{sw}$  refers to the switching frequency in application,  $D_{ox}$  refers to the dissipation factor of the capacitor's dielectric,  $R_{e0}$  refers to the temperature dependent resistance of the capacitor at room temperature,  $T_{s,Cap}$  refers to the surface temperature of the capacitor,  $h_{tot}$  refers to the total heat transfer coefficient of the capacitor,  $h_{free}$  refers to the convection heat transfer coefficient of the capacitor,  $h_{rad}$  refers to the radiation heat transfer coefficient of the capacitor,  $A_{Cap}$  refers to the surface area of the capacitor,  $D_{Cap}$  refers to the diameter of the capacitor, and  $L_{Cap}$  refers to the length of the capacitor.

For the switching device's junction temperature during an operating phase,  $T_{j-IGBT}$ :

$$T_{j-IGBT} = P_A R_{th}^{IGBT} + T_{Ref} \quad (33)$$

where

$$E_{sw} = E_{sw,ref} \cdot \left(\frac{i_c}{I_{ref}}\right)^{K_i} \left(\frac{V_{applied}}{V_{ref}}\right)^{K_v} \left(1 + TC_{sw} \cdot (T_{j-IGBT} = T_{j,SD,max} - T_{amb})\right) \quad (34)$$

$$P_{IGBT}^{Cond} = v_{ce0} \cdot i_c + R_{on,S} \cdot i_c^2 \quad (35)$$

$$P_{IGBT}^{SW} = \frac{E_{sw} \cdot f_{sw}}{\pi} \cdot \frac{\sqrt{2} \cdot i_c}{I_{ref}} \cdot \frac{\sqrt{2} \cdot V_{applied}}{V_{ref}} \quad (36)$$

$$P_A = P_{IGBT}^{Cond} + P(t)_{IGBT}^{SW} \quad (37)$$

From Eq. (38),  $P_A$  refers to the total power losses,  $R_{th}^{IGBT}$  refers to the thermal resistance of the switching device,  $E_{sw}$  refers to the total switching energy losses of the IGBT,  $E_{sw,ref}$  refers to the reference switching energy losses of the IGBT,  $i_c$  refers to the IGBT collector current,  $I_{ref}$  refers

to the nominal current,  $TC_{sw}$  refers to the temperature coefficient of switching losses,  $P_{IGBT}^{Cond}$  refers to the conduction losses in the switching device,  $P_{IGBT}^{SW}$  refers to the switching losses in the switching device,  $v_{ce0}$  refers to the collector-emitter voltage, and  $R_{on,S}$  refers to the on-state resistance of the IGBT.

The last equations to describe the rest of the variables are Eq. (38), Eq. (39), Eq. (40), and Eq. (41).

$$T_{max-cycling,Cap} = T_{c,Cap} + \frac{\Delta T_{cycling,Cap}}{2} \quad (38)$$

$$\Pi_{Ruggedizing} = e^{0.7(1-Recom\_Grade)} \quad (39)$$

$$\Delta T_{cycling,SD} = 0.1977 - 2.0113 * T_{j-IGBT} + 2.01 * T_{max-cycling} \quad (40)$$

$$T_{max-cycling} = T_{j-IGBT} + 0.2801 \quad (41)$$

where *Recom\_Grade* refers to the weighted recommendation score assigned to the capacitor or switching device.

### 3.3. COMPONENT LEVEL RELIABILITY MODELING

The component level reliability modeling is done through wear-out modeling to find lifetime coefficients such as  $N_f$  and  $L_0$ , which will determine the overall reliability on a component level. The general aim of the modeling at a component level is to be able to develop an equation that describes the capacitor's lifetime in years ( $L_{Cap}$ ) and an equation that describes the IGBT's cycles to failure ( $N_{f,IGBT}$ ), defined by Eq. (42) and Eq. (43) respectively.

$$L_{Cap} = L_0 \times K_T \times K_R \times K_V \quad (42)$$

$$N_{f,IGBT} = A \cdot \Delta T_{j-IGBT}^{\beta_1} \cdot \exp\left(\frac{\beta_2}{T_{j-IGBT}+273}\right) t_{on}^{\beta_3} \cdot I_{C,SD}^{\beta_4} \cdot V_{applied}^{\beta_5} \cdot D_{bw}^{\beta_6} \quad (43)$$

where  $L_0$  refers to the useful lifetime of the capacitor at nominal conditions,  $K_T$  refers to the model of lifetime on temperature,  $K_R$  refers to the model of lifetime on ripple current,  $K_V$  refers to the model of lifetime on voltage,  $A$  refers to the base number of cycles to failure of the IGBT,  $\beta_1 - \beta_6$  refers to lifetime model constants,  $\Delta T_{j-IGBT}$  refers to the junction temperature swing,  $T_{j-IGBT}$  defined in Eq. (33) refers to the switching device's junction temperature during an operating phase,  $t_{on}$  refers to the on-time of the IGBT,  $I_{C-SD}$  refers to the IGBT collector current,  $V_{applied}$  refers to the operation voltage, and  $D_{bw}$  refers to the bond wire diameter.

The variables aforementioned are defined by Eq. (44), Eq. (45), and Eq. (46), while the rest of variables are assumed constant.

$$K_T = 2^{\frac{T_{c,Cap} - T_{amb}}{10}} \quad (44)$$

$$K_R = K_i^{[1 - I_{rip}^2]} \times \frac{\Delta T_{cycling,Cap}}{10} \quad (45)$$

$$K_V = \left( \frac{V_{applied}}{V_{rated}} \right)^{-n} \quad (46)$$

where  $T_{c,Cap}$  is the core temperature of the capacitor defined by Eq. (47),  $T_{amb}$  is the ambient temperature,  $K_i$  is the empirical safety factor,  $I_{rip}$  is the percent ripple current in the application defined by Eq. (24),  $\Delta T_{cycling,Cap}$  is the amplitude of temperature variation associated with the capacitor's cycling phase defined by Eq. (23),  $V_{applied}$  is the operation voltage, and  $V_{rated}$  is the rated blocking voltage of the capacitor.

$$T_{c,Cap} = \Delta T_{cycling,Cap} + T_{s,Cap} \quad (47)$$

where  $T_{s,Cap}$  is the surface temperature of the capacitor.

### 3.4. RELIABILITY ENHANCEMENT

Once a system's reliability modeling is developed at each one of the levels (component level, sub-system level, and power system level), the reliability of this system can be predicted by studying its behavior. Therefore, the system can be improved by enhancing its reliability, and this can be done by taking various approaches.

One way to improve a system's reliability is by increasing its maintenance program and avoiding possible supply shortcomings in terms of demand. Still, this approach is hardly optimizable and efficient. The second approach is done by improving the design of the infrastructure used in the power system by targeting each system level to enhance its features. This research will focus on optimizing the parameters that could be controlled only at the sub-system level and at the component level to get the highest reliability possible for the overall power system.

The variables regarding the power system that can be controlled, therefore improving the overall performance, are the applied voltage ( $V_{applied}$ ), the switching frequency applied ( $f_{sw}$ ), the length of the capacitor ( $L^{elCap}$ ), the diameter of the capacitor ( $D^{elCap}$ ), the IGBT collector current ( $i_{c,SD}$ ), the diameter of the bond wire of the switching device ( $D_{bw,SD}$ ), the heat sink base thickness ( $t_{b,hs,SD}$ ), the number of capacitors ( $N_{Cap}$ ), and the number of switching devices ( $N_{SD}$ ). More variables could be considered, but this research aims to optimize just those.

These variables will be optimized to find the best possible converter. Still, the designer establishes boundaries that need to be considered in the optimization process, so the final goal will be to find the most optimum value between these limits. The lower and upper limits for these input variables proposed by the designer are presented in Table 3.1. It is essential to mention that the designer can change these boundaries depending on the application of the converter to be designed.

Table 3.1: Input variables boundaries

Variable	Lower boundary	Upper Boundary
$V_{applied} (V)$	500	650
$f_{sw} (kHz)$	5	40
$i_{c,SD} (A)$	10 A	20 A
$L^{elCap} (mm)$	[7.5, 17.5, 27.5, 37.5, 47.5, ... 175]	
$D^{elCap} (mm)$	[5, 15, 25, 35, 45, 55, ... 100]	
$D_{bw,SD} (\mu m)$	[300, 350, ... 500]	
$t_{b,hs,SD} (mm)$	[25, 30, ... 50]	
$N_{Cap} (\#)$	[2,4,6,8,10]	
$N_{SD} (\#)$	[2,4,6,8,10]	

In addition, the optimization problem is subject to certain maximum allowed parameters, which will be analyzed next. The parameters are related to the size, cost, space, and temperature of certain converter components, which are defined in Table 3.2.

Table 3.2: Parameters constrictions

Parameter	Maximum/Minimum value allowed
$A_{Cap,max} (m^2)$	$\leq \left(\frac{9\pi}{400}\right)$
$AR_{Cap,max} (ratio)$	$\leq 2$
$I_{rip,max} (\%)$	$\leq 50$
$T_{J,SD,max} (^\circ C)$	$\leq 125$
$A_{hs,SD,max} (m^2)$	$\leq [100 \times 10^{-3} \times 100 \times 10^{-3}]$
$I_{c,SD,rated} (A)$	$\leq 20$
$Der_{max} (\%)$	$\geq 80$
$Space_{pcb,max}$	$\leq [20 \cdot (64.3 \times 105.7)]mm^2$
$Cost_{comp,max}$	$\leq \$ 500$

## CHAPTER 4

### METAHEURISTIC OPTIMIZATION ALGORITHMS

The reliability model developed in Chapter 3 for a power electronic converter at the component, sub-system, and system levels will be used for optimization improvement as objective function input for the metaheuristic optimization algorithms previously mentioned: Harris Hawk Optimization, Particle Swarm Optimization, and Artificial Bee Colony Optimization.

In Chapter 5, these algorithms will be compared to find their respective convergence rates and determine which reaches the most optimum results. This comparison will be fundamental, as the performance of the algorithm will affect the design of the converter, affecting its reliability and the performance of the overall system where the converter is implemented.

#### 4.1. HARRIS HAWK OPTIMIZATION (HHO) ALGORITHM

The Harris Hawk optimization method is a novel nature-inspired, gradient-free, and population-based optimization algorithm that imitates the chasing style of Harris Hawks' birds. HHO is one of the newest metaheuristic optimization algorithms, and it was introduced recently by Heidari et al. in 2019 [62]. This algorithm follows the attacking behaviors of Harris hawks on the prey in nature, such as preaching, predation, and surprise pounce strategies. Like other metaheuristic algorithms, HHO includes two main phases: exploration and exploitation, shown in Fig. 4.1. The model implemented in this work was directly developed from [65].

HHO has previously been used for optimization with applications in the medical field such as [66], applications in EVs such as [67], applications in UAVs such as [68], applications in IoT such as [69], and applications in PV emulator control [70]. However, as this algorithm is new, much work has yet to be related to power systems and, more specifically, power converters. The power of this optimization algorithm is higher than that of other optimization algorithms, and it is expected to converge faster and to more optimum values.

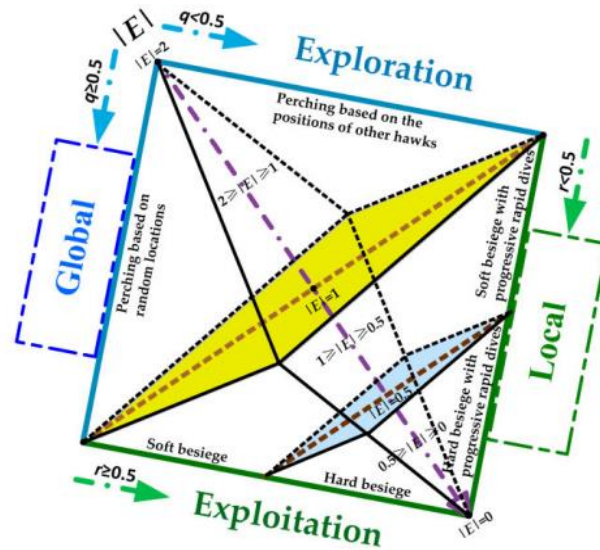


Fig. 4.1: Exploration and exploitation phases of Harris Hawks optimization (HHO) [65].

As seen from Fig. 4.1, the HHO’s two main phases (exploration and exploitation) are divided into two and four stages, respectively. The exploration phase is composed of perching based on random locations stage and the perching based on the position of other hawks. On the other hand, the exploitation phase comprises four main stages: Soft Besiege, Hard Besiege, Soft Besiege with progressive rapid dives, and Hard Besiege progressive rapid dives. To determine the phase and stage in which the Harris Hawk Optimization algorithm is used, the variables  $|E|$  (escaping energy of the rabbit) and  $r$  (probability of escaping of the rabbit) are used. Fig. 4.2 shows how the algorithm determines the next phase and stage that will be implemented.

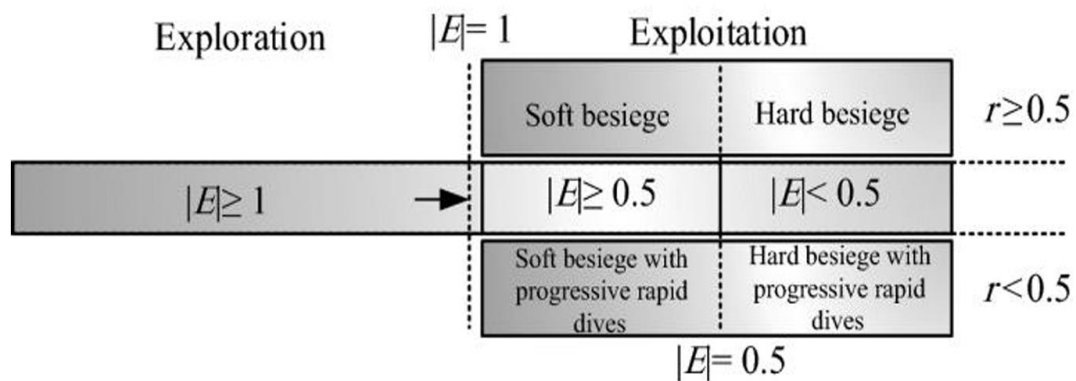


Fig. 4.2: The exploration phase and the four types of exploitation phases in HHO [65].

#### 4.1.1. INITIALIZATION PHASE

During this phase, the Harris Hawk population is initialized randomly between the upper and lower bounds provided. In addition, the objective function and its solution space for the population members to displace are defined. The equation used to initialize the population follows Eq. (48).

$$X_i(i = 1, 2, \dots, N) \quad (48)$$

#### 4.1.2. EXPLORATION PHASE

The exploration phase is where Harris Hawks search for the prey. In this stage, the fitness of each population member is calculated for each iteration. Still, as the prey is difficult to see in some cases, some members stay in their position, waiting to detect it, following Eq. (49).

$$X(t + 1) = \begin{cases} X_{rand}(t) - r_1 | X_{rand}(t) - 2r_2X(t) & q \geq 0.5 \\ (X_{rabbit}(t) - X_m(t)) - r_3(LB + r_4(UB - LB)) & q \leq 0.5 \end{cases} \quad (49)$$

where  $X(t + 1)$  is the position of the hawks in the next iteration  $t$ ,  $X_{rabbit}(t)$  is the rabbit position,  $X(t)$  is the current position of the Harris Hawk,  $X_m(t)$  is the average position of the population,  $r_1, r_2, r_3, r_4$ , and  $q$  are random number between 0 and 1. Last but not least,  $LB$  and  $UB$  represent the lower and upper bound of the variables to be generated.

#### 4.1.3. TRANSITION FROM EXPLORATION TO EXPLOITATION

The correct balance between metaheuristic algorithms' exploration and exploitation phases is fundamental for better performance. The variable that determines the transition from the exploration phase to the exploitation phase is the prey escaping energy, as defined by Eq. (50).

$$E = 2E_0 \left(1 - \frac{t}{T}\right) \quad (50)$$

where  $E$  is the escaping energy of the rabbit,  $E_0$  is the initial state of energy which corresponds to

a random value between -1 and 1, and  $T$  is the maximum number of iterations. Whenever the absolute value of the energy  $E$  is greater or equal to a value of 1 ( $|E| \geq 1$ ), the Hawks will be redirected to explore a different region of the plane, entering the exploration phase. However, when the absolute value of the energy  $E$  is less than a value of 1 ( $|E| < 1$ ), the Hawks search nearby locations for a possible solution, entering the exploitation phase.

#### 4.1.4. EXPLOITATION PHASE

The exploitation phase happens when the Harris Hawks attack the prey based on the position detected in the previous phase. During the exploration phase, each Hawk scouts the prey to gather information. Once they are in range to attack, they transition to the exploitation phase to avoid the rabbit's attempts to escape. This phase consists of four main stages: Soft Besiege, Hard Besiege, Soft Besiege with progressive rapid dives, and Hard Besiege with progressive rapid dives. To determine which stage the Harris Hawk will be in, the two variables used are  $|E|$ , referring to the escaping energy of the rabbit, and  $r$ , referring to the probability of the rabbit escaping.

#### 4.1.5. SOFT BESIEGE STAGE

If the probability of escaping  $r$  is greater or equal to 0.5 ( $r \geq 0.5$ ) and the escaping energy of the rabbit  $|E|$  is greater or equal to 0.5 ( $|E| \geq 0.5$ ), the rabbit still has some energy left and a low chance of escaping. Hence, the Harris Hawks begin the soft besiege stage to make the rabbit lose more energy before attacking it directly. Eq. (51) and Eq. (52) formulate the soft besiege stage.

$$X(t + 1) = \Delta X(t) - E |J X_{rabbit} - X(t)| \quad (51)$$

$$\Delta X(t) = \Delta X_{rabbit} - X(t) \quad (52)$$

where  $\Delta X(t)$  represents the difference between the position of the rabbit and the position of the Harris Hawk at iteration  $t$ , and  $J$  represents a random jump strength from the rabbit developed in Eq. (53).

$$J = 2(1 - r_5) \quad (53)$$

#### 4.1.6. HARD BESIEGE STAGE

If the probability of escaping  $r$  is greater or equal to 0.5 ( $r \geq 0.5$ ) and the escaping energy of the rabbit  $|E|$  is less than 0.5 ( $|E| < 0.5$ ), then it means that the rabbit doesn't have much energy left, and the chances of escaping are also low. Hence, the Harris Hawks begin the hard besiege stage to attack the rabbit directly to find the final solution. The hard besiege stage is formulated by Eq. (54).

$$X(t + 1) = X_{rabbit}(t) - E |\Delta X(t)| \quad (54)$$

#### 4.1.7. SOFT BESIEGE WITH PROGRESSIVE RAPID DIVES STAGE

Suppose the probability of escaping  $r$  is less than 0.5 ( $r < 0.5$ ), and the escaping energy of the rabbit  $|E|$  is greater or equal to 0.5 ( $|E| \geq 0.5$ ). In that case, the rabbit still has some energy left and a high chance of escaping, so the Harris Hawks begin the soft besiege with progressive rapid dives before switching to the hard besiege. Another name for this stage is smart soft besiege because the Hawks are performing a zigzag movement with multiple dives around the rabbit to approach it closer. The Hawk's position is updated in two steps for this stage. The first step is modeled by Eq. (55), where the Hawks decide what the next move should be. The second step is modeled by Eq. (56), where the Hawks perform rapid dives based on the Levy flight function.

$$Y = X_{rabbit}(t) - E |J X_{rabbit}(t) - X(t)| \quad (55)$$

$$Z = Y + S \times LF(dim) \quad (56)$$

where  $dim$  refers to the dimensions of the objective problem to be optimized,  $S$  is a randomly generated vector of size  $1 \times dim$ , and  $LF$  denotes the Levy flight function shown in Eq. (57) and Eq. (58).

$$LF(x) = 0.01 \times \frac{u \times \sigma}{|v|^{\frac{1}{\beta}}} \quad (57)$$

$$\sigma = \left( \frac{\Gamma(1 + \beta) \times \sin\left(\frac{\pi\beta}{2}\right)}{\Gamma\left(\frac{1 + \beta}{2}\right) \times \beta \times 2^{\left(\frac{\beta-1}{2}\right)}} \right)^{\frac{1}{\beta}} \quad (58)$$

where  $u$  and  $v$  are random values between 0 and 1, and  $\beta = 1.5$ .

Consequently, to update the position of the Harris Hawks in the soft besiege with progressive rapid dives stage, Eq. (59) is followed.

$$X(t + 1) = \begin{cases} Y & \text{if } F(Y) < F(X(t)) \\ Z & \text{if } F(Z) < F(X(t)) \end{cases} \quad (59)$$

where  $F$  is the cost value for Hawks' position given by the objective function when  $Y$  and  $Z$  are evaluated.

#### 4.1.8. HARD BESIEGE WITH PROGRESSIVE RAPID DIVES STAGE

If the probability of escaping  $r$  is less than 0.5 ( $r < 0.5$ ) and the escaping energy of the rabbit  $|E|$  is less than 0.5 ( $|E| < 0.5$ ), then the rabbit does not have enough energy to escape, even though its chances are high. Hence, the Harris Hawks begin the hard besiege with a progressive rapid dive stage to approach the prey and then attack it. The change in position of the Hawks is similar to the soft besiege but with different modeling equations, depicted by Eq. (60), Eq. (61), and Eq. (62).

$$X(t + 1) = \begin{cases} Y & \text{if } F(Y) < F(X(t)) \\ Z & \text{if } F(Z) < F(X(t)) \end{cases} \quad (60)$$

where

$$Y = X_{rabbit}(t) - E \cdot |J \cdot X_{rabbit}(t) - X_m(t)| \quad (61)$$

$$Z = Y + S \times LF(dim) \quad (62)$$



## 4.2. PARTICLE SWARM OPTIMIZATION (PSO) ALGORITHM

Particle Swarm Optimization (PSO) was developed by Kennedy and Eberhart in 1995 and inspired by biological systems' behavior, commonly called swarm intelligence algorithms. This is a metaheuristic optimization algorithm that resembles the movement of birds that could help find the optimum solution in a nonlinear optimization problem, which is the case when analyzing the reliability of power electronic converters [71]. PSO is also beneficial when dealing with other types of nonlinear optimization problems in the areas of sensing [72], control [73], and RFID network planning [74]. Some other applications are presented in Fig. 4.3.

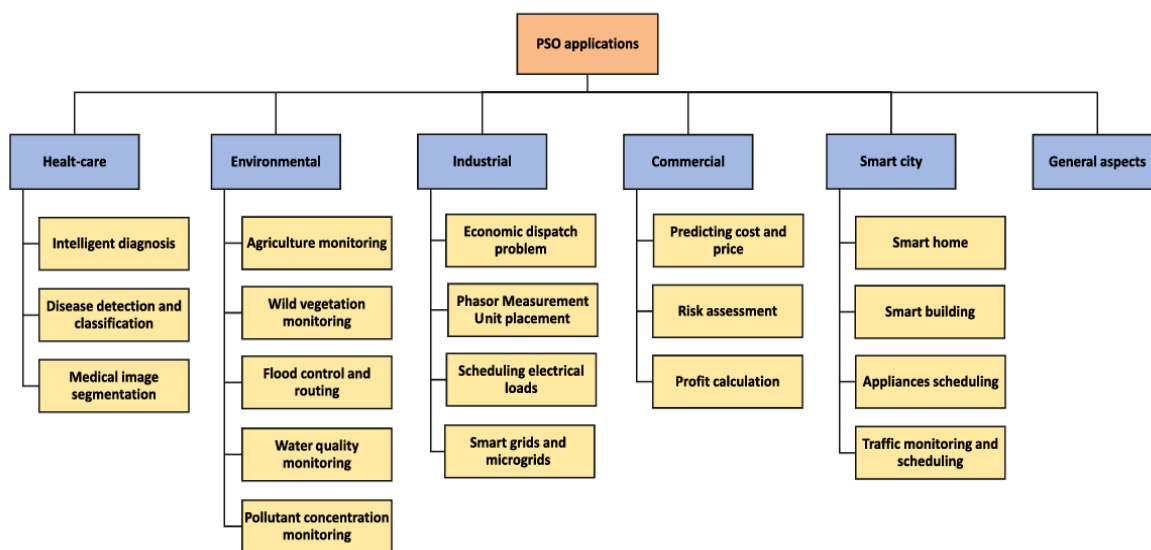


Fig. 4.3: The taxonomy of PSO applications [75].

### 4.2.1. PSO PRINCIPLES OF EXECUTION

Classically, the simulation is performed on a two-dimensional grid where the birds search for food, the location of which is unknown to them. The birds fly over space, including every possible solution in the food search to determine the optimum solution. The motion of the searching agents is governed by three aspects: inertia, local optima, and group optima. The first one, inertia, means that they will continue moving in the direction they have been moving. The second one, local optima, means that they will tend to move towards the position that gives them their personal best fitness value. The third one, group optima, means that they tend to move towards the position that

offers the best fitness within the same searching group. When simulating the search for an optimum solution using PSO in reliability analysis, all the temporal positions of the searching agents are recorded to ensure the finding of the most optimum solution at the end [76].

As with many biological system-based algorithms, this optimization algorithm relies on creating a population of agents that will cooperate using collective intelligence to achieve the most optimum results. This method could be adapted to power systems reliability analysis, producing excellent results when aiming to find the optimum values for multiple parameters when considering power electronic converters [76]. In addition, the particle swarm optimization algorithm is excellent for electrical engineering optimization problems that involve optimizing a multimodal cost function with continuous variables. Because traditional deterministic optimal methods cannot find the global optimal solutions to these problems, stochastic and heuristic algorithms are raised as potential solutions. This algorithm has been modified to control premature convergence to local values and improve its global search ability [77]. The flowchart of the PSO implemented is shown in Fig. 4.4.

#### 4.2.2. DEVELOPMENT OF THE ALGORITHM

The original PSO algorithm with velocity clamping presented in [78] was modified to include a relatively newer concept in PSO called constriction factor, presented in [79] and [80]. However, the main steps for the algorithm were preserved. As a traditional PSO algorithm, it has only three controlling parameters: the inertia weight, the cognitive ratio, and the social ratio. In addition, this algorithm has an outstanding balance between exploration and exploitation, which makes it an excellent candidate to find the best possible solution [79]. Any change in these three parameters will completely change the performance of the PSO algorithm, as shown in [81] and [82].

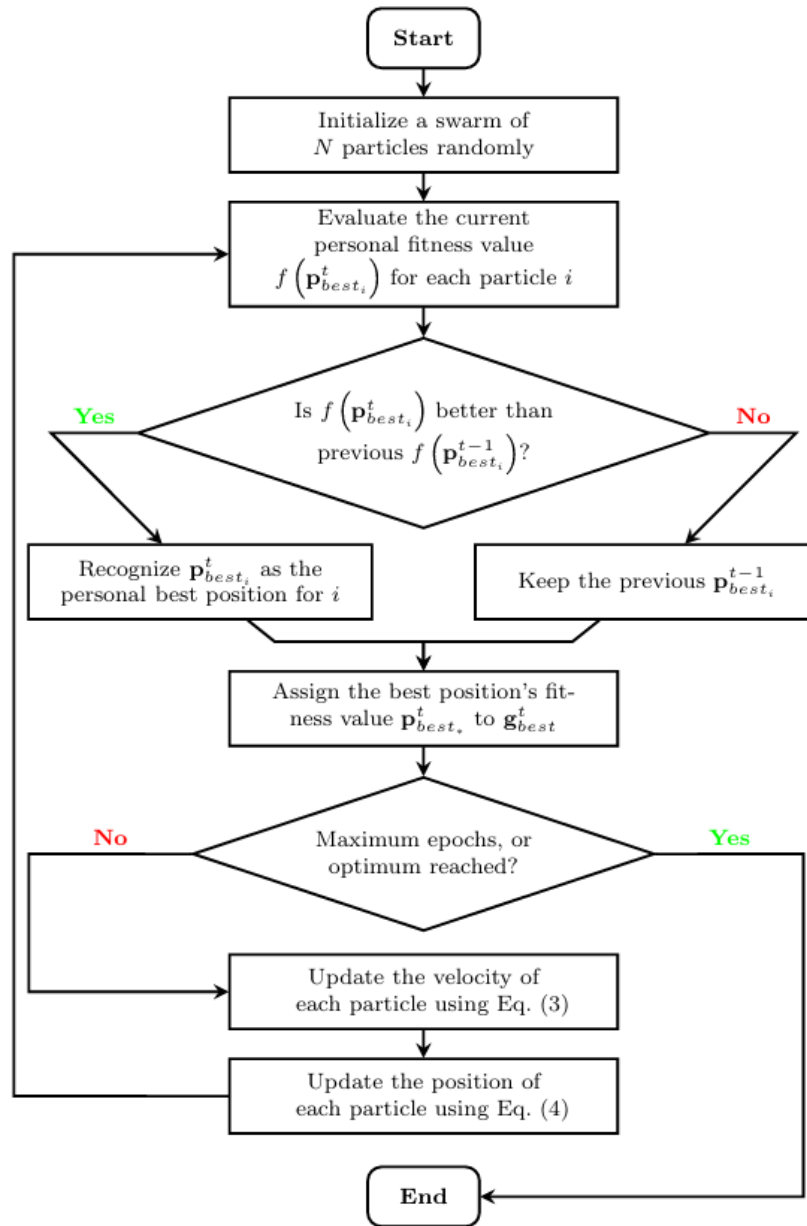


Fig. 4.4: The flowchart of PSO [75].

#### 4.2.3. INITIALIZATION PHASE

The PSO algorithm starts by initializing a random vector for the velocity of the particles initialized as a vector with the dimensions of the objective problem and a random vector for the position of the particles defined as Eq. (63).

$$particle(i).Position = unifrnd(VarMin, VarMax, VarSize) \quad (63)$$

where the function *unifrnd* generates random numbers from the continuous uniform distribution, *VarMin* represents the lower bound matrix for the objective function, *VarMax* represents the upper bound matrix for the objective function, and *VarSize* represents the size of the objective function matrix to optimize.

#### 4.2.4. EXPLORATION AND EXPLOITATION PHASE

Once the initial values for the position and the velocity are generated, each iteration will evaluate and save the best position found by the particle (*Pbest*) and the best position found by the whole swarm (*Gbest*). These two variables will be used to update the velocity and position in future iterations, as shown in Eq. (64) and Eq. (65).

$$v_{id}(t + 1) = v_{id}(t) + c_1 r_1 (Pbest_{id}(t) - x_{id}(t)) + c_2 r_2 (Gbest_{id}(t) - x_{id}(t)) \quad (64)$$

$$x_{id}(t + 1) = x_{id}(t) + v_{id}(t + 1) \quad (65)$$

where  $c_1$  and  $c_2$  are the personal and social acceleration coefficient, respectively, and  $r_1$  and  $r_2$  are two uniform random values generated between 0 and 1.

#### 4.2.5. CONSTRICTION COEFFICIENTS

The careful selection of constriction coefficients to prevent the PSO algorithm from accelerating too fast, leading to an explosion, is fundamental. The constriction coefficients used as input in the PSO developed are  $\kappa$ ,  $\phi_1$ , and  $\phi_2$ . After careful consideration of the objective problem and multiple attempts with different coefficients, the following values were selected for each coefficient:  $\kappa = 1$ ,  $\phi_1 = 2.05$ ,  $\phi_2 = 2.05$ .

The inertia coefficient  $\chi$  could then be calculated using the provided constriction coefficients, as shown in Eq. (66). However, as there was no damping in the constriction coefficients, the value

was assumed to be 1,  $\chi_{damp} = 1$ .

$$\chi = \frac{2\kappa}{|2 - \phi - \sqrt{\phi^2 - 4\phi}|} \quad (66)$$

where  $\phi = \phi_1 + \phi_2$

Using the inertia coefficient  $\chi$  previously calculated, the personal acceleration coefficient  $c_1$  and the social acceleration coefficient  $c_2$  are calculated in Eq. (67) and Eq. (68), respectively.

$$c_1 = \chi * \phi_1 \quad (67)$$

$$c_2 = \chi * \phi_2 \quad (68)$$

A widespread value to use as input for  $c_1$  and  $c_2$  is 1.49, but in this case, the value 2.05 brought better performance to the algorithm. In addition, it is traditionally recommended to ensure that  $c_1$  is a large value and  $c_2$  is a small value to ensure that the particles perform a complete space search without converging into local best values. On the other hand, setting a small  $c_1$  and a large  $c_2$  would make the algorithm focus more on the exploitation phase, which could be helpful depending on the purpose of the optimization problem. The acceleration coefficient could also change with the iterations of the PSO algorithm, like the algorithm proposed in [83].

## 4.2.6. PSO PSEUDOCODE

Algorithm 2 Particle Swarm Optimization [79]

---

**Input:** Converter: Function to be optimized, MaxIt: maximum number of iterations, nPop: population size,  $\kappa$ ,  $\phi_1$  and  $\phi_2$ : constriction coefficients, nVar: number of decision variables, lb: lower bound matrix, ub: upper bound matrix.

**Output:** out.BestSol: best fitness position found, out.BestCosts: best cost found for the best position.

Initialize the particle population randomly:  $particle(i).Position$  ( $i = 1, 2, \dots, nPop$ ) using **Eq. (63)**

Initialize the velocity of the particle related to the constriction coefficients:  $particle(i).Velocity$  ( $i = 1, 2, \dots, nPop$ ).

**While** (maximum iteration not reached ( $i < MaxIt$ )) **do**

Check the location boundaries for each parameter and input these values into the problem function to evaluate the fitness of these particles.

The best position and cost are set as  $GlobalBest$ , later outputted as  $out.BestSol$ .

**For** (each searching agent  $particle(i)$  ( $i = 1$  to  $nPop$ )) **do**

Generate  $r_1$  and  $r_2$

Update velocity of the particle:  $particle(i).Velocity$  using **Eq. (64)**

Apply lower and upper bound limits to velocity.

Update position:  $particle(i).Position$  using **Eq. (65)**

Apply lower and upper bound limits to position.

Reevaluate the fitness of the new particle position:  $particle(i).Cost$

**If**  $particle(i).Cost < particle(i).BestCost$  **then**

Update personal best position and cost for the particle:  $particle(i).Position$  &  $particle(i).BestCost$

**if**  $particle(i).Cost < particle(i).GlobalBestCost$  **then**

Update global best position and cost:  $GlobalBest.Position$  &  $GlobalBest.Cost$

**Return** the  $GlobalBest.Position$  &  $GlobalBest.Cost$

---

### 4.3. ARTIFICIAL BEE COLONY (ABC) ALGORITHM

The Artificial Bee Colony algorithm models the behavior of the bees when searching for food, which consists of two modes of behavior: gathering a food source (better solution) and abandoning the food source (worse solution) [85]. Karaboga proposed this algorithm in 2005 to solve a multivariate function optimization problem given the intelligent foraging behavior of a honeybee swarm [86]. An improved version of the algorithm was proposed in [87], but the traditional ABC algorithm was used for this work.

The Artificial Bee Colony algorithm is a powerful algorithm that has found successful applications in fields such as remote sensing [88], [89], and [90], construction cost minimization [91], and smart grids [92].

#### 4.3.1. ABC PRINCIPLES OF EXECUTION

The artificial bee colony algorithm population consists of three different types of agents in charge of finding the most optimum results: the employed bees, the scout bees, and the onlooker bees. The employed bees are the ones on the location of the food sources. These types of bees have the task of exploiting these food sources and informing onlooker bees about the location of the food. The scout bees search for food in random locations, and once they find food, they start exploiting it, becoming employed bees. Lastly, the onlooker bees are the ones that haven't yet got to explore, and they are resting in the hive, awaiting to be recruited [93]. Fig. 4.5 from [95] depicts the functioning of the ABC algorithm when searching for the most optimum solution.

Like all the optimization algorithms, the ABC algorithm begins by creating a randomly distributed initial population between the upper and lower bound provided. This initial population is created following Eq. (69).

$$X_i(i = 1, 2, \dots, nPop) \quad (69)$$

where  $nPop$  is the total size of the hive's population, and each vector has the dimensions of the variables to be optimized.

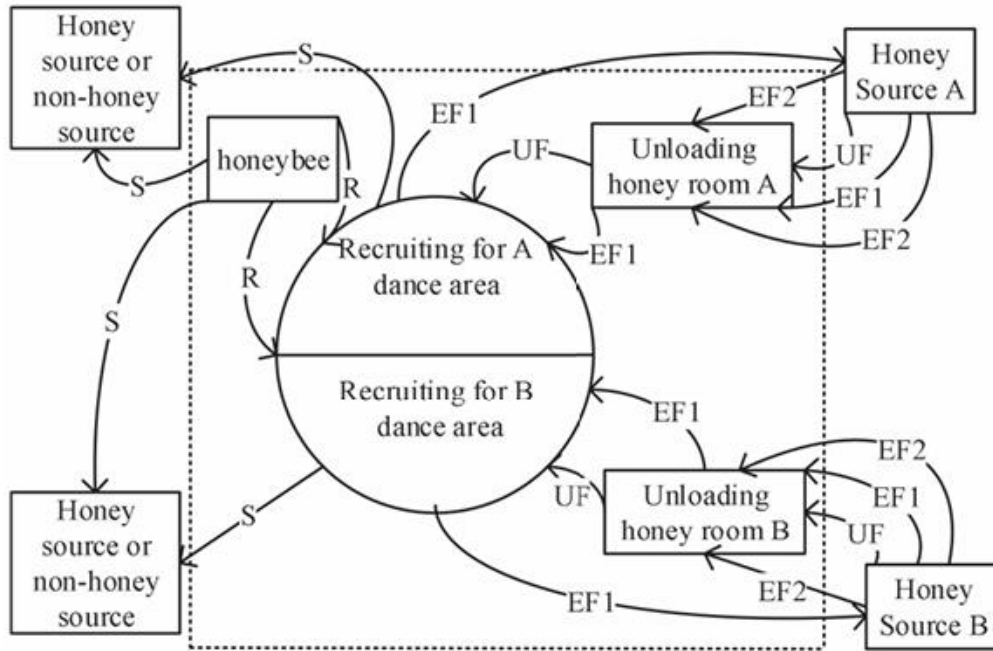


Fig. 4.5: Schematic diagram of the artificial bee colony algorithm [95].

Once the initial population is initialized, the position of a food source will be searched, with the most optimum position being where there is more nectar. Here, the hive population is divided into one of the three groups mentioned before, which are either an employed bee, an onlooker bee, or a scout bee. ABC algorithm was developed for this work based on [96].

#### 4.3.2. EMPLOYED BEES PHASE

Employed bees modify their position based on visual information. If the amount of food in the new position is higher than the old position, the employed bee automatically remembers the new position and forgets the old one. If the new position is not better than the old one, the bee keeps the old one in memory. Once they finish the search process, they share the information gathered with the onlooker bees waiting in the dance area [96].

In addition, each employed bee generates a neighbor food source position  $i + 1$  using Eq. (70) and compares the amount of food in this position to the amount of food in the last position  $i$ .

$$x_{ij}^{new} = x_{ij}^{old} + u(x_{ij}^{old} - x_{kj}) \quad (70)$$

where  $k \neq i$  and are numbers between 1 and the total number of employed bees,  $u$  is a random number between -1 and 1, and  $j$  is a number between 1 and the dimensions of the objective function to optimize. Therefore,  $x_{ij}$  is the  $j^{th}$  parameter of a solution  $x_i$ .

Once all the positions  $i$  are checked, if the amount of food is not greater than the amount of food in the old location, the employed bee transforms into a scout bee.

#### 4.3.3. ONLOOKER BEES PHASE

Onlooker bees will wait for information from the employed bees, and if they receive that information, they will evaluate which food source is the most convenient based on the level of food. Onlooker bees also select convenient food sources through visual information, and because of this, they can only find sources in the neighborhood of previous positions. The onlooker bees evaluate the probability  $p_i$  of selecting a food source based on Eq. (71).

$$p_i = \frac{fitness_i}{\sum_{i=1}^{E_b} fitness_i} \quad (71)$$

where  $fitness_i$  is the fitness evaluation of a solution  $i$ , and  $E_b$  is the total number of food-source positions, corresponding to half of the colony size.

Using Eq. (71), each onlooker bee will be able to determine the most optimum food source to migrate. In addition, each onlooker bee generates a neighbor food source position  $i + 1$  using Eq. (70) and compares the amount of food in this position to the amount of food in the last position  $i$ . Once an onlooker bee selects the most optimum position, it transforms into an employed bee at that selected position.

#### 4.3.4. SCOUT BEES PHASE

On the other hand, instead of using visual information to search for food, scout bees search for new possible positions without any information. In other words, they have the task of finding new

sources of food to be exploited by the employed bees. Once a scout bee finds a food source, this bee automatically transforms into an employed bee. Once a food position is detected as not worth it anymore, the employed bee in that source position transforms into a scout bee.

The scout bees find a new position for the food based on Eq. (72)

$$x_i^{j(new)} = \min x_i^j + u(\max x_i^j - x_i^j) \quad (72)$$

where  $j$  represents the total number of parameters and  $u$  is a random number between -1 and 1.

#### 4.3.5. ABC PSEUDOCODE

Algorithm 3 Artificial Bee Colony Algorithm [96]

---

**Input:** Converter: Function to be optimized,  $nPop$ : the population size (colony size),  $MaxIt$ : the maximum number of iterations,  $L$ : abandonment limit parameter,  $a$ : acceleration coefficient upper bound,  $lb$ : lower bound matrix,  $ub$ : upper bound matrix.

**Output:** out.BestSol: best fitness position found, out.BestCosts: best cost found for the best position.

Initialize the particle population randomly within limits:  $pop(i).Position$  ( $i = 1, 2, \dots, nPop$ )

**While** (maximum iteration not reached ( $it < MaxIt$ )) **do**

**For** ( $i = 1:nPop$ ) **do**

**%Employed bees**

        Recruit bees for the selected sites and to evaluate fitness

        Select the bee with the best fitness as BestSolution

        Calculate the position for the next iteration using **Eq. (70)**

**If** ( $pop(i).Cost \leq BestSol.Cost$ ) **then**

        Update the best solution

**end**

**For** ( $i = 1:nOnlooker$ ) **do**

**% Onlooker bees**

        Select sites for local search using  $RouletteWheelSelection(P)$

        Calculate selection probability  $p_i$  using **Eq. (71)**

        Determine position of new bee recruited  $newbee.Position$

```
Evaluate fitness of the new bee and compare it to current bee position  $pop(i).Cost$   
    If ( $newbee.Cost \leq pop(i).Cost$ ) then    %Selection probabilities  
        Update the current bee position and cost with the ones of the new bee  
        end  
end  
For ( $i = 1:nScout$ ) do    % Scout bees  
    Assign the remaining bees to looking for randomly using Eq. (72)  
    Evaluate the fitness of remaining bees  
    Update probabilities  
end  
end  
Return the best position (out. BestSol) and best cost (out. BestCosts)
```

---

## CHAPTER 5

### RELIABILITY STUDIES AND RESULTS

In previous chapters, reliability improvement optimization for power converters was discussed, as well as the approach to achieve this substantial improvement in the design of power converters. Multiple metaheuristic optimization algorithms were proposed to find the optimal parameters for the design of a power converter, considering the behavior of power converters modeled in Chapter 3 for each one of its levels.

It is important to mention that for this study, both the sub-system and component level reliability models were used, but not the power system level reliability model. This is because the sub-system and component levels are strongly related to the design of the converters, which was the main focus of this research, compared with the power system level, which will be more related to the design and optimization of the power system itself.

The metaheuristic optimization algorithms used were the Artificial Bee Colony (ABC) optimization algorithm, the Particle Swarm Optimization (PSO) algorithm, and the Harris Hawk Optimization (HHO) algorithm. As mentioned before, the algorithms were tested with the same input parameters for the component and sub-system levels and reliability models were developed. Firstly, the algorithms will be tested for their performance in each of the levels separately, and after, a multiobjective optimization will be made to determine the most efficient converter that could be designed. In addition, the convergence rate of each one of the optimization algorithms will be measured to compare and determine which algorithm is the most convenient.

The main indicators of the reliability of a system will be the failure rate  $\lambda$ , measured in *FIT* (failure in time); the reliability  $R$ , measured in %; the mean time to failure *MTTF* (mean time to failure), measured in hours; the lifetime of the component  $L$ , measured in years; and the cycles to failure  $N_f$ , measured in cycles. The failure rate ( $\lambda$ ), the reliability ( $R$ ), and the mean time to failure (*MTTF*) will correspond to the useful time phase presented in Fig. 2.1, which corresponds to the component level modeling presented in Chapter 3. On the other hand, the lifetime of the component ( $L$ ) and the cycles to failure ( $N_f$ ) will correspond to the wear-out phase presented in Fig. 2.1, which corresponds to the sub-system level modeling presented in Chapter 3.

Reliability  $R$  is defined as the success rate of a component's operation if operated within the specified time frame  $t_{phase}$ , which corresponds to 24 hours.

## 5.1 HARRIS HAWK OPTIMIZATION ALGORITHM RESULTS

The first optimization algorithm tested was the Harris Hawk Optimization algorithm, which focuses on the useful time phase of the converter, modeled at a component level. Table 5.1 models the capacitor failure rate optimized parameters using the HHO algorithm, and it analyzes the reliability of a single component (capacitor) and the reliability when redundancy of its components. In addition, Fig. 5.1 and Fig. 5.2 illustrate the convergence rate for the HHO algorithm when a single capacitor is considered and when multiple capacitors are considered respectively.

Table 5.1: Capacitor failure rate optimized parameters (HHO)

	<b>Design Parameter</b>	<b>Optimum value</b>	<b>Constraint</b>	<b>Actual Value</b>	<b>Min/Max value</b>
1Cap	$v_{applied}(V)$	520	$A_{cap,max}[m^2]$	5.7079 * $10^{-8}$	$\leq 0.0707$
	$f_{sw}(kHz)$	40	$AR_{cap}$	1.7632	$1 \leq AR_{cap} \leq 2$
	$L_{elCap}(mm)$	167.5	$I_{rip,max}[\%]$	10	$\leq 50$
	$D_{elCap}(mm)$	95	$Der(V)[\%]$	80	$\geq 80$
	$\lambda_{cap}[FIT]$		0.0650		
	$R_{cap}[\%]$		21		
	$MTTF[hrs]$		15.3796		
$\geq 2Cap$	$v_{applied}(V)$	520	$A_{cap,max}[m^2]$	5.7079 * $10^{-8}$	$\leq 0.0707$
	$f_{sw}(kHz)$	40	$AR_{cap}$	1.7632	$1 \leq AR_{cap} \leq 2$
	$L_{elCap}(mm)$	167.5	$I_{rip,max}[\%]$	10	$\leq 50\%$
	$D_{elCap}(mm)$	95	$Der(V)[\%]$	80	$\geq 80$
	$N_{cap}$	14	$Space_{pcb}[\#]$	14	$\leq 14$
	-	-	$Budget_{cap}[\$]$	738.64	$\leq 750$
	$\lambda_{cap}[FIT]$		0.00926		
	$R_{sys}[\%]$		96.314		
	$MTTF[hrs]$		50.0079		

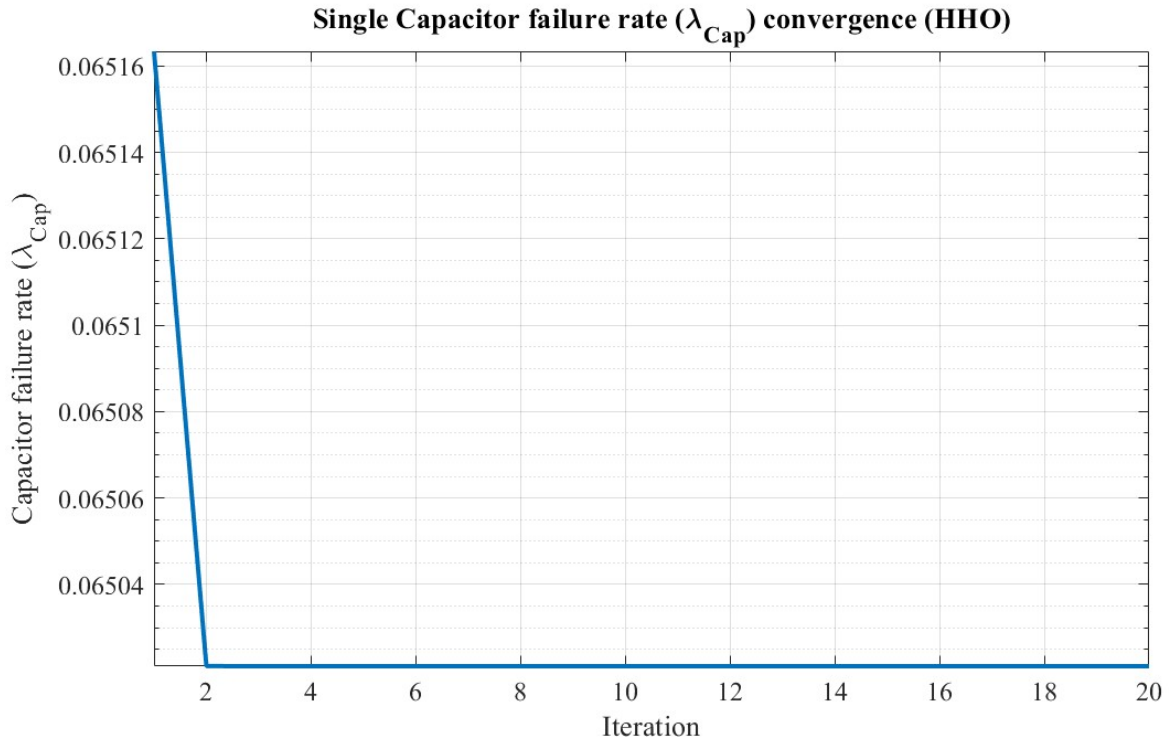


Fig. 5.1: Single capacitor failure rate ( $\lambda_{Cap}$ ) convergence (HHO)

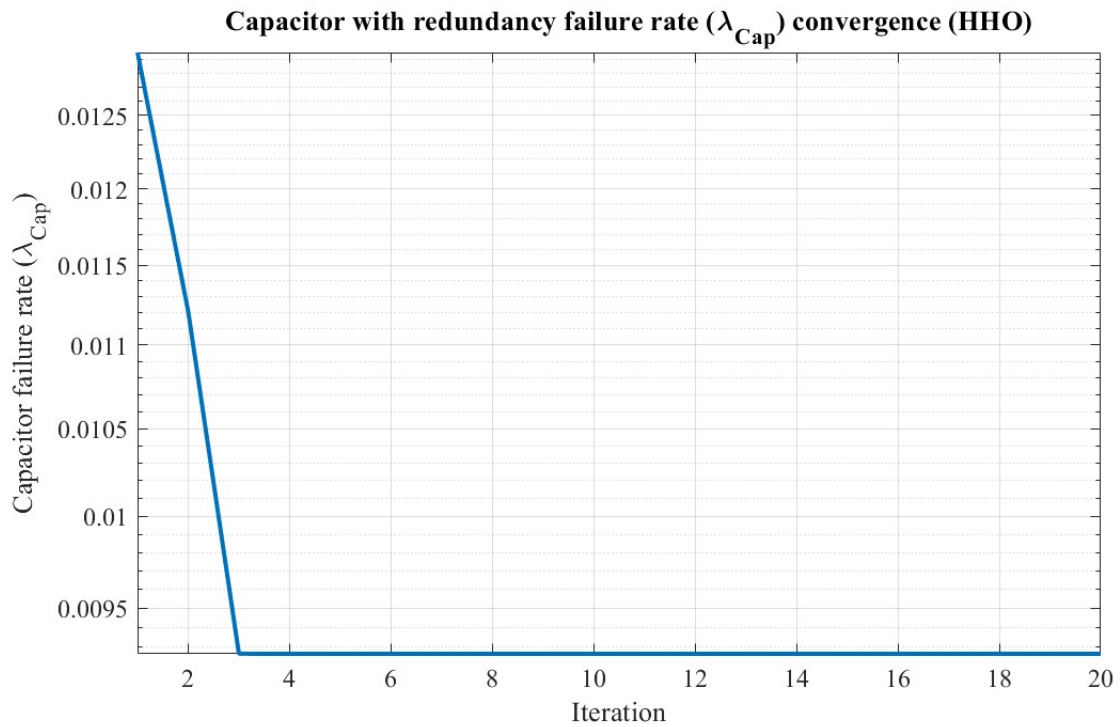


Fig. 5.2: Capacitor with redundancy failure rate ( $\lambda_{Cap}$ ) convergence (HHO)

Table 5.2: Single Capacitor lifetime optimized parameters (HHO)

$\Delta$	Design Parameter	Optimum value	Constraint	Actual Value	Min/Max value
–	$v_{applied}(V)$	520	$A_{cap,max}[m^2]$	$1.3744 * 10^{-4}$	$\leq 0.0707$
	$f_{sw}(kHz)$	8.0005	$AR_{cap}$	1.5	$1 \leq AR_{cap} \leq 2$
	$L_{elCap}(mm)$	7.5	$I_{rip,max} [\%]$	50	$\leq 50$
	$D_{elCap}(mm)$	5	$Der(V)[\%]$	80	$\geq 80$
	$L_0[yr]$		1		
	$L_{x,Cap}[yr]$		8.8566		
Der	$v_{applied}(V)$	422.5	$A_{cap,max}[m^2]$	$1.3744 * 10^{-4}$	$\leq 0.0707$
	$f_{sw}(kHz)$	8.0005	$AR_{cap}$	1.5	$1 \leq AR_{cap} \leq 2$
	$L_{elCap}(mm)$	7.5	$I_{rip,max} [\%]$	50	$\leq 50\%$
	$D_{elCap}(mm)$	5	$Der(V)[\%]$	65	$\geq 65$
	$L_0[yr]$		1		
	$L_{x,Cap}[yr]$		25.012		
$I_{rip}$	$v_{applied}(V)$	520	$A_{cap,max}[m^2]$	$1.3744 * 10^{-4}$	$\leq 0.0707$
	$f_{sw}(kHz)$	6.897	$AR_{cap}$	1.5	$1 \leq AR_{cap} \leq 2$
	$L_{elCap}(mm)$	7.5	$I_{rip,max} [\%]$	58	$\leq 58$
	$D_{elCap}(mm)$	5	$Der(V)[\%]$	80	$\geq 80$
	$L_0[yr]$		1		
	$L_{x,Cap}[yr]$		19.869		

On the other hand, Table 5.2 presents the optimized parameters for a single capacitor lifetime improvement without considering redundancy. The capacitor's lifetime will strictly depend on the constrictions imposed by the designer, and this can be demonstrated when the minimum deration is lowered and the capacitor's lifetime increases drastically. Another example is when the maximum allowed ripple current increases, and the capacitor's lifetime increases accordingly.

To illustrate the convergence rate of a single capacitor lifetime using the HHO algorithm Fig. 5.3 was included.

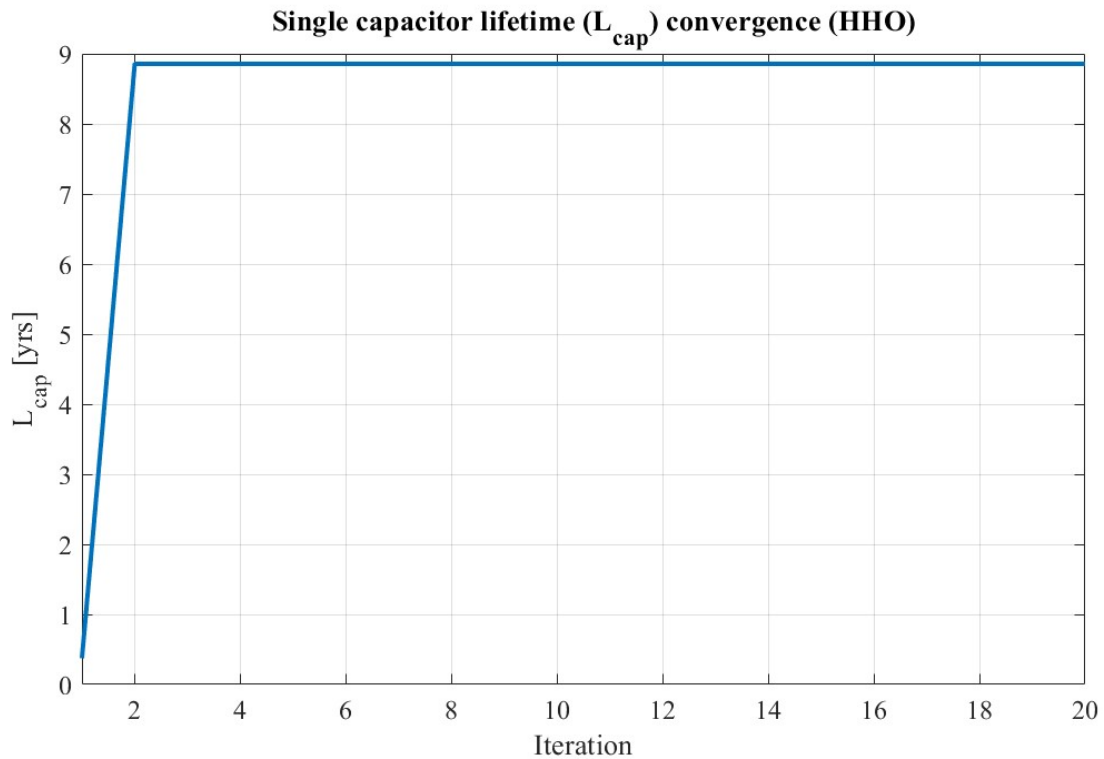


Fig. 5.3: Single capacitor lifetime ( $L_{cap}$ ) convergence (HHO)

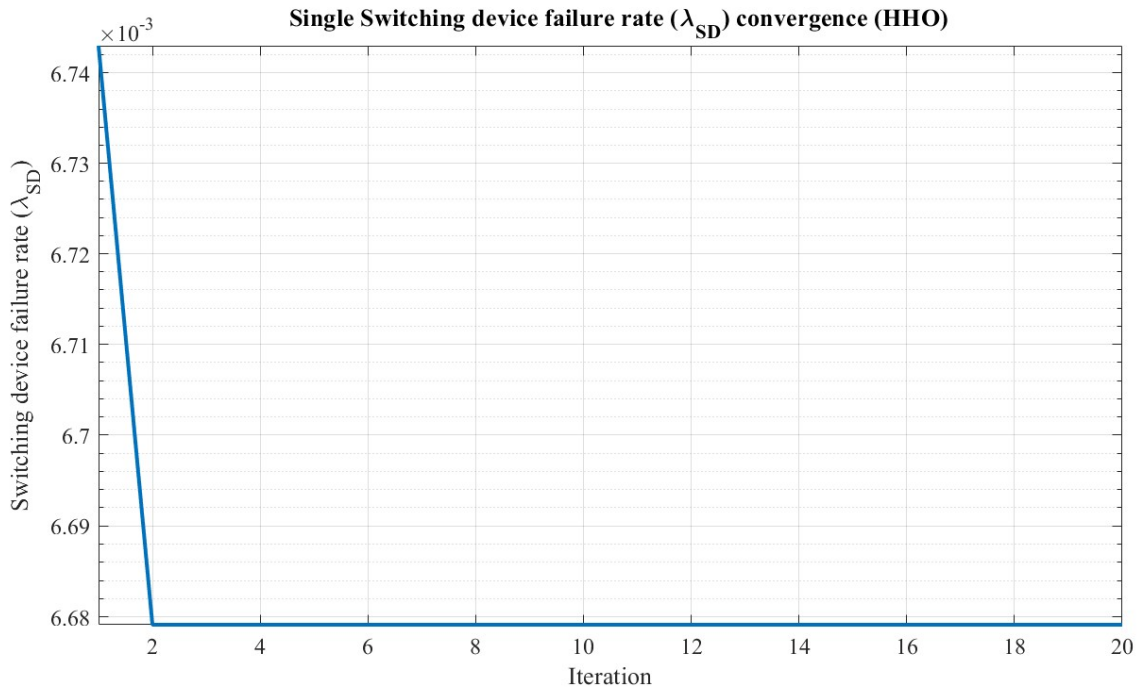
The switching device is another critical component of the converter on a component level. Table 5.3 analyzes the failure rate of the switching device, which will directly impact the overall reliability of the power converter. Once again, the possibility of just a single switching device and adding more than one switching device to the system to increase its reliability was analyzed.

From Table 5.3, it is clear that adding more switching devices to the system increases its overall reliability. The optimized value for the total number of switching devices in the system was 8, which brings the system's overall reliability up to almost a 100%.

Fig. 5.4 and Fig. 5.5 show the convergence of the Harris Hawk Optimization algorithm for a single switching device and multiple switching devices, respectively.

Table 5.3: Switching device failure rate optimized parameters (HHO)

	<b>Design Parameter</b>	<b>Optimum value</b>	<b>Constraint</b>	<b>Actual Value</b>	<b>Min/Max value</b>
1SD	$v_{applied}(V)$	520	$T_{j,SD}[^{\circ}C]$	72.9194	$\leq 125$
	$f_{sw}(kHz)$	8.0005	$Der(V)[\%]$	80	$\geq 80$
	$i_{SD,c}(A)$	16	$Der(I)[\%]$	80	$\geq 80$
	$t_{hs,b}(mm)$	25	$A_{hs,SD}[m^2]$	9.0843 $* 10^{-5}$	$\leq 0.01$
	$D_{SD,bw}(\mu m)$	300	$I_{bw,SD}[A]$	1.0017	$\leq 20$
	$\lambda_{SD}[FIT]$		$6.6792 * 10^{-3}$		
	$R_{SD}[\%]$		85.189		
	$MTTF[hrs]$		149.7185		
$\geq 2SD$	$v_{applied}(V)$	520	$T_{j,SD}[^{\circ}C]$	72.9194	$\leq 125$
	$f_{sw}(kHz)$	8.0005	$Der(V)[\%]$	80	$\geq 80$
	$i_{SD,c}(A)$	16	$Der(I)[\%]$	80	$\geq 80$
	$t_{hs,b}(mm)$	45	$A_{hs,SD}[m^2]$	1.6352 $* 10^{-4}$	$\leq 0.01$
	$D_{SD,bw}(\mu m)$	350	$I_{bw,SD}[A]$	1.8292	$\leq 20$
	$N_{SD}$	8	$Space_{pcb}[\#]$	8	$\leq 20$
	—	—	$Budget_{SD}[\$]$	485.04	$\leq 500$
	$\lambda_{SD}[FIT]$		$7.1173 * 10^{-8}$		
	$R_{sys}[\%]$		99.9999		
	$MTTF[hrs]$		406.9136		

Fig. 5.4: Single switching device failure rate ( $\lambda_{SD}$ ) convergence (HHO)

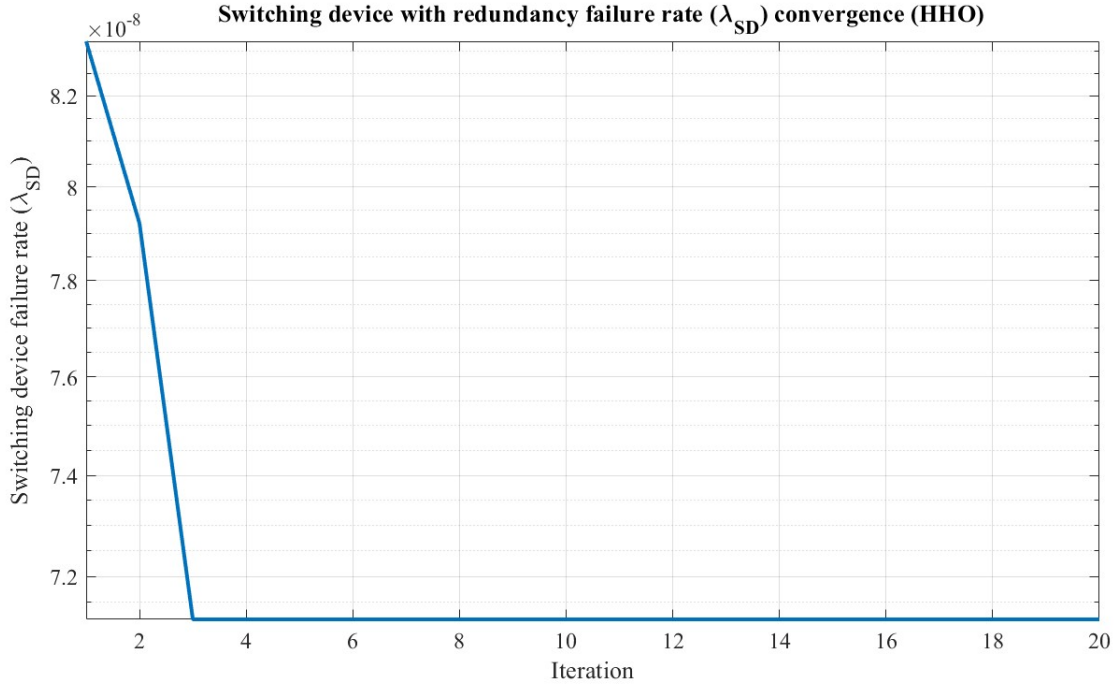


Fig. 5.5: Switching device with redundancy failure rate ( $\lambda_{SD}$ ) convergence (HHO)

Table 5.4: Single switching device lifetime optimized parameters (HHO)

$\Delta$	Design Parameter	Optimum value	Constraint	Actual Value	Min/Max value
-	$v_{applied}(V)$	520	$T_{j,SD}[^{\circ}C]$	72.9194	$\leq 125$
	$f_{sw}(kHz)$	8.0005	$Der(V)[\%]$	80	$\geq 80$
	$i_{SD,c}(A)$	16	$Der(I)[\%]$	80	$\geq 80$
	$t_{hs,b}(mm)$	25	$A_{hs,SD}[m^2]$	9.0843 $\times 10^{-5}$	$\leq 0.01$
	$D_{SD,bw}(\mu m)$	300	$I_{bw,SD}[A]$	1.0017	$\leq 20$
	$N_{f0,SD}[\text{cycles}]$		$28 * 10^3$		
	$N_{f,SD}[\text{cycles}]$		$24.581 * 10^3$		
Der	$v_{applied}(V)$	422.5	$T_{j,SD}[^{\circ}C]$	59.4147	$\leq 125$
	$f_{sw}(kHz)$	8.0005	$Der(V)[\%]$	65	$\geq 65$
	$i_{SD,c}(A)$	13	$Der(I)[\%]$	65	$\geq 65$
	$t_{hs,b}(mm)$	25	$A_{hs,SD}[m^2]$	9.0843 $\times 10^{-5}$	$\leq 0.01$
	$D_{SD,bw}(\mu m)$	300	$I_{bw,SD}[A]$	1.0017	$\leq 20$
	$N_{f0,SD}[\text{cycles}]$		$28 * 10^3$		
	$N_{f,SD}[\text{cycles}]$		$38.141 * 10^3$		

The last optimization done with the HHO algorithm corresponds to the lifetime optimization of the switching device, measured in cycles. These parameters are shown in Table 5.4, where it is shown how the lifetime of the component used will depend on the parameters of the designer, as stated with the capacitor. When the minimum deration is lowered, the switching device can have a longer lifetime with more than 50% extra cycles.

The convergence was also analyzed for the switching device cycles to failure using the HHO algorithm, and it is shown in Fig. 5.6.

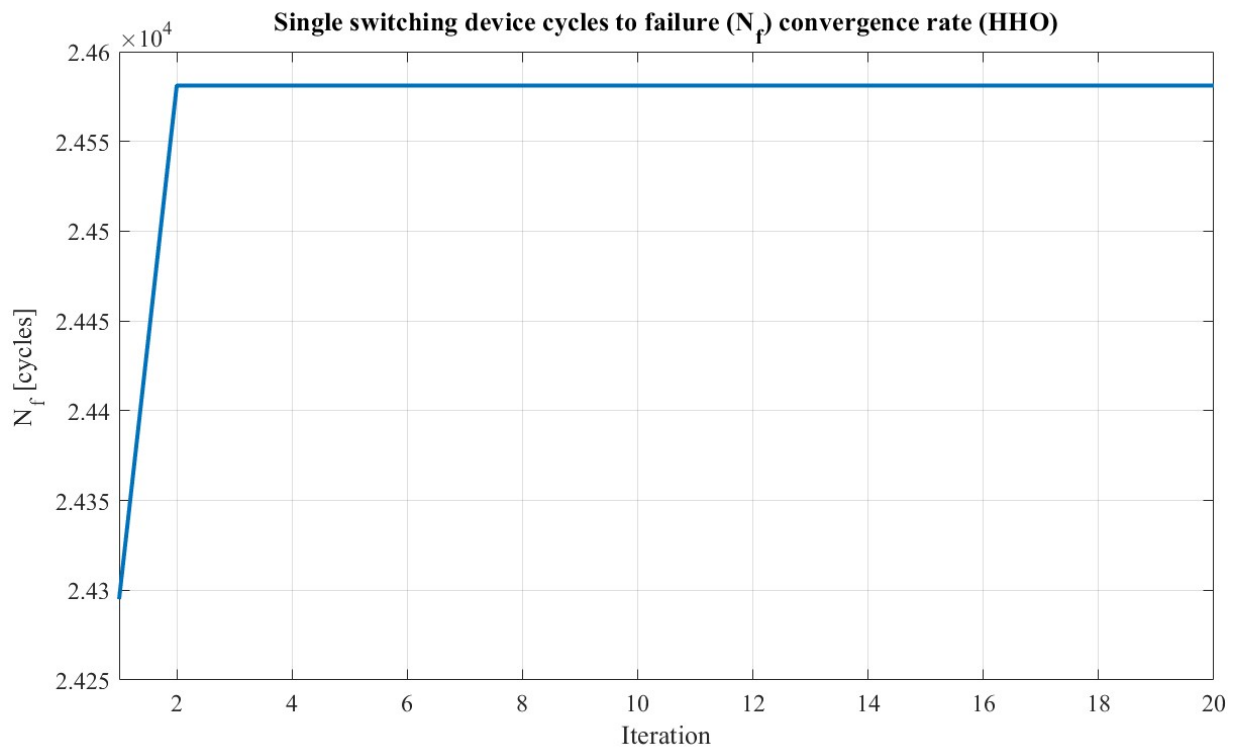


Fig. 5.6: Single switching device cycles to failure ( $N_f$ ) convergence (HHO)

## 5.2 PARTICLE SWARM OPTIMIZATION ALGORITHM RESULTS

The second optimization algorithm tested was the Particle Swarm optimization algorithm, first focusing on the converter's useful time phase, modeled at a component level. Table 5.5 models the capacitor failure rate optimized parameters using the PSO algorithm, and it analyzes the reliability of a single component (capacitor) and the reliability when the redundancy of this component is considered. In addition, Fig. 5.7 and Fig. 5.8 illustrate the convergence rate for the PSO algorithm when a single capacitor is considered and when multiple capacitors are considered respectively.

Table 5.5: Capacitor failure rate optimized parameters (PSO)

	<b>Design Parameter</b>	<b>Optimum value</b>	<b>Constraint</b>	<b>Actual Value</b>	<b>Min/Max value</b>
1Cap	$v_{applied}(V)$	520	$A_{cap,max}[m^2]$	6.2832 $* 10^{-8}$	$\leq 0.0707$
	$f_{sw}(kHz)$	40	$AR_{cap}$	1.75	$1 \leq AR_{cap} \leq 2$
	$L_{elCap}(mm)$	175	$I_{rip,max} [\%]$	10	$\leq 50$
	$D_{elCap}(mm)$	100	$Der(V)[\%]$	80	$\geq 80$
	$\lambda_{Cap}[FIT]$		0.0650		
	$R_{cap} [\%]$		21		
	$MTTF[hrs]$		15.3796		
$\geq 2Cap$	$v_{applied}(V)$	520	$A_{cap,max}[m^2]$	6.2832 $* 10^{-8}$	$\leq 0.0707$
	$f_{sw}(kHz)$	40	$AR_{cap}$	1.75	$1 \leq AR_{cap} \leq 2$
	$L_{elCap}(mm)$	175	$I_{rip,max} [\%]$	10	$\leq 50\%$
	$D_{elCap}(mm)$	100	$Der(V)[\%]$	80	$\geq 80$
	$N_{cap}$	14	$Space_{pcb}[\#]$	14	$\leq 14$
	-	-	$Budget_{cap}[\$]$	738.64	$\leq 750$
	$\lambda_{Cap}[FIT]$		0.00926		
	$R_{sys} [\%]$		96.314		
	$MTTF[hrs]$		50.0079		

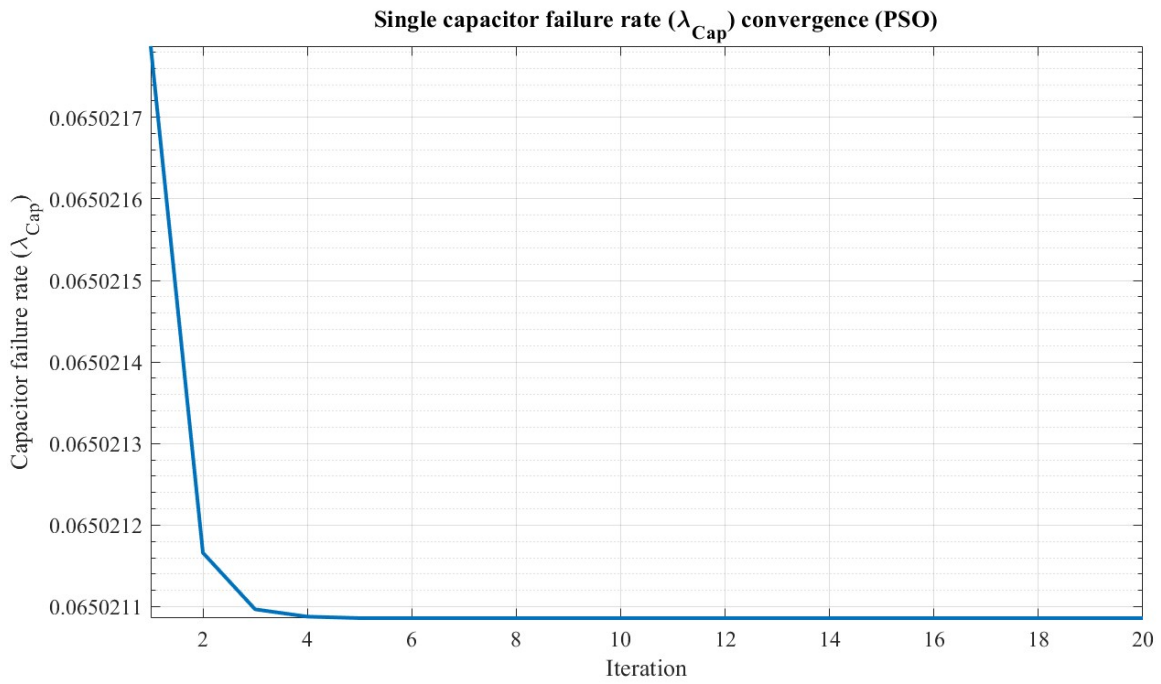


Fig. 5.7: Single capacitor failure rate ( $\lambda_{cap}$ ) convergence (PSO)

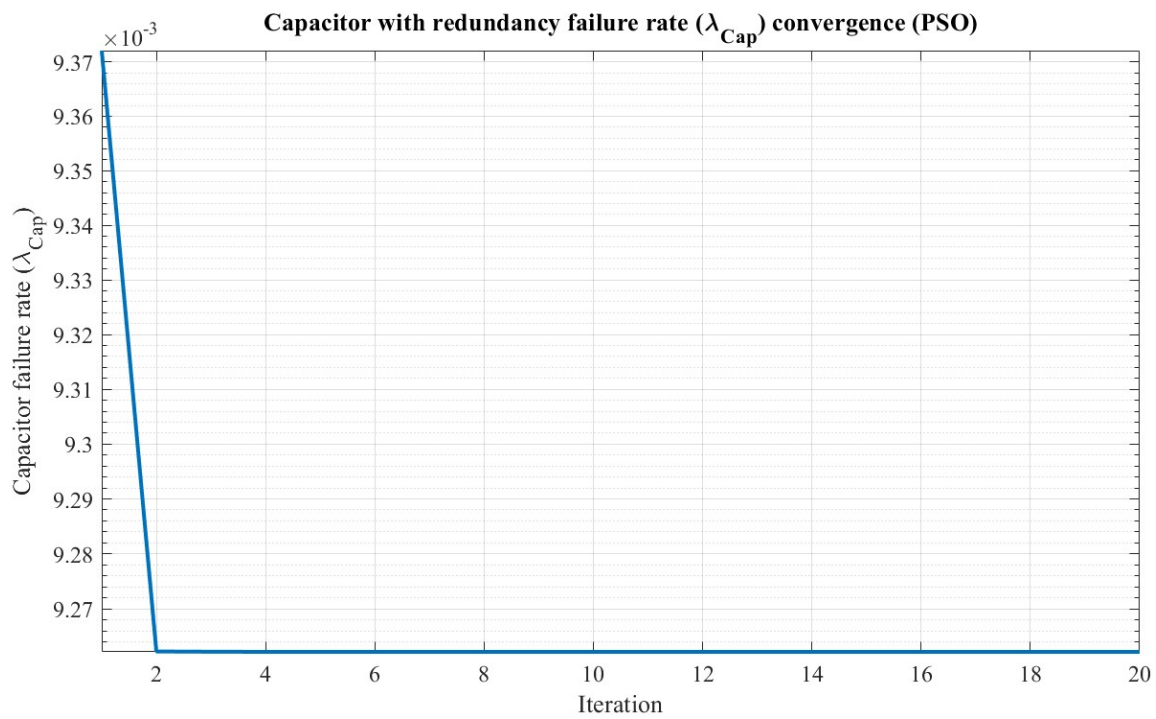


Fig. 5.8: Capacitor with redundancy failure rate ( $\lambda_{cap}$ ) convergence (PSO)

Table 5.6: Single capacitor lifetime optimized parameters (PSO)

$\Delta$	Design Parameter	Optimum value	Constraint	Actual Value	Min/Max value
–	$v_{applied}(V)$	520	$A_{cap,max}[m^2]$	$1.3744 * 10^{-4}$	$\leq 0.0707$
	$f_{sw}(kHz)$	8.0005	$AR_{cap}$	1.5	$1 \leq AR_{cap} \leq 2$
	$L_{elCap}(mm)$	7.5	$I_{rip,max} [\%]$	50	$\leq 50$
	$D_{elCap}(mm)$	5	$Der(V)[\%]$	80	$\geq 80$
	$L_0[yr]$		1		
	$L_{x,Cap}[yr]$		8.8566		
Der	$v_{applied}(V)$	422.5	$A_{cap,max}[m^2]$	$1.3744 * 10^{-4}$	$\leq 0.0707$
	$f_{sw}(kHz)$	8.0005	$AR_{cap}$	1.5	$1 \leq AR_{cap} \leq 2$
	$L_{elCap}(mm)$	7.5	$I_{rip,max} [\%]$	50	$\leq 50\%$
	$D_{elCap}(mm)$	5	$Der(V)[\%]$	65	$\geq 65$
	$L_0[yr]$		1		
	$L_{x,Cap}[yr]$		25.012		
$I_{rip}$	$v_{applied}(V)$	520	$A_{cap,max}[m^2]$	$1.3744 * 10^{-4}$	$\leq 0.0707$
	$f_{sw}(kHz)$	6.897	$AR_{cap}$	1.5	$1 \leq AR_{cap} \leq 2$
	$L_{elCap}(mm)$	7.5	$I_{rip,max} [\%]$	58	$\leq 58$
	$D_{elCap}(mm)$	5	$Der(V)[\%]$	80	$\geq 80$
	$L_0[yr]$		1		
	$L_{x,Cap}[yr]$		19.869		

On the other hand, Table 5.6 presents the optimized parameters for a single capacitor lifetime improvement without considering redundancy. From this table, it is clear that when the constrictions are changed, the lifetime can also change, as it happened with the changes in the minimum deration and maximum ripple current percentage. Because of this, it is implied that the converter's designer will have to choose the constrictions appropriately to get the maximum lifetime possible for each component.

To illustrate the convergence rate of a single capacitor lifetime using the PSO algorithm Fig. 5.9 was included.

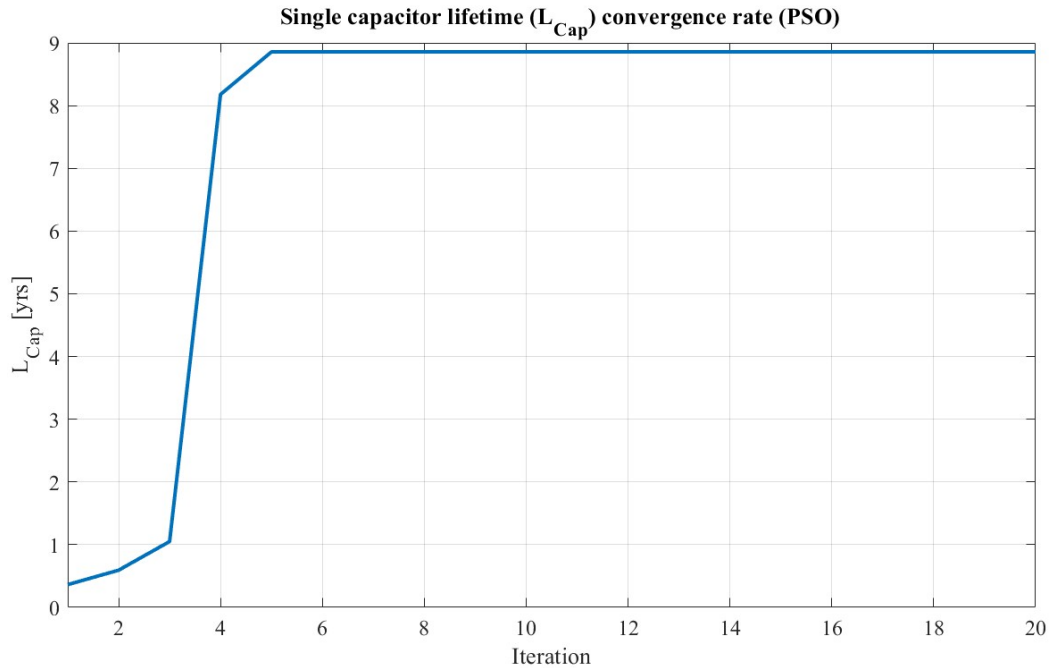


Fig. 5.9. Single capacitor lifetime ( $L_{Cap}$ ) convergence (PSO)

On the other hand, Table 5.7 analyzes the failure rate of the other crucial component, the switching device. Tuning the parameters corresponding to the switching device will directly impact the performance of the power electronic converter. As with the capacitor, the possibility of just a single switching device was analyzed, and more than one switching device was added to the system to increase its reliability.

Table 5.7 shows that including more components in the system will increase its overall reliability because a backup device keeps the system running when one fails. The optimized value for the total number of switching devices in the system was 8, which brings the system's overall reliability up to almost 100%.

Fig. 5.10 and Fig. 5.11 show the convergence of the Particle swarm optimization algorithm for a single switching device and multiple switching devices respectively.

Table 5.7. Switching device failure rate optimized parameters (PSO)

	<b>Design Parameter</b>	<b>Optimum value</b>	<b>Constraint</b>	<b>Actual Value</b>	<b>Min/Max value</b>
1SD	$v_{applied}(V)$	520	$T_{j,SD}[^{\circ}C]$	72.9194	$\leq 125$
	$f_{sw}(kHz)$	8.0005	$Der(V)[\%]$	80	$\geq 80$
	$i_{SD,c}(A)$	16	$Der(I)[\%]$	80	$\geq 80$
	$t_{hs,b}(mm)$	40	$A_{hs,SD}[m^2]$	$1.4535 * 10^{-4}$	$\leq 0.01$
	$D_{SD,bw}(\mu m)$	400	$I_{bw,SD}[A]$	1.6232	$\leq 20$
	$\lambda_{SD}[FIT]$	$6.6792 * 10^{-3}$			
	$R_{SD}[\%]$	85.189			
	$MTTF[hrs]$	149.7185			
$\geq 2SD$	$v_{applied}(V)$	520	$T_{j,SD}[^{\circ}C]$	72.9194	$\leq 125$
	$f_{sw}(kHz)$	8.0005	$Der(V)[\%]$	80	$\geq 80$
	$i_{SD,c}(A)$	16	$Der(I)[\%]$	80	$\geq 80$
	$t_{hs,b}(mm)$	40	$A_{hs,SD}[m^2]$	$1.4535 * 10^{-4}$	$\leq 0.01$
	$D_{SD,bw}(\mu m)$	350	$I_{bw,SD}[A]$	1.7246	$\leq 20$
	$N_{SD}$	8	$Space_{pcb}[\#]$	8	$\leq 20$
	—	—	$Budget_{SD}[\$]$	485.04	$\leq 500$
	$\lambda_{SD}[FIT]$	$7.1173 * 10^{-8}$			
	$R_{sys}[\%]$	99.9999			
	$MTTF[hrs]$	406.9136			

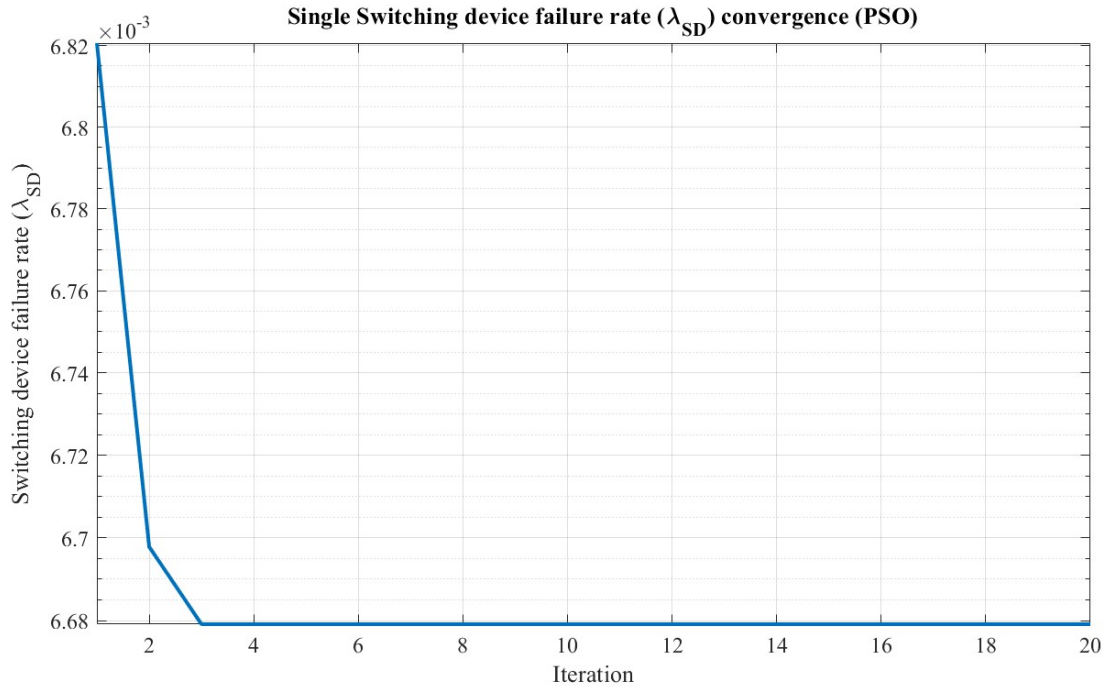


Fig. 5.10. Single switching device failure rate ( $\lambda_{SD}$ ) convergence (PSO)

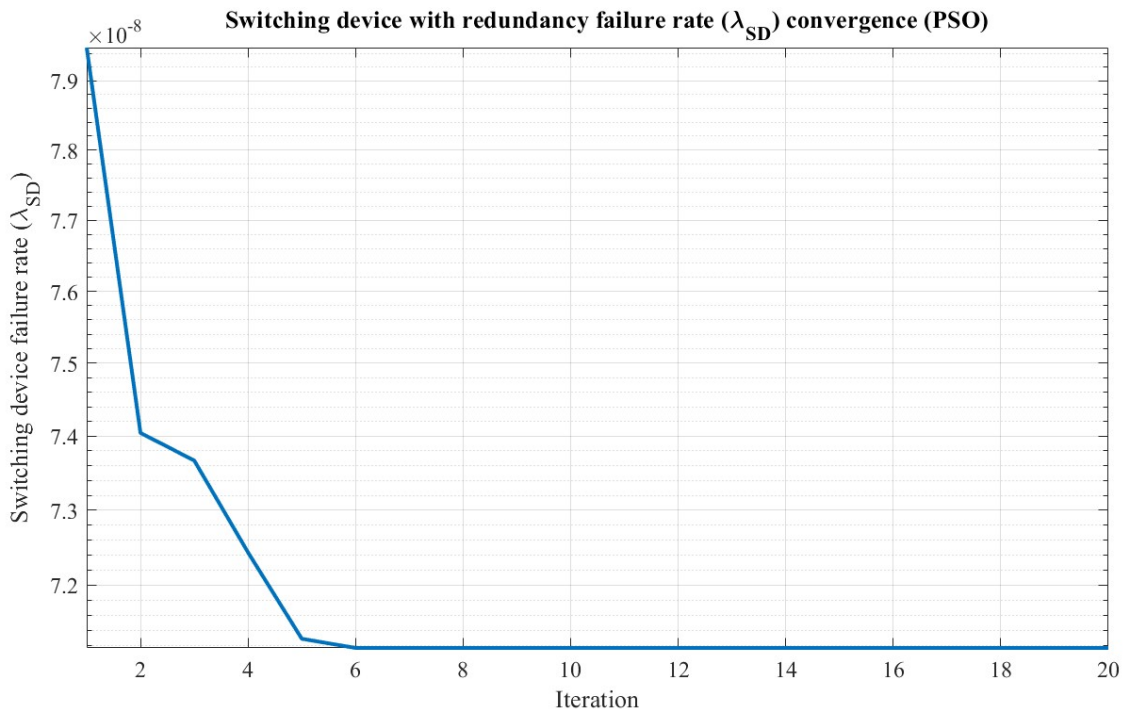


Fig. 5.11. Switching device with redundancy failure rate ( $\lambda_{SD}$ ) convergence (PSO)

Table 5.8: Single switching device lifetime optimized parameters (PSO)

$\Delta$	Design Parameter	Optimum value	Constraint	Actual Value	Min/Max value
–	$v_{applied}(V)$	520	$T_{j,SD}[^{\circ}C]$	72.9194	$\leq 125$
	$f_{sw}(kHz)$	8.0005	$Der(V)[\%]$	80	$\geq 80$
	$i_{SD,c}(A)$	16	$Der(I)[\%]$	80	$\geq 80$
	$t_{hs,b}(mm)$	25	$A_{hs,SD}[m^2]$	9.0843 $* 10^{-5}$	$\leq 0.01$
	$D_{SD,bw}(\mu m)$	300	$I_{bw,SD}[A]$	1.0017	$\leq 20$
	$N_{f0,SD}[\text{cycles}]$		$28 * 10^3$		
	$N_{f,SD}[\text{cycles}]$		$24.581 * 10^3$		
Der	$v_{applied}(V)$	422.5	$T_{j,SD}[^{\circ}C]$	59.4147	$\leq 125$
	$f_{sw}(kHz)$	8.0005	$Der(V)[\%]$	65	$\geq 65$
	$i_{SD,c}(A)$	13	$Der(I)[\%]$	65	$\geq 65$
	$t_{hs,b}(mm)$	25	$A_{hs,SD}[m^2]$	9.0843 $* 10^{-5}$	$\leq 0.01$
	$D_{SD,bw}(\mu m)$	300	$I_{bw,SD}[A]$	1.0017	$\leq 20$
	$N_{f0,SD}[\text{cycles}]$		$28 * 10^3$		
	$N_{f,SD}[\text{cycles}]$		$38.141 * 10^3$		

The last optimization done with the PSO corresponds to the lifetime optimization of the switching device, measured in cycles. These parameters are shown in Table 5.8. As with the capacitor, the designer-imposed parameter constrictions could affect the overall lifetime. For example, when the minimum deration is lowered, the switching device can have a longer life with more than 50% extra cycles, which could be considered to improve reliability when designed.

The convergence was also analyzed for the switching device cycles to failure using the PSO algorithm, shown in Fig. 5.12.

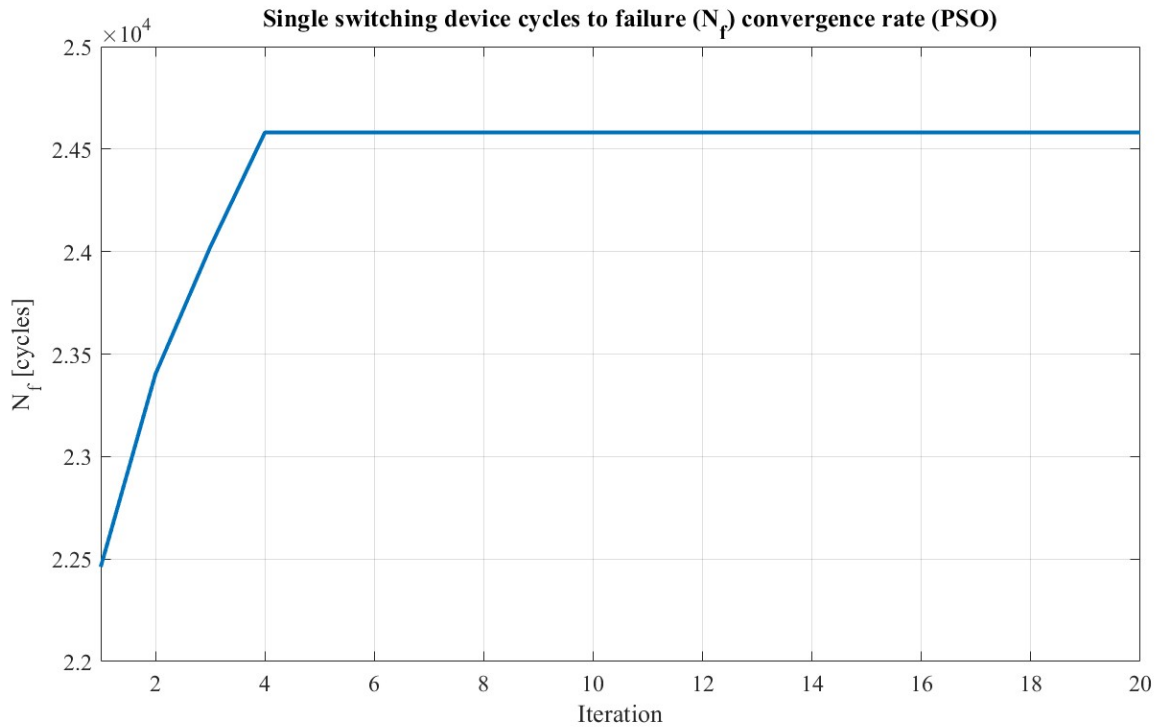


Fig. 5.12: Single switching device cycles to failure ( $N_f$ ) convergence (PSO)

### 5.3 ARTIFICIAL BEE COLONY OPTIMIZATION ALGORITHM RESULTS

The third optimization algorithm tested was the Artificial bee colony algorithm, firstly while focusing on the useful time phase of the converter, modeled at a component level. Table 5.9 models the capacitor failure rate optimized parameters using the ABC algorithm, and it analyzes the reliability of a single component (capacitor) as well as the reliability when the redundancy of its components is considered. In addition, Fig. 5.13 and Fig. 5.14 illustrate the convergence rate for the ABC algorithm when a single capacitor is taken into account and when multiple capacitors are taken into account respectively.

Table 5.9: Capacitor failure rate optimized parameters (ABC)

	<b>Design Parameter</b>	<b>Optimum value</b>	<b>Constraint</b>	<b>Actual Value</b>	<b>Min/Max value</b>
1Cap	$v_{applied}(V)$	520	$A_{cap,max}[m^2]$	5.7079 $* 10^{-8}$	$\leq 0.0707$
	$f_{sw}(kHz)$	40	$AR_{cap}$	1.7632	$1 \leq AR_{cap} \leq 2$
	$L_{elCap}(mm)$	167.5	$I_{rip,max}[\%]$	10	$\leq 50$
	$D_{elCap}(mm)$	95	$Der(V)[\%]$	80	$\geq 80$
	$\lambda_{Cap}[FIT]$			0.0650	
	$R_{cap}[\%]$			21	
	$MTTF[hrs]$			15.3796	
$\geq 2Cap$	$v_{applied}(V)$	520	$A_{cap,max}[m^2]$	6.2832 $* 10^{-8}$	$\leq 0.0707$
	$f_{sw}(kHz)$	40	$AR_{cap}$	1.75	$1 \leq AR_{cap} \leq 2$
	$L_{elCap}(mm)$	175	$I_{rip,max}[\%]$	10	$\leq 50\%$
	$D_{elCap}(mm)$	100	$Der(V)[\%]$	80	$\geq 80$
	$N_{cap}$	14	$Space_{pcb}[\#]$	14	$\leq 14$
	-	-	$Budget_{cap}[\$]$	738.64	$\leq 750$
	$\lambda_{Cap}[FIT]$			0.00926	
	$R_{sys}[\%]$			96.314	
	$MTTF[hrs]$			50.0079	

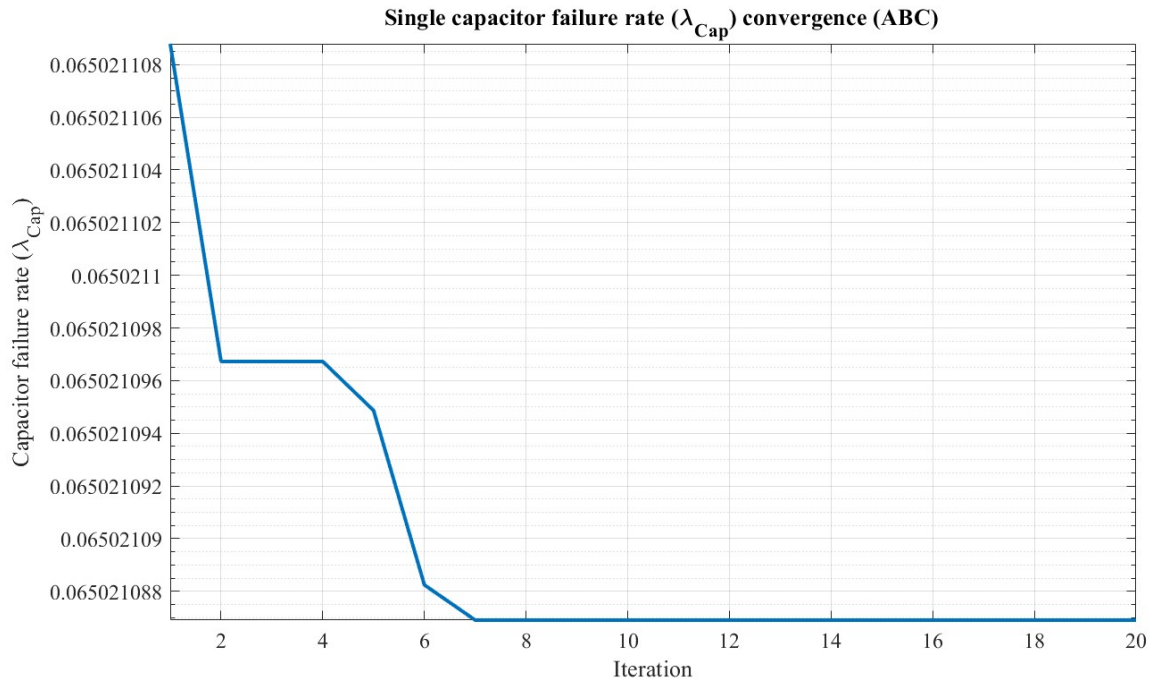


Fig. 5.13: Single capacitor failure rate ( $\lambda_{cap}$ ) convergence (ABC)

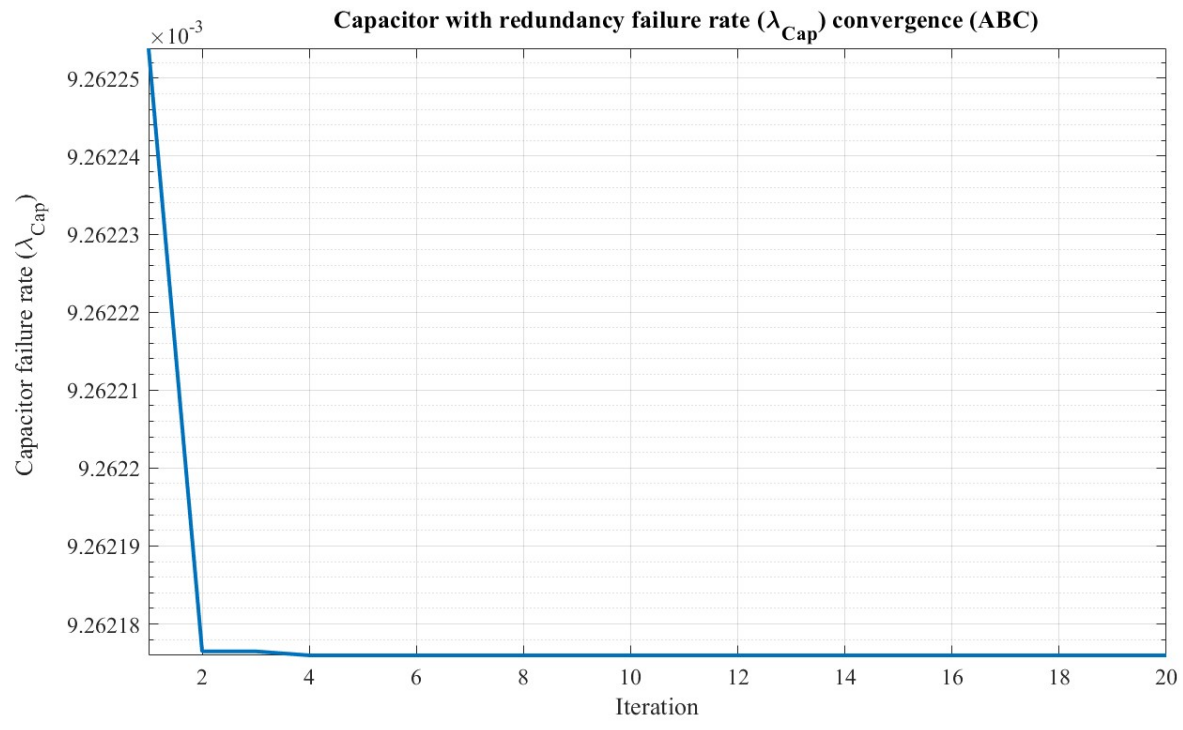


Fig. 5.14: Capacitor with redundancy failure rate ( $\lambda_{cap}$ ) convergence (ABC)

Table 5.10: Single capacitor lifetime optimized parameters (ABC)

$\Delta$	Design Parameter	Optimum value	Constraint	Actual Value	Min/Max value
–	$v_{applied}(V)$	520	$A_{cap,max}[m^2]$	$1.3744 * 10^{-4}$	$\leq 0.0707$
	$f_{sw}(kHz)$	8.0005	$AR_{cap}$	1.5	$1 \leq AR_{cap} \leq 2$
	$L_{elCap}(mm)$	7.5	$I_{rip,max} [\%]$	50	$\leq 50$
	$D_{elCap}(mm)$	5	$Der(V)[\%]$	80	$\geq 80$
	$L_0[yrs]$		1		
	$L_{x,Cap}[yrs]$		8.8566		
Der	$v_{applied}(V)$	422.5	$A_{cap,max}[m^2]$	$1.3744 * 10^{-4}$	$\leq 0.0707$
	$f_{sw}(kHz)$	8.0005	$AR_{cap}$	1.5	$1 \leq AR_{cap} \leq 2$
	$L_{elCap}(mm)$	7.5	$I_{rip,max} [\%]$	50	$\leq 50\%$
	$D_{elCap}(mm)$	5	$Der(V)[\%]$	65	$\geq 65$
	$L_0[yrs]$		1		
	$L_{x,Cap}[yrs]$		25.012		
$I_{rip}$	$v_{applied}(V)$	520	$A_{cap,max}[m^2]$	$1.3744 * 10^{-4}$	$\leq 0.0707$
	$f_{sw}(kHz)$	6.897	$AR_{cap}$	1.5	$1 \leq AR_{cap} \leq 2$
	$L_{elCap}(mm)$	7.5	$I_{rip,max} [\%]$	58	$\leq 58$
	$D_{elCap}(mm)$	5	$Der(V)[\%]$	80	$\geq 80$
	$L_0[yrs]$		1		
	$L_{x,Cap}[yrs]$		19.869		

The lifetime of a single capacitor without considering redundancy was also optimized, and its optimized parameters are shown in Table 5.10. Once again, a favorable change in the constrictions imposed by the designer can increase the capacitor's up to almost 200%. This is the case of the minimum deration, and maximum ripple current allowed, with noticeable increments in the total lifetime of the capacitor.

To illustrate the convergence rate of a single capacitor lifetime using the ABC algorithm, Fig. 5.15 was included.

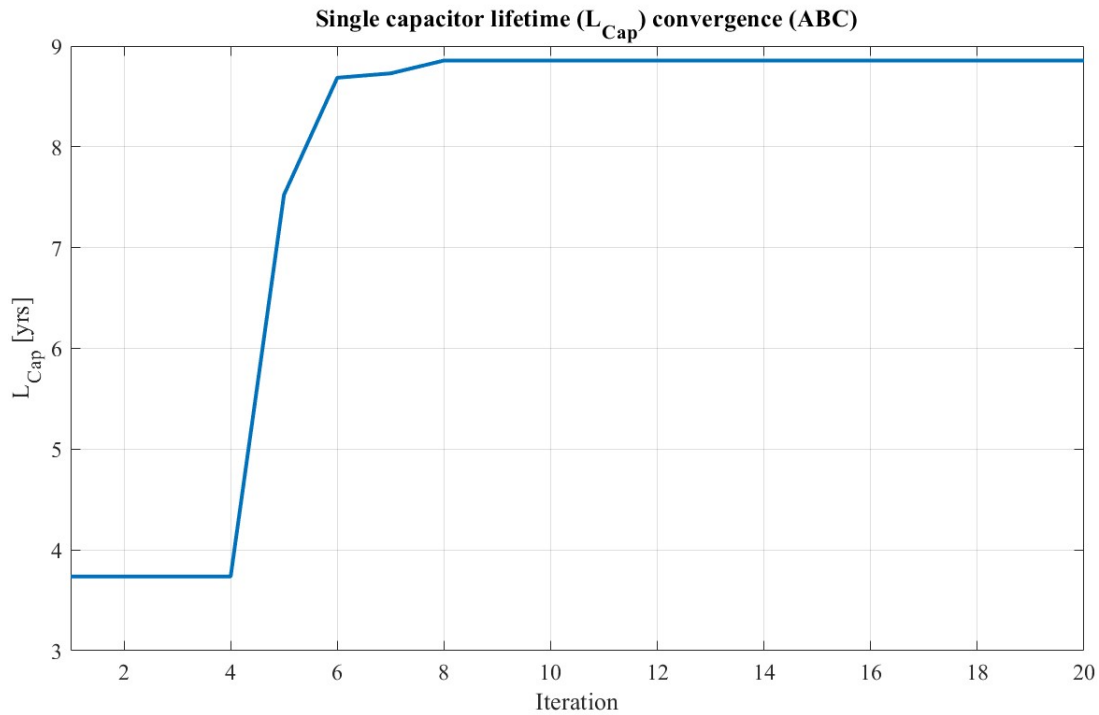


Fig. 5.15: Single capacitor lifetime  $L_{cap}$  convergence (ABC)

For a global system failure rate and reliability analysis, it is also essential to consider the switching device, which was analyzed in Table 5.11. This analysis of the most optimum parameters will allow the designer to decrease the failure rate of the switching device as much as possible and, therefore, the system's overall failure rate. As with the capacitor, the possibility of just a single switching device was analyzed, and more than one switching device was added to the system to increase its reliability.

As mentioned before, the more backup components a system has, the more reliable it is, and this possibility of redundancy is depicted in Table 5.11, where the usage of 8 switching devices increases the reliability of the overall system up to almost 100%.

Fig. 5.16 and Fig. 5.17 show the convergence of the Artificial bee colony algorithm for a single switching device and multiple switching devices algorithm respectively.

Table 5.11: Switching device failure rate optimized parameters (ABC)

	<b>Design Parameter</b>	<b>Optimum value</b>	<b>Constraint</b>	<b>Actual Value</b>	<b>Min/Max value</b>
1SD	$v_{applied}(V)$	520	$T_{j,SD}[^{\circ}C]$	72.9194	$\leq 125$
	$f_{sw}(kHz)$	8.0005	$Der(V)[\%]$	80	$\geq 80$
	$i_{SD,c}(A)$	16	$Der(I)[\%]$	80	$\geq 80$
	$t_{hs,b}(mm)$	35	$A_{hs,SD}[m^2]$	$1.2718 * 10^{-4}$	$\leq 0.01$
	$D_{SD,bw}(\mu m)$	400	$I_{bw,SD}[A]$	2.107	$\leq 20$
	$\lambda_{SD}[FIT]$	$6.6792 * 10^{-3}$			
	$R_{SD}[\%]$	85.189			
	$MTTF[hrs]$	149.7185			
$\geq 2SD$	$v_{applied}(V)$	520	$T_{j,SD}[^{\circ}C]$	72.9194	$\leq 125$
	$f_{sw}(kHz)$	8.0005	$Der(V)[\%]$	80	$\geq 80$
	$i_{SD,c}(A)$	16	$Der(I)[\%]$	80	$\geq 80$
	$t_{hs,b}(mm)$	40	$A_{hs,SD}[m^2]$	$1.4535 * 10^{-4}$	$\leq 0.01$
	$D_{SD,bw}(\mu m)$	400	$I_{bw,SD}[A]$	2.2525	$\leq 20$
	$N_{SD}$	8	$Space_{pcb}[\#]$	8	$\leq 20$
	—	—	$Budget_{SD}[\$]$	485.04	$\leq 500$
	$\lambda_{SD}[FIT]$	$7.1173 * 10^{-8}$			
	$R_{sys}[\%]$	99.9999			
	$MTTF[hrs]$	406.9136			

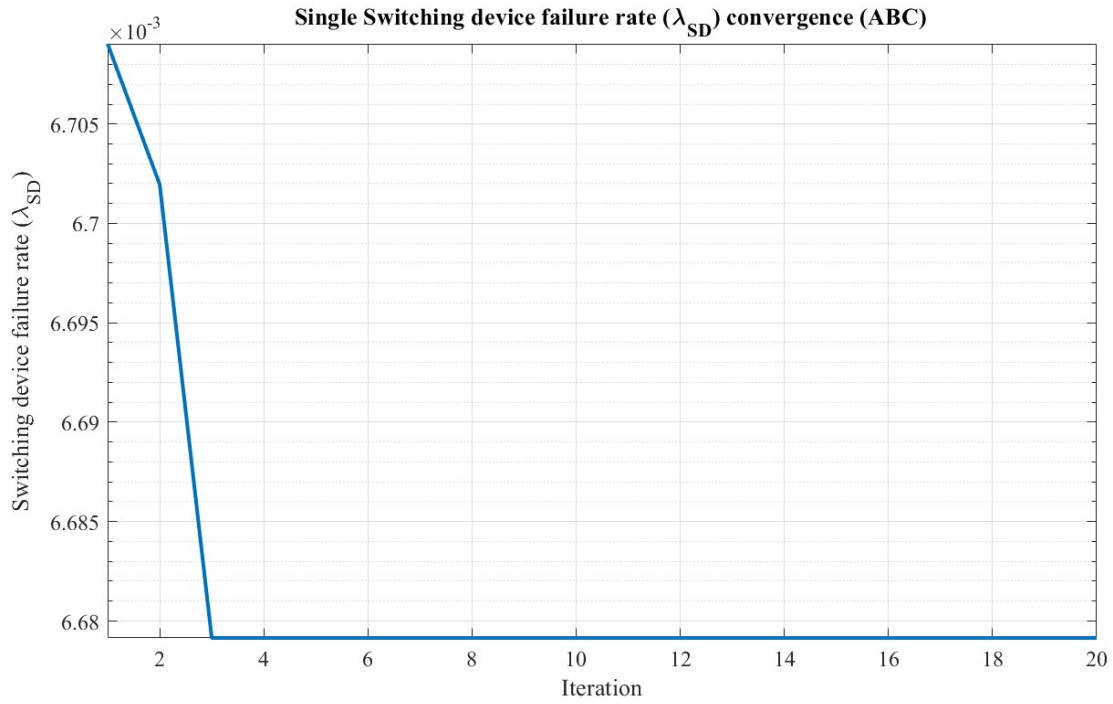


Fig. 5.16: Single switching device failure rate ( $\lambda_{SD}$ ) convergence (ABC)

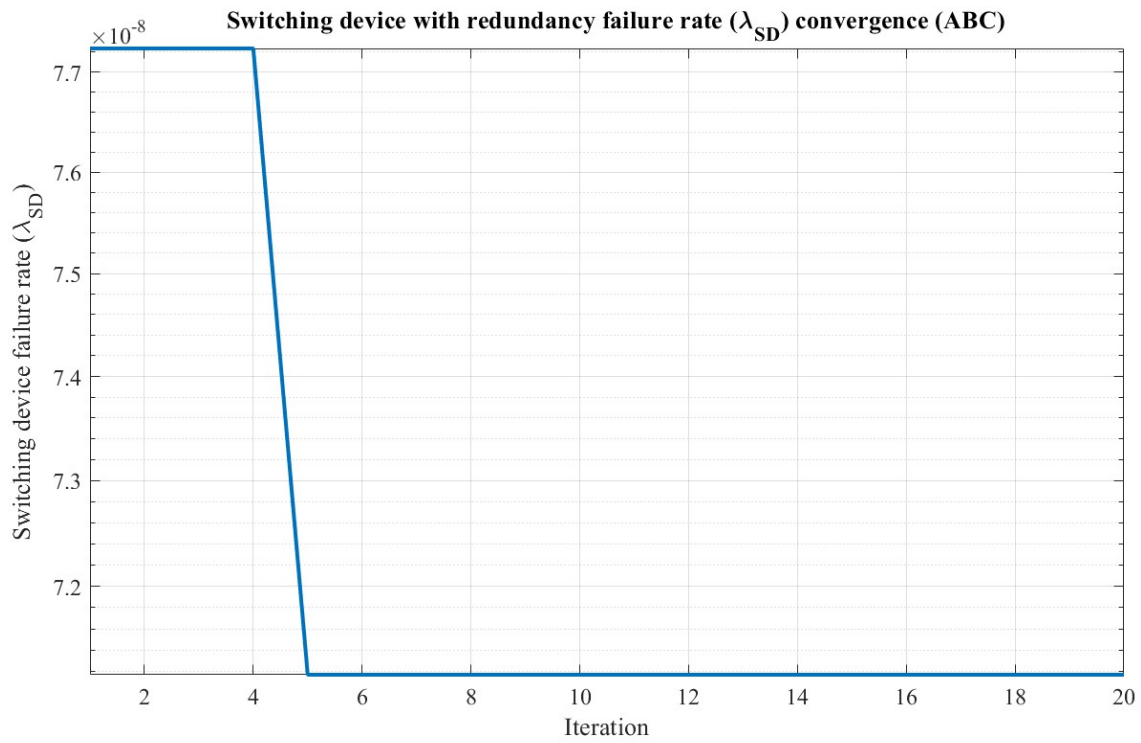


Fig. 5.17: Switching device with redundancy failure rate ( $\lambda_{SD}$ ) convergence (ABC)

Table 5.12: Single switching device lifetime optimized parameters (ABC)

$\Delta$	Design Parameter	Optimum value	Constraint	Actual Value	Min/Max value
–	$v_{applied}(V)$	520	$T_{j,SD}[^{\circ}C]$	72.9194	$\leq 125$
	$f_{sw}(kHz)$	8.0005	$Der(V)[\%]$	80	$\geq 80$
	$i_{SD,c}(A)$	16	$Der(I)[\%]$	80	$\geq 80$
	$t_{hs,b}(mm)$	25	$A_{hs,SD}[m^2]$	9.0843 $* 10^{-5}$	$\leq 0.01$
	$D_{SD,bw}(\mu m)$	300	$I_{bw,SD}[A]$	1.0017	$\leq 20$
	$N_{f0,SD}[\text{cycles}]$		$28 * 10^3$		
	$N_{f,SD}[\text{cycles}]$		$24.581 * 10^3$		
Der	$v_{applied}(V)$	422.5	$T_{j,SD}[^{\circ}C]$	59.4147	$\leq 125$
	$f_{sw}(kHz)$	8.0005	$Der(V)[\%]$	65	$\geq 65$
	$i_{SD,c}(A)$	13	$Der(I)[\%]$	65	$\geq 65$
	$t_{hs,b}(mm)$	35	$A_{hs,SD}[m^2]$	1.2718 $* 10^{-4}$	$\leq 0.01$
	$D_{SD,bw}(\mu m)$	300	$I_{bw,SD}[A]$	1.1852	$\leq 20$
	$N_{f0,SD}[\text{cycles}]$		$28 * 10^3$		
	$N_{f,SD}[\text{cycles}]$		$38.141 * 10^3$		

The last optimization done with the ABC corresponds to the lifetime optimization of the switching device, measured in cycles. These parameters are shown in Table 5.12, showing how important the designer's role will be in adequately tuning the parameter constrictions to extend the switching device's lifetime. As with the HHO and the PSO, a change in the deration brought the cycles to failure 50% higher, significantly extending the lifetime of the switching device.

The convergence was also analyzed for the switching device cycles to failure using the ABC algorithm, shown in Fig. 5.18.

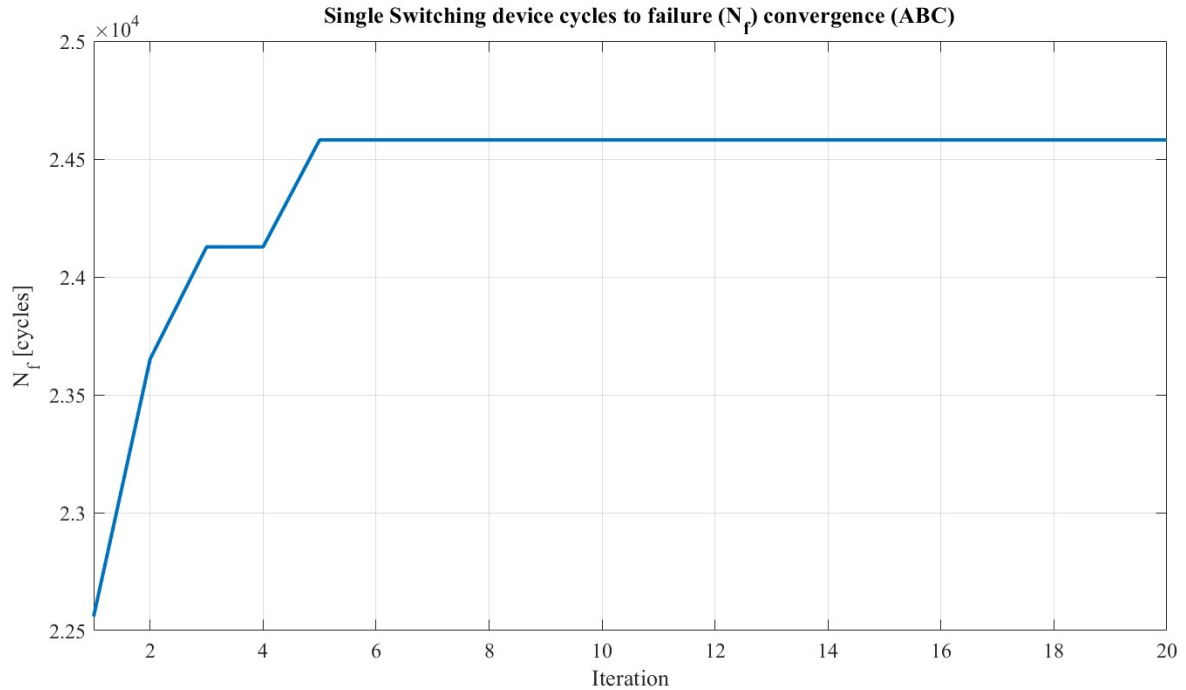


Fig. 5.18: Single switching device cycles to failure ( $N_f$ ) convergence (ABC)

#### 5.4 NUMBER OF COMPONENTS VS PERFORMANCE

The reliability of each system component can be optimized up to a certain point, where constrictions such as space and cost or parameters such as maximum current and voltage will restrict further optimization. However, even though the reliability of a single component in a system is not extremely high, the addition of duplicated components (redundancy) will allow the system to keep running if one of them happens to fail. This will allow the people in charge of the maintenance of the system to change the defective component for a fully functional one so that the system can function at its 100% capabilities again without stopping its functioning.

Because of the improvement in the overall reliability and lifetime of a system, including redundancy, the number of components in a system was analyzed in terms of the performance that they bring. Fig. 5.19 illustrates the improvement in a system in terms of system failure rate and system mean time to failure when more capacitors are added. The best value optimized for the system failure rate was found with  $N_{cap} = 14$ , which was restricted by the overall cost of the system being \$750. The system failure rate was approximately  $\lambda_{sys} = 0.00926$ , which translates into an overall reliability of 96.314%.

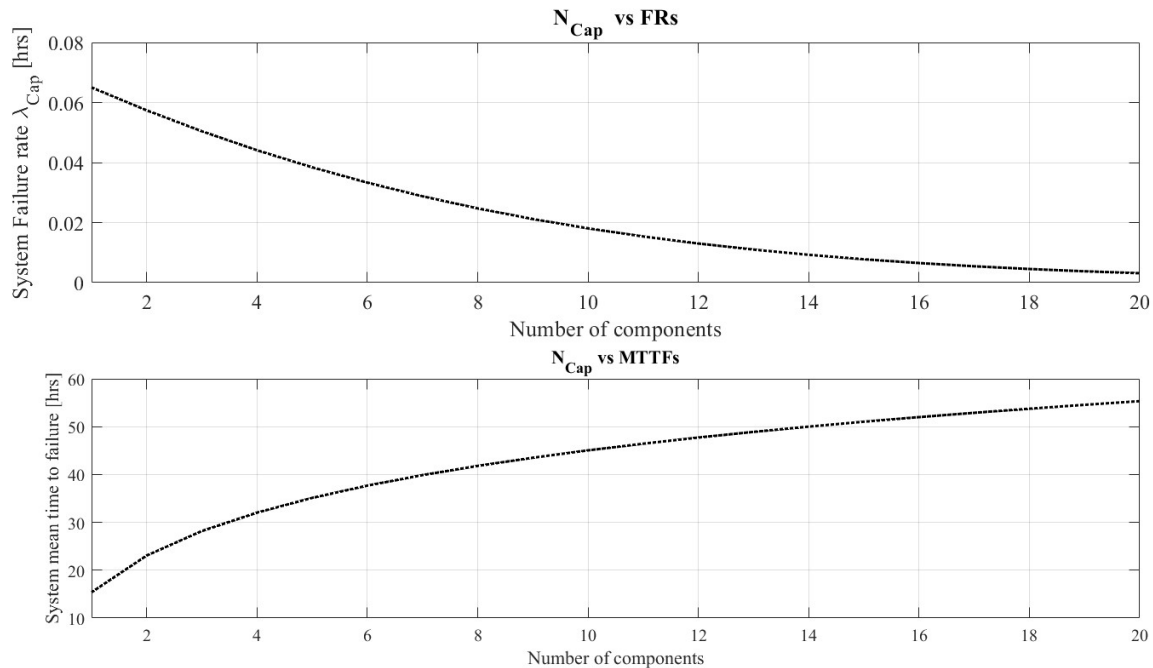


Fig. 5.19: Number of capacitors vs performance

The concept of redundancy also applies to the switching device, where an outstanding improvement was made when including redundancy, reaching an overall system's reliability of almost 100%. The number of components in a system was analyzed in terms of the performance that they bring. Fig. 5.20 illustrates the improvement in a system in terms of system failure rate and system mean time to failure when more switching devices are added. The best value optimized for the system failure rate was found with  $N_{SD} = 8$ , which was restricted by the overall cost of the system being \$500. The system failure rate was approximately  $\lambda_{sys} = 7.1173 * 10^{-8}$ , translating into an overall reliability of 99.9999%.

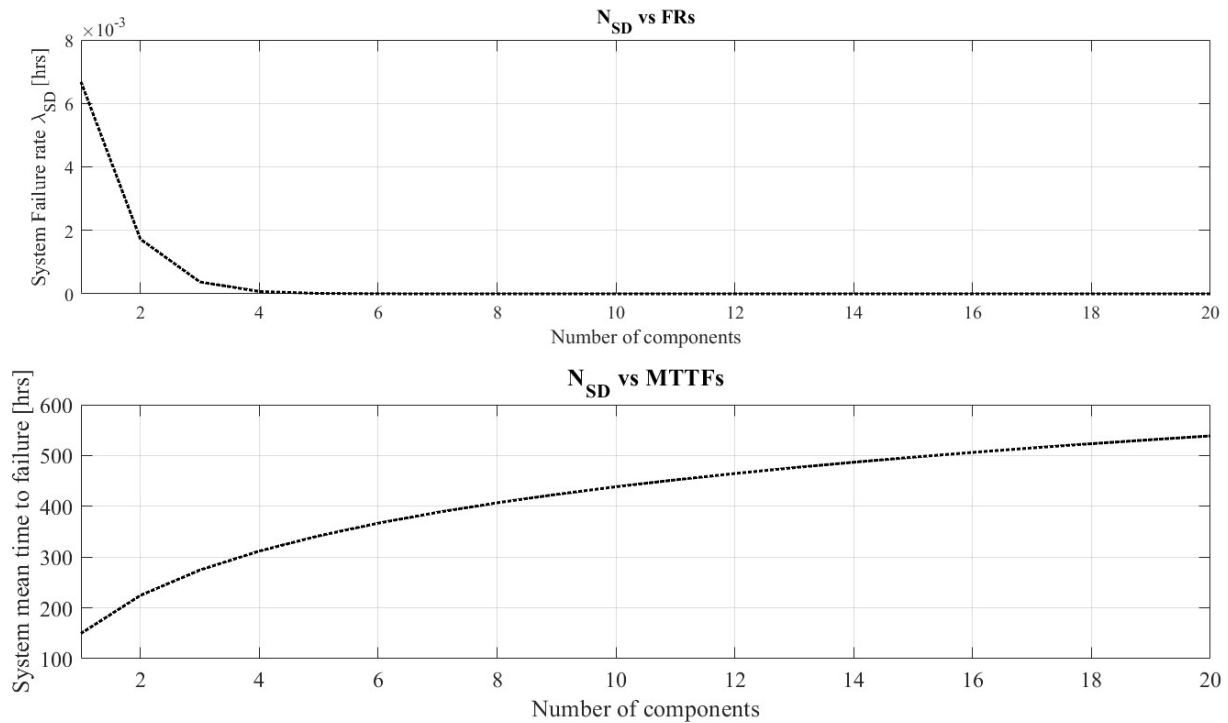


Fig. 5.20: Number of switching devices vs performance

## 5.5 GLOBAL OPTIMIZATION (USEFUL TIME PHASE)

The global optimization of the system was firstly done considering the useful time phase, directly related to the component level modeling, with  $\lambda_{cap}$  and  $\lambda_{SD}$  as a target to minimize. Table 5.13 and Table 5.14 show the useful time phase optimized results considering the modeling on a component level for each one of the algorithms proposed. The system's reliability overall was also considered, considering the reliability of the capacitor system and the switching device system individually. The overall reliability was found to be 96.3139 %, which could be improved if designer changes the parameter constrictions.

Table 5.13: Useful time phase optimized results

Algorithm	Design Parameter	Optimum value	Constraint	Actual Value	Min/Max value
HHO	$v_{applied}(V)$	520	$A_{cap,max}[m^2]$	$5.7079 * 10^{-8}$	$\leq 0.0707$
	$f_{sw}(kHz)$	8.0055	$AR_{cap}$	1.7632	$1 \leq AR_{cap} \leq 2$
	$i_{SD,c}(A)$	16	$I_{rip,max}[\%]$	50	$\leq 50$
	$L_{elCap}(mm)$	167.5	$Der(V)[\%]$	80	$\geq 80$
	$D_{elCap}(mm)$	95	$Der(I)[\%]$	80	$\geq 80$
	$D_{SD,bw}(\mu m)$	450	$A_{hs,SD}[m^2]$	$9.0843 * 10^{-5}$	$\leq 0.01$
	$t_{hs,b}(mm)$	25	$I_{bw,SD}[A]$	2.2538	$\leq 20$
	$N_{cap}$	14	$T_{j,SD}[^{\circ}C]$	72.9194	$\leq 125$
	$N_{SD}$	8	$Space_{pcb}[\#]$	[8, 14]	$\leq 20$
	–	–	$Budget_{cap}[\$]$	738.64	$\leq 750$
	–	–	$Budget_{SD}[\$]$	485.04	$\leq 500$
		$\lambda_{Cap}[FIT]$		0.009264	
	$R_{sys,cap}[\%]$		96.314		
	$\lambda_{SD}[FIT]$		$7.1173 * 10^{-8}$		
	$R_{sys,SD}[\%]$		99.9999		
	$R_{total}[\%]$		96.3139		

Table 5.14: Useful time phase optimized results

Algorithm	Design Parameter	Optimum value	Constraint	Actual Value	Min/Max value
PSO	$v_{applied}(V)$	520	$A_{cap,max}[m^2]$	$6.2832 * 10^{-8}$	$\leq 0.0707$
	$f_{sw}(kHz)$	8.0055	$AR_{cap}$	1.75	$1 \leq AR_{cap} \leq 2$
	$i_{SD,c}(A)$	16	$I_{rip,max}[\%]$	50	$\leq 50$
	$L_{elCap}(mm)$	175	$Der(V)[\%]$	80	$\geq 80$
	$D_{elCap}(mm)$	100	$Der(I)[\%]$	80	$\geq 80$
	$D_{SD,bw}(\mu m)$	300	$A_{hs,SD}[m^2]$	$1.2718 * 10^{-4}$	$\leq 0.01$
	$t_{hs,b}(mm)$	35	$I_{bw,SD}[A]$	1.1852	$\leq 20$
	$N_{cap}$	14	$T_{j,SD}[^{\circ}C]$	72.9194	$\leq 125$
	$N_{SD}$	8	$Space_{pcb}[\#]$	[8, 14]	$\leq 20$
	—	—	$Budget_{cap}[\$]$	738.64	$\leq 750$
	—	—	$Budget_{SD}[\$]$	485.04	$\leq 500$
	$\lambda_{Cap}[FIT]$		0.009264		
	$R_{sys,cap}[\%]$		96.314		
	$\lambda_{SD}[FIT]$		$7.1173 * 10^{-8}$		
	$R_{sys,SD}[\%]$		99.9999		
	$R_{total}[\%]$		96.3139		
ABC	$v_{applied}(V)$	520	$A_{cap,max}[m^2]$	0.0571	$\leq 0.0707$
	$f_{sw}(kHz)$	8.0055	$AR_{cap}$	1.5	$1 \leq AR_{cap} \leq 2$
	$i_{SD,c}(A)$	16	$I_{rip,max}[\%]$	50	$\leq 50$
	$L_{elCap}(mm)$	167.5	$Der(V)[\%]$	80	$\geq 80$
	$D_{elCap}(mm)$	95	$Der(I)[\%]$	80	$\geq 80$
	$D_{SD,bw}(\mu m)$	300	$A_{hs,SD}[m^2]$	$9.0843 * 10^{-5}$	$\leq 0.01$
	$t_{hs,b}(mm)$	25	$I_{bw,SD}[A]$	1.0017	$\leq 20$
	$N_{cap}$	14	$T_{j,SD}[^{\circ}C]$	72.9194	$\leq 125$
	$N_{SD}$	8	$Space_{pcb}[\#]$	[8, 14]	$\leq 20$
	—	—	$Budget_{cap}[\$]$	738.64	$\leq 750$
	—	—	$Budget_{SD}[\$]$	485.04	$\leq 500$
	$\lambda_{Cap}[FIT]$		0.009264		
	$R_{sys,cap}[\%]$		96.314		
	$\lambda_{SD}[FIT]$		$7.1173 * 10^{-8}$		
	$R_{sys,SD}[\%]$		99.9999		
	$R_{total}[\%]$		96.3139		

In addition, Fig. 5.21 and Table 5.15 elaborate on the convergence rate for each one of the algorithms proposed. From the graph and the table, the algorithm with the highest convergence rate is the HHO, which converges to the optimal value in 2 iterations out of 20, and with only 50 population members. However, it is the algorithm that takes the longest to execute each iteration with 0.00554 seconds per iteration.

The slowest convergence algorithm was the ABC, which converged in iteration 12 out of 20, also with 50 population members, but with the difference of spending just 0.0012 seconds per iteration. In the middle, the most balanced algorithm was the PSO algorithm, which converged in 5 iterations out of 20, with 50 population members and only 0.00076 seconds per iteration.

A change in the algorithm's parameters could change the overall rate of convergence, but it could also bring down the performance by adding more time per iteration execution. For example, each algorithm could be run with more population members, which would make the algorithm find the solution in an earlier iteration, but with the downside of spending more time per iteration.

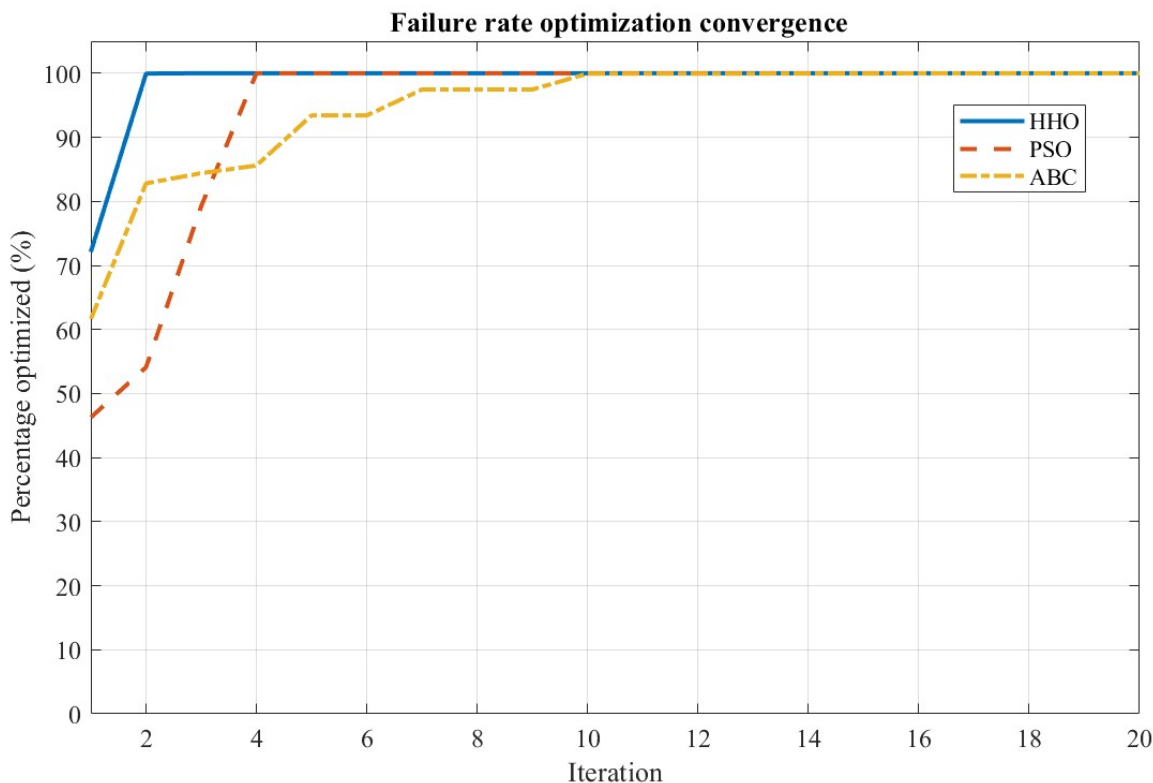


Fig. 5.21: Failure rate optimization convergence.

Table 5.15: Failure rate optimization parameters

Algorithm	Total # of iterations	Population members	# of Iterations for convergence	Time per iteration (#20) (sec)	Total time (sec)
<i>HHO</i>	20	50	2	0.00554	0.1108
<i>PSO</i>	20	50	5	$7.6 * 10^{-4}$	0.0152
<i>ABC</i>	20	50	12	0.0012	0.0248

### 5.6 GLOBAL OPTIMIZATION (WEAR OUT PHASE)

The global optimization of the system was secondly done considering the wear-out phase, directly related to the sub-system-level modeling, with  $L_{cap}$  and  $N_{SD}$  as a target to maximize. Table 5.16 and Table 5.17 show the wear-out phase optimized results considering the modeling on a sub-system level for each one of the algorithms proposed.

Table 5.16: Wear out phase optimized results

Algorithm	Design Parameter	Optimum value	Constraint	Actual Value	Min/Max value
<i>HHO</i>	$v_{applied}(V)$	520	$A_{cap,max}[m^2]$	$1.3744 * 10^{-4}$	$\leq 0.0707$
	$f_{sw}(kHz)$	8.0055	$AR_{cap}$	1.5	$1 \leq AR_{cap} \leq 2$
	$i_{SD,c}(A)$	16	$I_{rip,max}[\%]$	50	$\leq 50$
	$L_{elCap}(mm)$	7.5	$Der(V)[\%]$	80	$\geq 80$
	$D_{elCap}(mm)$	5	$Der(I)[\%]$	80	$\geq 80$
	$D_{SD,bw}(\mu m)$	300	$A_{hs,SD}[m^2]$	$9.0843 * 10^{-5}$	$\leq 0.01$
	$t_{hs,b}(mm)$	25	$I_{bw,SD}[A]$	1.0017	$\leq 20$
	$N_{cap}$	—	$T_{j,SD}[^{\circ}C]$	72.9194	$\leq 125$
	$N_{SD}$	—	$Space_{pcb}[\#]$	[8, 14]	$\leq 20$
	—	—	$Budget_{cap}[\$]$	—	$\leq 750$
—	—	$Budget_{SD}[\$]$	—	$\leq 500$	
	$L_{cap}[yrs]$	8.8566			
	$N_{SD}[cycles]$	24581.153			

Table 5.17: Wear out phase optimized results

Algorithm	Design Parameter	Optimum value	Constraint	Actual Value	Min/Max value
PSO	$v_{applied}(V)$	520	$A_{cap,max}[m^2]$	$1.3744 * 10^{-4}$	$\leq 0.0707$
	$f_{sw}(kHz)$	8.0055	$AR_{cap}$	1.5	$1 \leq AR_{cap} \leq 2$
	$i_{SD,c}(A)$	16	$I_{rip,max}[\%]$	50	$\leq 50$
	$L_{elCap}(mm)$	7.5	$Der(V)[\%]$	80	$\geq 80$
	$D_{elCap}(mm)$	5	$Der(I)[\%]$	80	$\geq 80$
	$D_{SD,bw}(\mu m)$	300	$A_{hs,SD}[m^2]$	$1.0901 * 10^{-4}$	$\leq 0.01$
	$t_{hs,b}(mm)$	30	$I_{bw,SD}[A]$	1.0973	$\leq 20$
	$N_{cap}$	–	$T_{j,SD}[^{\circ}C]$	72.9194	$\leq 125$
	$N_{SD}$	–	$Space_{pcb}[\#]$	[8, 14]	$\leq 20$
	–	–	$Budget_{cap}[\$]$	–	$\leq 750$
	–	–	$Budget_{SD}[\$]$	–	$\leq 500$
		$L_{cap}[yrs]$	8.8566		
	$N_{SD}[cycles]$	24581.153			
ABC	$v_{applied}(V)$	520	$A_{cap,max}[m^2]$	$1.3744 * 10^{-4}$	$\leq 0.0707$
	$f_{sw}(kHz)$	8.0055	$AR_{cap}$	1.5	$1 \leq AR_{cap} \leq 2$
	$i_{SD,c}(A)$	16	$I_{rip,max}[\%]$	50	$\leq 50$
	$L_{elCap}(mm)$	7.5	$Der(V)[\%]$	80	$\geq 80$
	$D_{elCap}(mm)$	5	$Der(I)[\%]$	80	$\geq 80$
	$D_{SD,bw}(\mu m)$	300	$A_{hs,SD}[m^2]$	$1.6352 * 10^{-4}$	$\leq 0.01$
	$t_{hs,b}(mm)$	45	$I_{bw,SD}[A]$	1.3439	$\leq 20$
	$N_{cap}$	–	$T_{j,SD}[^{\circ}C]$	72.9194	$\leq 125$
	$N_{SD}$	–	$Space_{pcb}[\#]$	[8, 14]	$\leq 20$
	–	–	$Budget_{cap}[\$]$	–	$\leq 750$
	–	–	$Budget_{SD}[\$]$	–	$\leq 500$
		$L_{cap}[yrs]$	8.8566		
	$N_{SD}[cycles]$	24581.153			

In addition, Fig. 5.22 and Table 5.18 elaborate on the convergence rate for each one of the algorithms proposed. From the graph and the table, the algorithm with the highest convergence rate is again the HHO, which converges to the most optimum value in 2 iterations out of 20, and with only 50 population members. However, it is the algorithm that takes the longest to execute each iteration with 0.00549 seconds per iteration.

The slowest convergence algorithm was the ABC, which converged in iteration 12 out of 20, also with 50 population members, but with the difference of spending just 0.0017 seconds per iteration. In the middle, the most balanced algorithm was the PSO algorithm, which converged in 5 iterations out of 20, with 50 population members and only 0.00065 seconds per iteration.

When considering other optimization problems, there is a high chance that more iterations will be needed, as well as the possibility of more population members needed to find the optimum answer. However, for this optimization problem and to find a balance between convergence and time of convergence, the parameters were kept to 20 total iterations and 50 total population members.

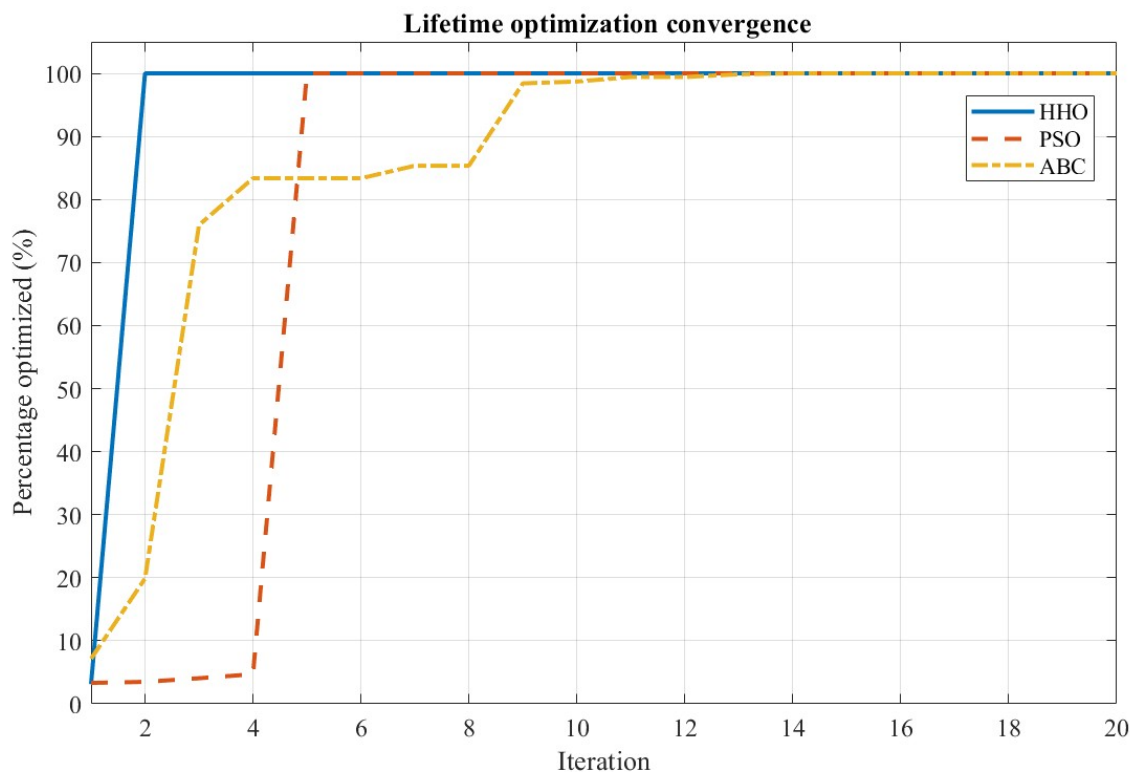


Fig. 5.22: Lifetime optimization convergence.

Table 5.18: Lifetime optimization parameters

<b>Algorithm</b>	<b>Total # of iterations</b>	<b>Population members</b>	<b># of Iterations for convergence</b>	<b>Time per iteration (#20) (sec)</b>	<b>Total time (sec)</b>
<i>HHO</i>	20	50	2	0.00549	0.1098
<i>PSO</i>	20	50	5	$6.5 * 10^{-4}$	0.0130
<i>ABC</i>	20	50	12	0.0017	0.0335

## CHAPTER 6

### CONCLUSION AND FUTURE WORKS

This work introduced the concept of reliability in power electronic converters and the importance of improving this reliability for the overall functioning of the power system. Reliability modeling was done for a power converter at its component and subsystem levels by analyzing its useful time and wear-out phases. This modeling was successfully used to determine the reliability of a power converter under certain conditions and to improve this reliability by using optimization algorithms such as HHO, PSO, and ABC algorithms. From the proposed algorithms, the HHO was the algorithm that demonstrated a superior convergence rate while consuming more computational resources. On the other hand, the PSO was the algorithm that demonstrated a balance between convergence rate and computational resources consumed.

The methods used in this research should be employed as a base for further optimization into more detailed parameters that could model the converter's behavior under other critical circumstances. The modeling done in this work just covers failures resulting from errors in development or manufacturing, as well as overstresses (electrical, mechanical, and thermal).

## REFERENCES

- [1] C. Singh, P. Jirutitijaroen, and J. Mitra, "Electric power grid reliability evaluation: Models and methods," *Chichester: Wiley Blackwell*, 2019.
- [2] S. Padmanaban, S. Chenniappan, and S. Palanisamy, "Power systems operation with 100% renewable energy sources," *Elsevier*, 2023.
- [3] M. A. Hannan, M. S. H. Lipu, P. J. Ker, R. A. Begum, V. G. Agelidis, and F. Blaabjerg, "Power electronics contribution to renewable energy conversion addressing emission reduction: Applications, issues, and recommendations," *Applied Energy*, vol. 251, p. 113404, Oct. 2019.
- [4] M. Davari, M. P. Aghababa, F. Blaabjerg, and M. Saif, "A Modular adaptive robust nonlinear control for resilient integration of VSIs into emerging modernized microgrids," *IEEE Journal of Emerging and Selected Topics in Power Electronics*, vol. 9, no. 3, pp. 2907–2925, Jun. 2021.
- [5] A. Afshari, M. Davari, M. Karrari, W. Gao, and F. Blaabjerg, "A multivariable, adaptive, robust, primary control enforcing predetermined dynamics of interest in islanded microgrids based on grid-forming inverter-based resources," *IEEE Transactions on Automation Science and Engineering*, May 2023.
- [6] S. Yazdani, M. Ferdowsi, M. Davari, and P. Shamsi, "Robust sliding mode control of a three-phase grid-forming inverter in non-ideal grid conditions and isolated mode of operation," in *Proceedings of the IEEE 2020 IEEE Applied Power Electronics Conference and Exposition (APEC), New Orleans, LA, USA, 2020*, pp. 3087–3091, Jun. 2020.
- [7] M. Davari and Y. A. -R. I. Mohamed, "Robust multi-objective control of VSC-based DC-voltage power port in hybrid AC/DC multi-terminal micro-grids," *IEEE Transactions on Smart Grid*, vol. 4, no. 3, pp. 1597–1612, Sep. 2013.
- [8] M. Davari and Y. A. -R. I. Mohamed, "Robust vector control of a very weak-grid-connected voltage-source converter considering the phase-locked loop dynamics," *IEEE Transactions on Power Electronics*, vol. 32, no. 2, pp. 977–994, Feb. 2017.
- [9] M. Davari, W. Gao, and F. Blaabjerg, "Analysing dynamics and synthesizing a robust vector control dc-voltage power port based on the modular multilevel converter in multi-infeed AC/DC smart grids," *IET Smart Grid*, vol. 2, no. 4, pp. 645–658, Sep. 2019.
- [10] M. Davari and Y. A. -R. I. Mohamed, "Dynamics and robust control of a grid-connected VSC in multiterminal dc grids considering the instantaneous power of DC- and AC-Side filters and dc grid uncertainty," *IEEE Transactions on Power Electronics*, vol. 31, no. 3, pp. 1942–1958, Mar. 2016.
- [11] Z. Wang, Y. Yu, W. Gao, M. Davari, and C. Deng, "Adaptive, optimal, virtual synchronous generator control of three-phase grid-connected inverters under different grid conditions—An adaptive dynamic programming approach," *IEEE Transactions on Industrial Informatics*, vol. 18, no. 11, pp. 7388–7399, Nov. 2022.

- [12] M. Davari, M. P. Aghababa, F. Blaabjerg, and M. Saif, "An innovative, adaptive faulty signal rectifier along with a switching controller for reliable primary control of GC-VSIs in CPS-Based modernized microgrids," *IEEE Transactions on Power Electronics*, vol. 36, no. 7, pp. 8370–8387, Jul. 2021.
- [13] Z. Wang, Y. Wang, M. Davari, and F. Blaabjerg, "An effective PQ-decoupling control scheme using adaptive dynamic programming approach to reducing oscillations of virtual synchronous generators for grid connection with different impedance types," *IEEE Transactions on Industrial Electronics*, vol. 71, no. 4, pp. 3763–3775, Apr. 2024.
- [14] M. Davari, W. Gao, A. Aghazadeh, F. Blaabjerg, and F. L. Lewis, "An optimal synchronization control method of PLL utilizing adaptive dynamic programming to synchronize inverter-based resources with unbalanced, low-inertia, and very weak grids," *IEEE Transactions on Automation Science and Engineering*, Mar. 2024.
- [15] M. Davari, A. Aghazadeh, W. Gao, and F. Blaabjerg, "Detailed dynamic dc models of VSC considering controls for DC-fault simulations in modernized microgrid protection," *IEEE Journal of Emerging and Selected Topics in Power Electronics*, vol. 9, no. 4, pp. 4514–4532, Aug. 2021.
- [16] M. Davari, W. Gao, and F. Blaabjerg, "A fault-tolerant, passivity-based controller enhanced by the equilibrium-to-equilibrium maneuver capability for the DC-voltage power port VSC in multi-feed AC/DC modernized grids," *IEEE Journal of Emerging and Selected Topics in Power Electronics*, vol. 8, no. 3, pp. 2484–2507, Sep. 2020.
- [17] S. Yazdani, M. Ferdowsi, M. Davari, and P. Shamsi, "Internal model based control to tackle non-minimum phase behavior in three-phase Z-source inverters," in *Proceedings of the IEEE 2020 IEEE Applied Power Electronics Conference and Exposition (APEC), New Orleans, LA, USA, 2020*, pp. 1904–1910, Jun. 2020.
- [18] O. Qasem, M. Davari, W. Gao, D. R. Kirk, and T. Chai, "Hybrid iteration ADP algorithm to solve cooperative, optimal output regulation problem for continuous-time, linear, multiagent systems: Theory and application in islanded modern microgrids with IBRs," *IEEE Transactions on Industrial Electronics*, vol. 71, no. 1, pp. 834–845, Jan. 2024.
- [19] S. Yazdani, M. Ferdowsi, M. Davari, and P. Shamsi, "Advanced current-limiting and power-sharing control in a PV-based grid-forming inverter under unbalanced grid conditions," *IEEE Journal of Emerging and Selected Topics in Power Electronics*, vol. 8, no. 2, pp. 1084–1096, Jun. 2020.
- [20] S. Yazdani, M. Davari, M. Ferdowsi, and P. Shamsi, "Internal model power synchronization control of a PV-based voltage-source converter in weak-grid and islanded conditions," *IEEE Transactions on Sustainable Energy*, vol. 12, no. 2, pp. 1360–1371, Apr. 2021.
- [21] M. Davari, S. M. Ale-Emran, H. Yazdanpanahi, and G. B. Gharehpetian, "Modeling the combination of UPQC and photovoltaic arrays with multi-input single-output DC-DC converter," in *Proceedings of the IEEE 2009 IEEE/PES Power Systems Conference and Exposition, Seattle, WA, USA, 2009*, pp. 1–7, Apr. 2009.

- [22] M. Davari and Y. A. -R. I. Mohamed, "Robust DC-link voltage control of a full-scale PMSG wind turbine for effective integration in DC grids," *IEEE Transactions on Power Electronics*, vol. 32, no. 5, pp. 4021–4035, May 2017.
- [23] M. Davari and Y. A. -R. I. Mohamed, "Robust droop and DC-Bus voltage control for effective stabilization and power sharing in VSC multiterminal DC grids," *IEEE Transactions on Power Electronics*, vol. 33, no. 5, pp. 4373–4395, May 2018.
- [24] A. Aghazadeh, N. Khodabakhshi-Javinani, H. Nafisi, M. Davari, and E. Pouresmaeil, "Adapted near-state PWM for dual two-level inverters in order to reduce common-mode voltage and switching losses," *IET Power Electronics*, vol. 12, no. 4, pp. 676–685, Feb. 2019.
- [25] A. Aghazadeh, M. Davari, H. Nafisi, and F. Blaabjerg, "Grid integration of a dual two-level voltage-source inverter considering grid impedance and phase-locked loop," *IEEE Journal of Emerging and Selected Topics in Power Electronics*, vol. 9, no. 1, pp. 401–422, Feb. 2021.
- [26] A. Sangwongwanich and F. Blaabjerg, "Monte Carlo simulation with incremental damage for reliability assessment of power electronics," *IEEE Transactions on Power Electronics*, vol. 36, no. 7, pp. 7366–7371, Jul. 2021.
- [27] M. Novak, A. Sangwongwanich, and F. Blaabjerg, "Monte Carlo-based reliability estimation methods for power devices in power electronics systems," *IEEE Open Journal of Power Electronics*, vol. 2, pp. 523–534, Sep. 2021.
- [28] N. Shahidirad, M. Niroomand, and R. -A. Hooshmand, "Investigation of PV power plant structures based on Monte Carlo reliability and economic analysis," *IEEE Journal of Photovoltaics*, vol. 8, no. 3, pp. 825–833, May 2018.
- [29] B. Zhang, M. Wang and W. Su, "Reliability analysis of power systems integrated with high-penetration of power converters," *IEEE Transactions on Power Systems*, vol. 36, no. 3, pp. 1998–2009, May 2021.
- [30] S. Peyghami, Z. Wang and F. Blaabjerg, "A guideline for reliability prediction in power electronic converters," *IEEE Transactions on Power Electronics*, vol. 35, no. 10, pp. 10958–10968, Oct. 2020.
- [31] Z. Tang, Y. Yang and F. Blaabjerg, "Power electronics: The enabling technology for renewable energy integration," *CSEE Journal of Power and Energy Systems*, vol. 8, no. 1, pp. 39–52, Jan. 2022.
- [32] G. Zhang, Z. Li, B. Zhang, and W. A. Halang, "Power electronics converters: Past, present and future," *Renewable and Sustainable Energy Reviews*, vol. 81, pp. 2028–2044, Jan. 2018
- [33] Y. Baazizi, et. al., "Experimental study of a three-phase diode rectifier operating at cryogenic temperature," *IEEE Transactions on Applied Superconductivity*, vol. 34, no. 3, pp. 1–5, May 2024.
- [34] M. Basler, et. al., "GaN active rectifier diode," *IEEE Open Journal of Power Electronics*, vol. 3,

pp. 876–885, Nov. 2022.

- [35] K. Dang et al., “Self-aligned and low-capacitance lateral GaN diode for x-band high-efficiency rectifier,” *IEEE Electron Device Letters*, vol. 43, no. 4, pp. 537–540, Apr. 2022.
- [36] G. T. Bui, D. A. Nguyen and C. Seo, “A novel design of dual-band inverse class-F shunt-diode rectifier for energy harvesting,” *IEEE Transactions on Circuits and Systems II: Express Briefs*, vol. 70, no. 7, pp. 2345–2349, Jul. 2023.
- [37] Y. He, et. al., “A compact single-phase cascaded three-level ac/dc converter with variable dc bus voltage and low CM noise,” *IEEE Transactions on Power Electronics*, vol. 39, no. 1, pp. 398–408, Jan. 2024.
- [38] L. Tan, B. Wu, S. Rivera and V. Yaramasu, “Comprehensive dc power balance management in high-power three-level dc–dc converter for electric vehicle fast charging,” *IEEE Transactions on Power Electronics*, vol. 31, no. 1, pp. 89–100, Jan. 2016.
- [39] F. Deng and Z. Chen, “Control of improved full-bridge three-level dc/dc converter for wind turbines in a dc grid,” *IEEE Transactions on Power Electronics*, vol. 28, no. 1, pp. 314–324, Jan. 2013.
- [40] J. Yang, Z. He, H. Pang and G. Tang, “The hybrid-cascaded dc–dc converters suitable for HVDC applications,” *IEEE Transactions on Power Electronics*, vol. 30, no. 10, pp. 5358–5363, Oct. 2015.
- [41] M. Ashraf, et. al., “A new hybrid dual active bridge modular multilevel based dc–dc converter for HVDC networks,” *IEEE Access*, vol. 9, pp. 62055–62073, Apr. 2021.
- [42] M. Basirifar and A. Shoulaie, “A comparative study of circulating current free and circulating current cycloconverters,” in *Proceedings of the IEEE 2010 First Power Quality Conference, Tehran, Iran*, Jan. 2010, pp. 1–4.
- [43] T. Xu, C. Klumpner and J. Clare, “Assessing the benefits of hybrid cycloconverters,” *IEEE Transactions on Industrial Electronics*, vol. 59, no. 1, pp. 47–57, Jan. 2012.
- [44] R. K. Burra, S. K. Mazumder and Rongjun Huang, “DV/DT related spurious gate turn-on of bidirectional switches in a high-frequency cycloconverter,” *IEEE Transactions on Power Electronics*, vol. 20, no. 6, pp. 1237–1243, Nov. 2005.
- [45] Y. Liu, G. T. Heydt, and R. F. Chu, “The power quality impact of cycloconverter control strategies,” *IEEE Transactions on Power Delivery*, vol. 20, no. 2, pp. 1711–1718, Apr. 2005.
- [46] D. Chen and Y. Chen, “Step-up ac voltage regulators with high-frequency link,” *IEEE Transactions on Power Electronics*, vol. 28, no. 1, pp. 390–397, Jan. 2013.
- [47] P. N. Wijesooriya, N. Kularatna and D. A. Steyn-Ross, “Efficiency enhancements to a linear ac voltage regulator: Multiwinding versus multitransformer design,” *IEEE Journal of Emerging and Selected Topics in Industrial Electronics*, vol. 1, no. 2, pp. 192–199, Oct. 2020.

- [48] J. W. Kolar, T. Friedli, J. Rodriguez and P. W. Wheeler, "Review of three-phase PWM ac–ac converter topologies," *IEEE Transactions on Industrial Electronics*, vol. 58, no. 11, pp. 4988–5006, Nov. 2011.
- [49] W. Wu, J. Ji and F. Blaabjerg, "Aalborg inverter – A new type of "Buck in buck, boost in boost" grid-tied inverter," *IEEE Transactions on Power Electronics*, vol. 30, no. 9, pp. 4784–4793, Sep. 2015.
- [50] F. Blaabjerg, M. Liserre and K. Ma, "Power electronics converters for wind turbine systems," *IEEE Transactions on Industry Applications*, vol. 48, no. 2, pp. 708–719, Apr. 2012.
- [51] F. Blaabjerg and K. Ma, "Future on power electronics for wind turbine systems," *IEEE Journal of Emerging and Selected Topics in Power Electronics*, vol. 1, no. 3, pp. 139–152, Sep. 2013.
- [52] D. Meneses, F. Blaabjerg, Ó. García and J. A. Cobos, "Review and comparison of step-up transformerless topologies for photovoltaic ac-module application," *IEEE Transactions on Power Electronics*, vol. 28, no. 6, pp. 2649–2663, Jun. 2013.
- [53] X. Xie, et. al., "Guest editorial: Control interactions in power electronic converter dominated power systems," *International Journal of Electrical Power & Energy Systems*, vol. 155, Part A, Jan. 2024.
- [54] S. Peyghami, F. Blaabjerg and P. Palensky, "Incorporating power electronic converters reliability into modern power system reliability analysis," *IEEE Journal of Emerging and Selected Topics in Power Electronics*, vol. 9, no. 2, pp. 1668–1681, Apr. 2021.
- [55] F. Hosseinabadi, et. al., "A comprehensive overview of reliability assessment strategies and testing of power electronics converters," *IEEE Open Journal of Power Electronics*, vol. 5, pp. 473–512, Mar. 2024.
- [56] S. Peyghami, P. Davari, M. Fotuhi-Firuzabad, and F. Blaabjerg, "Standard test systems for modern power system analysis: An overview," *IEEE Industrial Electronics Magazine*, vol. 13, no. 4, pp. 86–105, Dec. 2019.
- [57] P. Ferro Ferdinand, L. Nurdiana, and A. Irman, "Evaluation of power plant reliability using index loss of load in the Suralaya power plant," *IOP Conference Series: Materials Science and Engineering*, vol. 909, no. 1, p. 012070, Dec. 2020.
- [58] A. Volkanovski, M. Čepin, and B. Mavko, "Application of the fault tree analysis for assessment of power system reliability," *Reliability Engineering & System Safety*, vol. 94, no. 6, pp. 1116–1127, Jun. 2009.
- [59] M. Qawaqzeh, et al., "The assess reduction of the expected energy not-supplied to consumers in medium voltage distribution systems after installing a sectionalizer in optimal place," *Sustainable energy, grids and networks*, vol. 34, pp. 101035–101035, Jun. 2023.
- [60] T. X. Zhu, "A new methodology of analytical formula deduction and sensitivity analysis of EENS in bulk power system reliability assessment," in *Proceedings of the IEEE 2006 IEEE PES Power*

*Systems Conference and Exposition, Atlanta, GA, USA, 2006*, pp. 825–831, Feb. 2007.

- [61] *FIDES Guide 2022 – A reliability methodology for electronic systems*, Edition A, Institut pour la Maîtrise des Risques, France, 2023. [Online]. Available: [www.fides-reliability.org](http://www.fides-reliability.org) (Accessed: October 2023).
- [62] A. A. Heidari, et al., “Harris hawks optimization: Algorithm and applications,” *Future Generation Computer Systems*, vol. 97, pp. 849–872, Jun. 2018.
- [63] S. Oviedo, M. Davari, S. Zhao, and F. Blaabjerg, "Artificial-intelligence-enabled lifetime estimation of photovoltaic systems considering the mission profile of the DC–AC inverter," in *Proceedings of the IEEE SoutheastCon 2024, Atlanta, United States*, Apr. 2024.
- [64] I. D. Woodruff and M. Davari, "An optimization approach based on the interior-point methodology for the tertiary control of modernized microgrids," in *Proceedings of the IEEE 2019 SoutheastCon, Huntsville, AL, USA*, 2019, pp. 1-8, Mar. 2020.
- [65] R. Sihwail, K. Omar, K. A. Z. Ariffin, and M. Tubishat, “Improved Harris hawks optimization using elite opposition-based learning and novel search mechanism for feature selection,” *IEEE Access*, vol. 8, pp. 121127–121145, Jul. 2020.
- [66] Z. M. Elgamal, et al., “An improved Harris hawks optimization algorithm with simulated annealing for feature selection in the medical field,” *IEEE Access*, vol. 8, pp. 186638–186652, Oct. 2020.
- [67] V. M. Kumar, B. Chokkalingam, and L. Mihet-Popa, “Mitigation of complexity in charging station allocation for EVs using chaotic Harris hawks optimization charge scheduling algorithm,” *IEEE Access*, vol. 11, pp. 130466–130482, Nov. 2023.
- [68] J. Xie, S. Huang, D. Wei, and Z. Zhang, “Scheduling of multisensor for UAV cluster based on Harris hawks optimization with an adaptive golden sine search mechanism,” *IEEE Sensors Journal*, vol. 22, no. 10, pp. 9621-9635, May 2022.
- [69] K. Dev, et al., “Energy optimization for green communication in IoT using Harris hawks optimization,” *IEEE Transactions on Green Communications and Networking*, vol. 6, no. 2, pp. 685–694, Jun. 2022.
- [70] S. Esfandiari, M. Davari, W. Gao, Y. Yang, and K. Al-Haddad, "A novel converter-based PV emulator control using Lambert W method and fractional-order fuzzy proportional-integral controller trained by Harris hawks optimization," *IEEE Journal of Emerging and Selected Topics in Industrial Electronics*, pp. 1–15, Jan. 2024, doi: 10.1109/JESTIE.2024.3396140.
- [71] S. E. De León-Aldaco, H. Calleja and J. Aguayo Alquicira, “Metaheuristic optimization methods applied to power converters: A review,” *IEEE Transactions on Power Electronics*, vol. 30, no. 12, pp. 6791–6803, Dec. 2015.
- [72] R. V. Kulkarni and G. K. Venayagamoorthy, “Particle swarm optimization in wireless-sensor networks: A brief survey,” *IEEE Transactions on Systems, Man, and Cybernetics, Part C*

(Applications and Reviews), vol. 41, no. 2, pp. 262–267, Mar. 2011.

- [73] P. W. Shaikh, M. El-Abd, M. Khanafer, and K. Gao, “A review on swarm intelligence and evolutionary algorithms for solving the traffic signal control problem,” *IEEE Transactions on Intelligent Transportation Systems*, vol. 23, no. 1, pp. 48–63, Jan. 2022.
- [74] W. Yejiao, et al., “RFID network planning of smart factory based on swarm intelligent optimization algorithm: A review,” *IEEE Access*, vol. 12, pp. 64980–64996, May. 2024.
- [75] A. G. Gad, “Particle swarm optimization algorithm and its applications: A systematic review,” *Archives of Computational Methods in Engineering*, vol. 29, no. 5, pp. 2531–2561, Apr. 2022.
- [76] S. Patra, J. Mitra, and R. Earla, “A new intelligent search method for composite system reliability analysis,” in *Proceedings of the IEEE 2005/2006 IEEE/PES Transmission and Distribution Conference and Exhibition, Dallas, TX*, pp. 803-807, Sep. 2006
- [77] S. U. Khan, S. Yang, L. Wang, and L. Liu, “A modified particle swarm optimization algorithm for global optimizations of inverse problems,” *IEEE Transactions on Magnetics*, vol. 52, no. 3, pp. 1–4, Mar. 2016.
- [78] R. C. Eberhart, R. C. Dobbins, P. K. Simpson, and R. W. Dobbins, *Computational Intelligence PC Tools*. Morgan Kaufmann Pub, 1996.
- [79] T. M. Shami, et al., “Particle swarm optimization: A comprehensive survey,” *IEEE Access*, vol. 10, pp. 10031–10061, Jan. 2022.
- [80] M. Clerc and J. Kennedy, “The particle swarm – explosion, stability, and convergence in a multidimensional complex space,” *IEEE Transactions on Evolutionary Computation*, vol. 6, no. 1, pp. 58–73, Feb. 2002.
- [81] A. M. Eltamaly, “A novel strategy for optimal PSO control parameters determination for PV energy systems,” *Sustainability*, vol. 13, no. 2, p. 1008, Jan. 2021.
- [82] K. R. Harrison, A. P. Engelbrecht, and B. M. Ombuki-Berman, “Optimal parameter regions and the time-dependence of control parameter values for the particle swarm optimization algorithm,” *Swarm and Evolutionary Computation*, vol. 41, pp. 20–35, Aug. 2018.
- [83] A. Ratnaweera, S. K. Halgamuge, and H. C. Watson, “Self-organizing hierarchical particle swarm optimizer with time-varying acceleration coefficients,” *IEEE Transactions on Evolutionary Computation*, vol. 8, no. 3, pp. 240–255, Jun. 2004.
- [84] J. Kennedy and R. Eberhart, “Particle swarm optimization,” in *Proceedings of ICNN'95 - International Conference on Neural Networks, Perth, WA, Australia*, pp. 1942–1948 vol.4, Nov. 1995.
- [85] M. Xu, Y. Zhang, Y. Fan, Y. Chen and D. Song, “Linear spectral mixing model-guided artificial bee colony method for endmember generation,” *IEEE Geoscience and Remote Sensing Letters*,

vol. 17, no. 12, pp. 2145–2149, Dec. 2020.

- [86] D. Karaboga, “An idea based on honey bee swarm for numerical optimization,” *Computer and Communications*, vol. 2, no. 4, Oct. 2014.
- [87] H. Gao, Y. Shi, C. -M. Pun, and S. Kwong, “An improved artificial bee colony algorithm with its application,” *IEEE Transactions on Industrial Informatics*, vol. 15, no. 4, pp. 1853–1865, Apr. 2019.
- [88] B. Zhang, X. Sun, L. Gao, and L. Yang, “Endmember extraction of hyperspectral remote sensing images based on the discrete particle swarm optimization algorithm,” *IEEE Transactions on Geoscience and Remote Sensing*, vol. 49, no. 11, pp. 4173–4176, Nov. 2011.
- [89] X. Sun, L. Yang, B. Zhang, L. Gao, and J. Gao, “An endmember extraction method based on artificial bee colony algorithms for hyperspectral remote sensing images,” *Remote Sensing*, vol. 7, no. 12, pp. 16363–16383, Dec. 2015.
- [90] X. Lu, H. Sun and X. Zheng, “A feature aggregation convolutional neural network for remote sensing scene classification,” *IEEE Transactions on Geoscience and Remote Sensing*, vol. 57, no. 10, pp. 7894–7906, Oct. 2019.
- [91] A. H. Gandomi, and A. R. Kashani, “Construction cost minimization of shallow foundation Using recent swarm intelligence techniques,” *IEEE Transactions on Industrial Informatics*, vol. 14, no. 3, pp. 1099–1106, Mar. 2018.
- [92] D. Li, W. Chiu, H. Sun, and H. V. Poor, “Multiobjective optimization for demand side management program in smart grid,” *IEEE Transactions on Industrial Informatics*, vol. 14, no. 4, pp. 1482–1490, Apr. 2018
- [93] D. Karaboga and B. Basturk, “A powerful and efficient algorithm for numerical function optimization: Artificial bee colony (ABC) algorithm,” *Global Optimization*, vol. 39, no. 3, pp. 459–471, Apr. 2007.
- [94] J. Tang, G. Liu, and Q. Pan, “A review on representative swarm intelligence algorithms for solving optimization problems: Applications and trends,” *IEEE/CAA Journal of Automatica Sinica*, vol. 8, no. 10, pp. 1627–1643, Oct. 2021.
- [95] X. Zhang, W. Li, H. Li, B. Zhao, J. Li, and F. Liu, “Research on AGV path planning based on improved artificial bee colony algorithm,” in *Proceedings of the IEEE 2023 35th Chinese Control and Decision Conference (CCDC), Yichang, China*, pp. 703–708, Dec. 2023
- [96] F. S. Abu-Mouti and M. E. El-Hawary, “Overview of artificial bee colony (ABC) algorithm and its applications,” in *Proceedings of the IEEE 2012 IEEE International Systems Conference SysCon 2012, Vancouver, BC, Canada*, pp. 1–6 , Apr. 2012.
- [97] A. Hamideh, “Reliability analysis of power-converters-based power systems using artificial intelligence,” *Electronic Theses and Dissertation*, 2483, Jun. 2022.  
<https://digitalcommons.georgiasouthern.edu/etd/2483>.